

Fault Diagnosis and Fault-Tolerant Control of Unmanned Aerial Vehicles

Ban Wang

A Thesis

In the Department

of

Mechanical, Industrial & Aerospace Engineering

Presented in Partial Fulfillment of the Requirements

for the Degree of

Doctor of Philosophy (Mechanical Engineering) at

Concordia University

Montréal, Québec, Canada

June 2018

© Ban Wang, 2018

CONCORDIA UNIVERSITY
SCHOOL OF GRADUATE STUDIES

This is to certify that the thesis prepared

By: **Ban Wang**

Entitled: **Fault Diagnosis and Fault-Tolerant Control of Unmanned Aerial Vehicles**

and submitted in partial fulfillment of the requirements for the degree of

Doctor of Philosophy (Mechanical Engineering)

complies with the regulations of this University and meets the accepted standards with respect to originality and quality.

Signed by the Final Examining Committee:

Dr. Catherine Mulligan Chair

Dr. Xiang Chen External Examiner

Dr. Weiping Zhu External to Program

Dr. Wenfang Xie Examiner

Dr. Ramin Sedaghati Examiner

Dr. Youmin Zhang Thesis Supervisor

Approved by

Dr. Ali Dolatabadi Chair of Department or Graduate Program Director

August 7th, 2018

Date of Defense Dr. Amir Asif Dean, Faculty of Engineering and Computer Science

Abstract

Fault Diagnosis and Fault-Tolerant Control of Unmanned Aerial Vehicles

Ban Wang, Ph.D.

Concordia University, 2018

With the increasing demand for unmanned aerial vehicles (UAVs) in both military and civilian applications, critical safety issues need to be specially considered in order to make better and wider use of them. UAVs are usually employed to work in hazardous and complex environments, which may seriously threaten the safety and reliability of UAVs. Therefore, the safety and reliability of UAVs are becoming imperative for development of advanced intelligent control systems. The key challenge now is the lack of fully autonomous and reliable control techniques in face of different operation conditions and sophisticated environments. Further development of unmanned aerial vehicle (UAV) control systems is required to be reliable in the presence of system component faults and to be insensitive to model uncertainties and external environmental disturbances.

This thesis research aims to design and develop novel control schemes for UAVs with consideration of all the factors that may threaten their safety and reliability. A novel adaptive sliding mode control (SMC) strategy is proposed to accommodate model uncertainties and actuator faults for an unmanned quadrotor helicopter. Compared with the existing adaptive SMC strategies in the literature, the proposed adaptive scheme can tolerate larger actuator faults without stimulating control chattering due to the use of adaptation parameters in both continuous and discontinuous control parts. Furthermore, a fuzzy logic-based boundary layer and a nonlinear disturbance observer are synthesized to further improve the capability of the designed control scheme for tolerating model uncertainties, actuator faults, and unknown external disturbances while preventing

overestimation of the adaptive control parameters and suppressing the control chattering effect. Then, a cost-effective fault estimation scheme with a parallel bank of recurrent neural networks (RNNs) is proposed to accurately estimate actuator fault magnitude and an active fault-tolerant control (FTC) framework is established for a closed-loop quadrotor helicopter system. Finally, a reconfigurable control allocation approach is combined with adaptive SMC to achieve the capability of tolerating complete actuator failures with application to a modified octorotor helicopter. The significance of this proposed control scheme is that the stability of the closed-loop system is theoretically guaranteed in the presence of both single and simultaneous actuator faults.

Acknowledgments

This thesis is submitted in partial fulfillment of the requirements for the degree of philosophy doctor (Ph.D.) at Concordia University (CU) under the financial support of Chinese Scholarship Council (CSC) and Concordia University. The presented research has been conducted under the supervision of Prof. Youmin Zhang in the Diagnosis, Flight Control and Simulation Laboratory (DFCSL) and Networked Autonomous Vehicles Laboratory (NAVL) at the Department of Mechanical, Industrial & Aerospace Engineering, Concordia University.

My deepest gratitude and appreciation go to my supervisor, Prof. Youmin Zhang, for offering me this valuable and unique opportunity to pursue my Ph.D. degree under his supervision. I have been very fortunate to join his research group. His serious attitude towards research has taught me quite a lot. Without his consistent support and great help as well as valuable and insightful guidance, my research progress would probably be slowed and unsatisfactory. There are no words that can express my sincere gratitude for his outstanding supervision.

I would like to thank Prof. W.-F. Xie, Prof. C.-Y. Su, Prof. R. Sedaghati, and Prof. W.-P. Zhu for joining my examination committee and providing brilliant feedback and insightful comments during my comprehensive exam, research proposal exam, and thesis defense exam. I would also like to thank all my colleagues in my research group and collaborators who have helped me a lot during my four years of Ph.D. study. It is my great pleasure to do research and share opinions with them and learn from them.

Finally, I would like to extend my deepest gratitude and appreciation to my parents for their

love, understanding, consistent support, and countless sacrifices, which have played an indispensable role in my life. It can never be enough for me to thank them.

Table of Contents

List of Figures	xi
List of Tables	xvi
Nomenclature	xvii
Acronyms	xx
Chapter 1: Introduction	1
1.1 Background	1
1.1.1 Unmanned Aerial Vehicles	1
1.1.2 Structure of an Unmanned Aerial Vehicle	5
1.2 Fault-Tolerant Control	7
1.2.1 Actuator Faults and Failures	8
1.2.2 Sliding Mode Control	9
1.2.3 Control Allocation	12
1.3 Fault Detection and Diagnosis	14
1.4 Active Disturbance Rejection	17
1.5 Objectives of The Dissertation	19
1.6 Contributions of The Dissertation	21
1.7 Organization of The Dissertation	22
Chapter 2: Aircraft Model	25
2.1 Modeling of a Quadrotor Helicopter	26
2.1.1 Kinematic Equations	26

2.1.2	Dynamic Equations	28
2.1.3	Control Mixing	30
2.1.4	Model Linearization	32
2.2	Actuator Fault Formulation	35
2.3	Environmental Disturbance Formulation	36
Chapter 3: Adaptive Fault-Tolerant Control		37
3.1	Introduction	37
3.2	Adaptive Fault-Tolerant Control Design	39
3.2.1	Problem Formulation	39
3.2.2	Integral-Type Sliding Surface Design	40
3.2.3	Fault-Tolerant Control with Bounded Uncertainty	42
3.2.4	Adaptive Fault-Tolerant Control	45
3.3	Modeling of an Unmanned Quadrotor Helicopter	49
3.4	Simulation Results	51
3.4.1	Case 1: 20% Loss of Control Effectiveness in One Actuator	51
3.4.2	Case 2: 50% Loss of Control Effectiveness in One Actuator	54
3.4.3	Case 3: 3D Trajectory Tracking with 50% Loss of Control Effectiveness in Two Different Actuators	58
3.5	Conclusion	61
Chapter 4: Disturbance Observer-Based Adaptive Fuzzy Fault-Tolerant Control		63
4.1	Introduction	64
4.2	Problem Formulation	67
4.2.1	Modeling of a Quadrotor Helicopter	67
4.2.2	System Formulation	67
4.2.3	Problem Statement	70
4.3	Design of Adaptive Fuzzy Fault-Tolerant Flight Control	71
4.3.1	Integral Sliding Mode Control	71

4.3.2	Adaptive Sliding Mode Control Design	75
4.3.3	Fuzzy Boundary Layer Design	77
4.4	Active Disturbance Rejection	80
4.4.1	Design of Disturbance Observer	81
4.4.2	Synthesize of Disturbance Observer	82
4.5	Simulation Results	84
4.6	Experimental Results	87
4.6.1	Experiment Setup	89
4.6.2	Real Flight Test Results	89
4.7	Conclusion	94
Chapter 5: Active Fault-Tolerant Control		97
5.1	Introduction	98
5.2	Problem Formulation	103
5.2.1	Modeling of a Quadrotor Helicopter	103
5.2.2	Problem Statement	104
5.3	Design of Active FTC	105
5.3.1	Adaptive Sliding Mode Control	106
5.3.2	Construction of Reconfigurable Mechanism	108
5.4	Simulation Results	117
5.4.1	Actuator Faults	117
5.4.2	Construction of Recurrent Neural Networks	118
5.4.3	Learning Phase	119
5.4.4	Fault Diagnosis Case Studies	119
5.5	Experimental Results	121
5.5.1	Description of the Experiment Setup	122
5.5.2	Real Flight Fault Estimation and Accommodation Results	122
5.6	Conclusion	126

5.7	Appendix	126
Chapter 6:	Adaptive Fault-Tolerant Control Allocation	129
6.1	Introduction	130
6.2	Problem Formulation	133
6.2.1	Modeling of an Octorotor Helicopter	133
6.2.2	Problem Statement	135
6.2.3	Formulation of the Transformed System	136
6.3	Adaptive Fault-Tolerant Control Allocation	138
6.3.1	Fault-Tolerant Control Allocation	138
6.3.2	Design of High-Level Sliding Mode Control	140
6.3.3	Adaptive Sliding Mode Control Allocation	143
6.4	Simulation Results	146
6.4.1	Case 1: Single Actuator Fault/Failure	147
6.4.2	Case 2: Simultaneous Actuator Faults	150
6.5	Experimental Results	151
6.5.1	Description of the Experiment Setup	153
6.5.2	Case 1: Single Actuator Complete Failure	153
6.5.3	Case 2: Simultaneous Actuator Faults	155
6.6	Conclusion	158
Chapter 7:	Conclusions and Future Works	159
7.1	Conclusions	159
7.2	Future Works	161
Bibliography		163
List of Publications		182

List of Figures

Figure 1.1	The commonly used small-scale UAVs	3
Figure 1.2	The compound UAVs	3
Figure 1.3	The fundamental architecture of a typical UAV system.	6
Figure 1.4	Actuator fault classification with respect to time.	10
Figure 1.5	General modular structure of control allocation.	13
Figure 2.1	Illustration of the studied quadrotor helicopter.	25
Figure 2.2	Configuration of the quadrotor helicopter.	26
Figure 3.1	Schematic of the proposed adaptive SMC.	46
Figure 3.2	Configuration of the unmanned quadrotor helicopter.	49
Figure 3.3	Tracking performance using nominal SMC with 20% loss of control effectiveness in actuator #1.	52
Figure 3.4	Control input of the faulty actuator using nominal SMC with 20% loss of control effectiveness in actuator #1.	53
Figure 3.5	Tracking performance using adaptive SMC with 20% loss of control effectiveness in actuator #1.	53
Figure 3.6	Control input of the faulty actuator using adaptive SMC with 20% loss of control effectiveness in actuator #1.	54
Figure 3.7	Adaptive control gain using adaptive SMC with 20% loss of control effectiveness in actuator #1.	54

Figure 3.8 Tracking performance using nominal SMC with 50% loss of control effectiveness in actuator #1.	55
Figure 3.9 Control input of the faulty actuator using nominal SMC with 50% loss of control effectiveness in actuator #1.	56
Figure 3.10 Tracking performance using adaptive SMC with 50% loss of control effectiveness in actuator #1.	56
Figure 3.11 Control input of the faulty actuator using adaptive SMC with 50% loss of control effectiveness in actuator #1.	57
Figure 3.12 Adaptive control gain using adaptive SMC with 50% loss of control effectiveness in actuator #1.	57
Figure 3.13 3D trajectory tracking with 50% loss of control effectiveness in actuators #1 and #4 sequentially.	58
Figure 3.14 x position tracking and tracking error with 50% loss of control effectiveness in actuators #1 and #4 sequentially.	59
Figure 3.15 y position tracking and tracking error with 50% loss of control effectiveness in actuators #1 and #4 sequentially.	59
Figure 3.16 z position tracking and tracking error with 50% loss of control effectiveness in actuators #1 and #4 sequentially.	60
Figure 3.17 Roll angle tracking and tracking error with 50% loss of control effectiveness in actuators #1 and #4 sequentially.	60
Figure 3.18 Pitch angle tracking and tracking error with 50% loss of control effectiveness in actuators #1 and #4 sequentially.	60
Figure 3.19 Control inputs of the four motors.	61
Figure 4.1 Configuration of the studied quadrotor helicopter.	68
Figure 4.2 The schematic of the proposed control strategy.	72
Figure 4.3 The membership functions.	78
Figure 4.4 The schematic of the proposed disturbance observer-based control strategy. .	81

Figure 4.5	Tracking performances of height motion with different control approaches.	85
Figure 4.6	Tracking performances of pitch motion with different control approaches.	86
Figure 4.7	Estimation of the total mass of the quadrotor helicopter.	86
Figure 4.8	Tracking performance of pitch motion without disturbance observer.	87
Figure 4.9	Tracking performance of pitch motion with disturbance observer.	87
Figure 4.10	Estimation of the imposed disturbance.	88
Figure 4.11	Fuzzy surface for pitch motion.	89
Figure 4.12	The schematic of the experiment setup.	90
Figure 4.13	Tracking performance of pitch motion in the presence of 30% loss of control effectiveness fault in real flight test.	90
Figure 4.14	Control input of actuator #1 with proposed ASMC in the presence of 30% loss of control effectiveness fault in real flight test.	91
Figure 4.15	Control input of actuator #1 with compared ASMC in the presence of 30% loss of control effectiveness fault in real flight test.	91
Figure 4.16	Tracking performance of pitch motion in the presence of 50% loss of control effectiveness fault in real flight test.	92
Figure 4.17	Control input of actuator #1 with proposed ASMC in the presence of 50% loss of control effectiveness fault in real flight test.	93
Figure 4.18	Control input of actuator #1 with proposed AFSMC in the presence of 50% loss of control effectiveness fault in real flight test.	93
Figure 4.19	Adaptive control parameter related to pitch motion with proposed AFSMC in the presence of 50% loss of control effectiveness fault in real flight test.	94
Figure 4.20	Boundary layer thickness related to pitch motion with proposed AFSMC in the presence of 50% loss of control effectiveness fault in real flight test.	94
Figure 5.1	Configuration of the studied quadrotor helicopter.	103
Figure 5.2	The schematic of the proposed active FTC strategy.	105
Figure 5.3	Architecture of the recurrent neural network.	110

Figure 5.4 Two types of faults injected to actuators.	118
Figure 5.5 Fault estimation performance of RNN1 for actuator #1 in the presence of abrupt fault.	120
Figure 5.6 Fault estimation performance of RNN1 for actuator #1 in the presence of incipient fault.	121
Figure 5.7 Fault estimation performance of RNN1 and RNN2 for actuator #1 and actuator #2, respectively, in the presence of multiple faults.	121
Figure 5.8 The schematic of the experiment setup.	122
Figure 5.9 Fault estimation performance of RNN1 for actuator #1 in the presence of multiple abrupt faults in real flight test.	124
Figure 5.10 Tracking performance of pitch motion in the presence of multiple abrupt faults in real flight test.	124
Figure 5.11 Fault estimation performance of RNN1 for actuator #1 in the presence of incipient and abrupt faults in real flight test.	125
Figure 5.12 Tracking performance of pitch motion in the presence of incipient and abrupt faults in real flight test.	125
Figure 6.1 Configuration of the modified octorotor helicopter.	134
Figure 6.2 The schematic of the proposed adaptive fault-tolerant control strategy. . . .	138
Figure 6.3 Tracking performances of height and pitch motion in the presence of single actuator fault/failure.	148
Figure 6.4 Control inputs for actuators #1 and #5.	148
Figure 6.5 Sliding surfaces and virtual control inputs for height and pitch motion in the presence of single actuator fault/failure.	149
Figure 6.6 Tracking performances of height and pitch motion in the presence of simultaneous actuator faults.	149
Figure 6.7 Control inputs of motors in the presence of simultaneous actuator faults. . .	151

Figure 6.8 The change of adaptive parameter for pitch motion in the presence of simultaneous actuator faults.	151
Figure 6.9 Sliding surfaces and virtual control inputs for height and pitch motion in the presence of simultaneous actuator faults.	152
Figure 6.10 The schematic of the experiment setup.	153
Figure 6.11 Tracking performance of pitch motion in the presence of single actuator failure in real flight test.	154
Figure 6.12 Sliding surface of ASMCA for pitch motion in the presence of single actuator failure in real flight test.	154
Figure 6.13 Control inputs of related actuators for pitch motion in the presence of single actuator failure in real flight test.	155
Figure 6.14 Tracking performance of pitch motion in the presence of simultaneous actuator faults in real flight test.	155
Figure 6.15 Control inputs of related actuators for pitch motion in the presence of simultaneous actuator faults in real flight test.	156
Figure 6.16 Sliding surface of ASMCA for pitch motion in the presence of simultaneous actuator faults in real flight test.	156
Figure 6.17 Virtual control input for pitch motion in the presence of simultaneous actuator faults in real flight test.	157
Figure 6.18 Adaptive parameter of ASMCA for pitch motion in the presence of simultaneous actuator faults in real flight test.	157

List of Tables

Table 3.1	System Parameters	50
Table 4.1	Nomenclature	70
Table 4.2	Fuzzy Rules	78
Table 4.3	Fault Scenarios Considered in Real Flight Experiment	88
Table 4.4	Performance Indices	93
Table 5.1	Nomenclature	104
Table 5.2	Fault Scenarios Considered for Fault Diagnosis Problem in Simulation . . .	119
Table 5.3	Fault Scenarios Considered in Real Flight Experiment	123

Nomenclature

ω	The actuator bandwidth
ω^B	The rotational velocity vector
Ω_i	The i th propeller's rotational speed
ϕ	The roll angle
ψ	The yaw angle
τ^B	The moment vector
τ_x	The total torque along x_b -axis
τ_y	The total torque along y_b -axis
τ_z	The total torque along z_b -axis
θ	The pitch angle
Θ^I	The Euler angle vector
D	The translational motion induced drag force vector
F^I	The force vector
F_x	The total force along x_e -axis
F_y	The total force along y_e -axis

F_z	The total force along z_e -axis
G	The gravitaion vector
g	The acceleration of gravity
I	The diagonal inertial matrix
I_r	The inertial moment of the propeller
I_{xx}	The moment of inertia along x_b -axis
I_{yy}	The moment of inertia along y_b -axis
I_{zz}	The moment of inertia along z_b -axis
K_u	A positive gain related to propeller generated thrust
K_y	A positive gain related to propeller generated torque
L_d	The distance between motor and the center of mass of the quadrotor helicopter
m	The total mass of the quadrotor helicopter
M_f	The rotational motion induced torque vector
M_g	The gyroscopic torque vector
M_T	The torque vector generated by the propellers
p	The rotational velocity along x_b -axis
q	The rotational velocity along y_b -axis
r	The rotational velocity along z_b -axis
T	The thrust vector
u	The translational velocity along x_b -axis

U_ϕ	The generated torque along x_b -axis
U_ψ	The generated torque along z_b -axis
U_θ	The generated torque along y_b -axis
u_i	The pulse-width modulation input of the i th motor
U_z	The total thrust along z_b -axis
v	The translational velocity along y_b -axis
V^B	The translational velocity vector
w	The translational velocity along z_b -axis
X^I	The position vector
x_e	The position along x_e -axis
y_e	The position along y_e -axis
z_e	The position along z_e -axis

Acronyms

AFTCS Active fault-tolerant control system

ASMCA Adaptive sliding mode control allocation

COM Center of mass

DOBC Disturbance observer-based control

FAA Federal Aviation Administration

FDD Fault detection and diagnosis

FTC Fault-tolerant control

FTCS Fault-tolerant control system

GNC Guidance, navigation, and control

GPS Global positioning system

IMU Inertial measurement unit

LQR Linear quadratic regulator

LQRCA Linear quadratic regulator control allocation

MLP Multilayer perceptron

MPC Model predictive control

NSMCA Normal sliding mode control allocation

PFTCS Passive fault-tolerant control system

PID Proportional-integral-derivative

PWM Pulse-width modulation

RNN Recurrent neural network

RNNs Recurrent neural networks

SMC Sliding mode control

UASs Unmanned aerial systems

UAV Unmanned aerial vehicle

UAVs Unmanned aerial vehicles

VSS Variable structure system

VTOL Vertical take-off and landing

Chapter 1

Introduction

1.1 Background

1.1.1 Unmanned Aerial Vehicles

Over the last decades, unmanned aerial vehicles (UAVs) have been widely used by commercial industries, research institutes, and military sectors with applications to payload transportation [1, 2], forest fire detection and fighting [3], surveillance [4, 5], environmental monitoring [6], remote sensing [7], and aerial mapping [8], etc. More recently, with the development of automation technologies, more and more small-scale UAVs are coming out, which can further extend the applications of UAVs. New generations of UAVs need to be designed to achieve their missions with not only increased efficiency but also more safety and security. Future UAVs will be operated with algorithms capable of monitoring the aircraft's health status and of taking actions if needed [9]. Generally speaking, the commonly used UAVs can be classified into three types according to their configuration and flying mechanism [10].

- 1) Fixed-wing aircraft. As shown in Fig. 1.1(a), the wing of the aircraft is permanently attached to its airframe. Its propulsion system generates a forward thrust, which can make the aircraft produce the lift force to balance its weight with certain airspeed. Based on this principle, fixed-wing aircraft must maintain certain forward airspeed, and therefore cannot

vertically take off and land. In comparison with traditional helicopters, a fixed-wing aircraft has a much simpler structure and is able to carry heavier payloads over a longer flight range while consuming less power energy. The main disadvantage of fixed-wing aircraft lies in the requirement of a runway or launcher for take-off and landing.

- 2) Traditional helicopter. As shown in Fig. 1.1(b), a traditional helicopter is a type of rotorcraft in which the aerodynamic forces and moments are mainly supplied by the main rotor blades. To tilt the helicopter forward and backward or sideways, it is required to alter the angle of attack of the main rotor blades cyclically during rotation, creating a different amount of lift forces at different points in the cycle. Whereas, to increase or decrease the overall lift force, it is required to alter the angle of attack of the main rotor blades collectively by equal amounts at the same time, resulting in ascent or descent of the helicopter. Compared to fixed-wing aircraft, although it is capable of vertical take-off and landing (VTOL), its complex structure incurs high maintenance cost.
- 3) Multirotor helicopter. Multirotor helicopter is also called multicopter or multirotor in short. It can be considered as a special type of helicopter, which has three or more propellers. The most popular multirotor helicopter is the quadrotor helicopter as shown in Fig. 1.1(c). A typical quadrotor helicopter has four control inputs, which are the angular speeds of the four propellers. Unlike the traditional single-rotor helicopter, the aerodynamic forces and moments for the multirotor helicopter are generated by change of propellers' angular speeds. Thanks to its simple structure, a multirotor helicopter features high reliability and low maintenance cost. Whereas, its payload capacity and flight endurance are both compromised.

Besides the three types of UAVs mentioned above, there are some combinations of them. As shown in Fig. 1.2(a), a type of compound aircraft combines a quadrotor helicopter and a fixed-wing aircraft, which has capabilities of both high-speed forward flight and VTOL. Another type of compound aircraft, as shown in Fig. 1.2(b), combines a traditional helicopter and a fixed-wing aircraft, which features more payload capacity and higher efficiency due to the lower disc loading

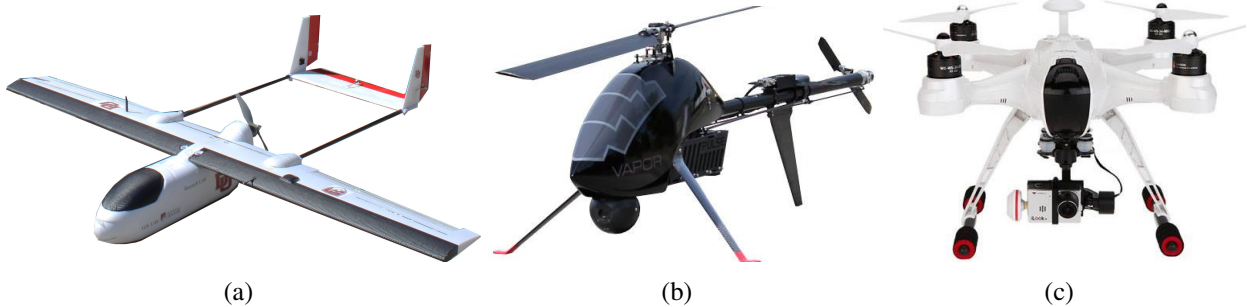


Figure 1.1: The commonly used small-scale UAVs.

compared to the previous one. Among those different types of UAVs, in recent years, multirotor helicopters have drawn more and more attention in both industrial and academic communities due to the capability of VTOL, affordable price, and strong potential for both indoor and outdoor flight.



Figure 1.2: The compound UAVs.

For many applications, in order to accomplish the specific task, different sensors and instrument systems need to be incorporated into the assigned unmanned aerial vehicle (UAV) to make it fully functional. In this sense, a UAV can be regarded as an aerial sensor/payload carrier, and usually the cost of those onboard instruments can easily exceed the cost of the UAV itself, especially for small-scale UAVs. Moreover, UAVs are usually employed to work in complex and hazardous environments, such as urban surveillance, fire fighting, and special military actions. These situations may seriously threaten the safety and reliability of the UAVs and the expensive onboard instruments/payloads. Especially, for those applications carried out in urban area, in-flight faults

exposed on UAVs may endanger human life and property in addition to the loss of the UAV itself. Therefore, the reliability and survivability of UAVs are becoming imperative, and critical safety issues need to be specially considered. As argued in [11–13], the increasing demands for safety, reliability, and high system performance have stimulated research in the area of fault-tolerant control (FTC) with the development in control theory and computer technology. Fault-tolerant capability is an important feature for safety-critical systems [11], such as aircraft [14, 15], spacecraft [16, 17], and wind turbines [18].

To ensure safety and reliability of UAVs, the capability of fault-tolerance is a key subject, but not the only one, to be considered. Depending on different applications, the weights and locations of the configured sensors or payloads may vary, which brings a big challenge for the onboard flight controller. In fact, a lot of uncertain factors often occur in real applications. Among civilian applications such as forest fire fighting and parcel delivery, to name a few, payload transportation is a basic requirement for UAVs. For those applications, due to the added/released payload and external disturbances, the stability of UAVs can be seriously affected, which is normally beyond the ability of a conventional flight controller [19]. For controlling UAVs, a lot of control strategies have been proposed to achieve good tracking performance [20–23]. Nevertheless, among most of the studies, the total take-off weight is assumed constant throughout the entire flight phase. For UAVs, especially small-scale UAVs, adding or releasing payload will significantly affect the tracking performance of the onboard flight controller. Furthermore, UAVs are expected to be cheap and low-cost, and unlike conventional manned aircraft, a very accurate mathematical model may not be available for designing the control system. In this case, the designed control system for UAVs should have the capability of tolerating certain level of model uncertainties. This presents another motivation for this thesis which aims to propose an effective control strategy to accommodate system model uncertainties and external disturbances to ensure the safety and reliability of UAVs.

It turns out that, it will be beneficial to have a UAV system with the capability of tolerating certain faults, model uncertainties, and external disturbances without imperiling itself and its surroundings. From the control point of view, it is to design a so-called self-repairing “smart” flight

control system to improve reliability and survivability of UAVs, which is also the requirement for the next generation flight control system according to unmanned aircraft systems roadmap released in 2005 by the U.S. Department of Defense.

1.1.2 Structure of an Unmanned Aerial Vehicle

In current usage, UAVs refer to aircraft that fly without human operators onboard. They can span a wide range in terms of size and complexity. The largest UAVs, such as Predator and Global Hawk, can weigh several thousand pounds and have wingspans on the order of 10 to 100 *ft*. In general, UAVs serve primarily as flying platforms for sensor payloads that can be as simple as electro-optical cameras or as complex as synthetic aperture radars depending on different applications. The flight of UAVs may be controlled either autonomously by onboard computers or by remote control from human operators on the ground.

Regardless of their sizes and applications, all UAVs share the same composition of basic subsystems as shown in Fig. 1.3. The function of each subsystem is outlined as follows:

- 1) *The aircraft:* The type and performance of aircraft is principally determined by the needs of the operational mission. The task of the aircraft is primarily to carry the mission payload to its point of application, while it also has to carry the necessary subsystems for it to operate. The significant determinants in the design of an aircraft configuration are the operational range, airspeed, and demanded endurance. The endurance and range requirement will determine the fuel load to be carried. Achievement of a small fuel load and maximized performance will require an efficient propulsion system and optimum airframe aerodynamics. The airspeed requirement will determine whether a lighter-than-air aircraft or a heavier-than-air fixed-wing or rotary-wing aircraft to be employed.
- 2) *Propulsion system:* Propulsion system is a critical and indispensable subsystem of the UAV system structure. Propulsion system provides the necessary thrust to maintain the flight of a UAV. The UAV performance, effectiveness, and utility depend strongly on the capabilities of



Figure 1.3: The fundamental architecture of a typical UAV system.

onboard propulsion system. Together with other UAV design considerations, the propulsion system determines the endurance, size, and weight of the UAV.

- 3) *Guidance, navigation, and control (GNC) system*: It is necessary for an aircraft to know where it is at any time during the flight. For fully autonomous operation, sufficient navigation equipment must be carried in the aircraft, such as global positioning system (GPS) and inertial measurement unit (IMU). All UAVs share the same need for onboard sensors to provide an estimate of the aircraft's full state vector. In addition to state estimation, UAVs need guidance and control systems that allow them to accomplish the assigned mission. In simple terms, the guidance system provides instructions on which state trajectory the UAV should follow in order to accomplish its mission, while the control system operates the actuators to make the aircraft follow the trajectory generated by the guidance system.

- 4) *Communication system*: The principal and probably the most demanding requirement for the communication system is to provide the data links (up and down) between the ground station

and the aircraft. Besides this requirement, the onboard wired/wireless communication with a variety of sensors, actuators, and other subsystems is also included in the communication system.

- 5) *The payload:* The type and performance of the payloads are driven by the needs of the operational mission. They can range from a relatively simple unstabilized video camera with a fixed lens having a mass as little as 200 g to a high-power radar with a mass of possibly up to 1000 kg . Some more sophisticated UAVs carry a combination of different types of sensors within a payload module or a series of modules. The data from these sensors can be processed and integrated to provide enhanced information, or information that cannot be obtained by using a single type of sensor.
- 6) *Ground station:* Ground station is the control center of the operation and the man-machine interface, which can be located in a fixed facility or a mobile vehicle. Usually, the UAV mission is pre-planned in the ground station and assigned to the UAV for its execution through the wireless communication system. Similarly, via the communication down-link, the aircraft returns its status information and captured data from the payloads to the operators.

1.2 Fault-Tolerant Control

As modern technological systems become complex, their corresponding control systems are designed more and more sophisticated, including the urgent need to increase reliability of the systems. This stimulates the study of reconfigurable control systems. Most research works in reconfigurable control systems focus on fault detection and diagnosis (FDD) that can serve as a monitoring system by detecting, localizing, and identifying faults in a system. FDD is a very important procedure but it is not sufficient to ensure safe operation of the system. For some safety-critical systems such as aircraft and spacecraft, the continuation of operation is a key feature and the closed-loop system should be capable of maintaining its pre-specified performance in terms of quality, safety, and stability despite the presence of faults. This calls for the appearance of

fault-tolerant control system (FTCS). More precisely, FTCS is a control system that can accommodate system component faults and is able to maintain system stability and performance in both fault-free and faulty conditions [24]. Generally speaking, FTCS can be classified into two types known as passive fault-tolerant control system (PFTCS) and active fault-tolerant control system (AFTCS) [11]. A PFTCS is designed to be robust against a class of presumed faults without requiring on-line detection of faults [25, 26], while an AFTCS is based on controller reconfiguration or selection of pre-designed controllers with the help of a FDD unit [27, 28]. A comparative study between AFTCS and PFTCS is presented by Jiang and Yu in [29]. From performance perspective, a PFTCS focuses more on the robustness of the control system to accommodate multiple system faults without striving for optimal performance for any specific faulty conditions. Since stability is the prior consideration in a passive approach, the designed controller turns to be more conservative from the performance point of view. An AFTCS typically consists of a FDD unit, a reconfigurable controller, and a controller reconfiguration mechanism. These three units have to work in harmony to complete successful control tasks, and an optimal solution with certain preset performance criteria can be found. However, there are other issues which can impair an AFTCS to achieve its mission. Usually, system component faults can render the system unstable, and therefore there is only a limited amount of time available for an AFTCS to react to the faults and to make corrective control actions [11].

1.2.1 Actuator Faults and Failures

Generally speaking, a fault is an unpermitted deviation of at least one characteristic property of the system from the acceptable, usual, and standard condition, whereas a failure is a permanent interruption of a system's ability to perform a required function under specified operating conditions [30]. Based on this definition, the impact of a fault can be a small reduction in efficiency, that may degrade the overall functioning of the system. Resulting from one or more faults, a failure is therefore an event that terminates the functioning of a unit in the system. Faults can take place in different parts of the controlled system. According to their occurrence location, faults can be

classified into actuator faults, sensor faults, and other system component faults [11, 31]. Since actuators play an important role of connecting control signals to physical movements of the system to accomplish specific objectives, there will be an emphasis on actuator faults and failures in this thesis. Indeed, a sensor fault/failure does not directly affect the flight performance of the aircraft. The sensor fault/failure can be handled either by using a redundant sensor if available, or by reconstructing the missing measurement data with the knowledge of the system and the measurement data furnished by the remaining sensors [32]. However, as soon as there is an actuator fault/failure, the aircraft flight performance will be inevitably degraded, and immediate action must be taken to preserve its original performance. Partial loss of control effectiveness of an actuator is a common fault occurring in aircraft systems which can result from hydraulic or pneumatic leakage, increased resistance or a fall in the supply voltage. Moreover, duplicating the actuators in the system in order to achieve increased fault-tolerance is often not an option due to their high price and large size and mass compared to sensors in the system.

Furthermore, actuator faults can also be classified according to their time characteristics as abrupt, incipient, and intermittent faults. Abrupt faults, as shown in Fig. 1.4(a), occur instantaneously often as a result of hardware damages. These faults are very severe since they can significantly affect the performance and stability of the controlled system. Incipient faults, as shown in Fig. 1.4(b), represent slow parametric changes often as a result of hardware aging. These faults are more difficult to be detected due to their slow time characteristics. Intermittent faults, as shown in Fig. 1.4(c), appear and disappear repeatedly in the system, for instance due to partially damaged wiring. Since intermittent faults are not common faults in aircraft systems, abrupt and incipient faults are mainly considered in this thesis.

1.2.2 Sliding Mode Control

Sliding mode control (SMC) theory was introduced for the first time in the context of the variable structure system (VSS) [33]. It was developed for the control of electric drives by Utkin [34]. During the last three decades, it has shown to be a very effective approach in robust control area.

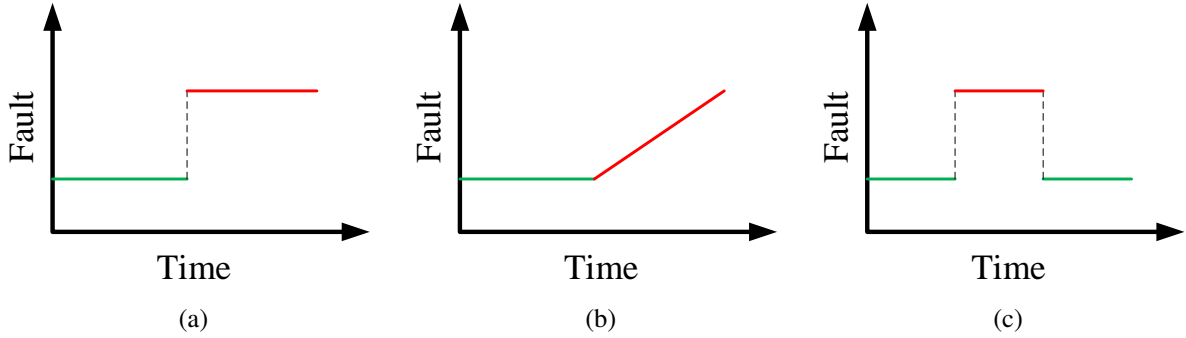


Figure 1.4: Actuator fault classification with respect to time.

Various books on SMC have also been published recently by Utkin *et. al.* [35], Edwards and Spurgeon [36], and Fridman *et. al.* [37]. Studies by Alwi and Edwards [38] and Wang *et. al.* [39] show some of the most recent researches in FTC area using SMC technique. SMC is an approach to design robust control systems handling large uncertainties with discontinuous control strategy, which demonstrates invariance to so-called matched uncertainties while on a reduced order sliding surface [40, 41]. To be more precise, SMC utilizes a high-speed switching control law to achieve two objectives. Firstly, it drives the nonlinear system's state trajectory onto a specified surface in the state space which is called sliding surface. Secondly, it maintains the system's state trajectory on this surface for all subsequent times. During this process, the structure of the control system varies from one to another and thereby it is called as SMC to emphasize the importance of the sliding mode [36]. Intuitively, SMC uses practically infinite gain to force the trajectory of a dynamic system to slide along the restricted sliding mode subspace, which leads to significant control performance. The main advantage of SMC over the other nonlinear control approaches is its robustness to external disturbances, model uncertainties, and system parametric variations. One design parameter is synthesized in the discontinuous control part and the control can be as simple as a switching between two states, therefore it does not need to be precise and will not be sensitive to parameter variations that enter into the control channel [42]. The property of insensitivity to parametric uncertainties and external disturbances makes SMC as one of the most promising control approaches. The robust characteristics of SMC provides a natural environment

for the use of such a technique on designing PFTCS [16, 38, 43–45]. There are two stages involved in the design of SMC. The first step features the construction of a sliding surface, on which the system performance can be maintained as expected. The second step is concerned with the selection of appropriate control law to force the sliding variable reach the designed sliding surface, and thereafter keep the sliding motion within the close neighborhood of the designed sliding surface. In [46], SMC approach is intended to serve as an alternative to truly reconfigurable systems for maintaining the desired performance without requiring any fault information. However, this kind of traditional robust control algorithm makes trade-off between system performance and robustness in order to accommodate certain faults and parametric uncertainties. Moreover, in order to effectively implement the conventional SMC, the bound of uncertainty is always required at the design stage. In fact, at most time, real systems work under fault-free conditions, and faults and parametric variations can occur at any time with unknown magnitudes, thus it is difficult to obtain the exact uncertainty bounds in advance. The consideration of faults at the system design stage will largely degrade system performance under fault-free conditions. Moreover, if an excessive amount of faults are prescribed, the big trade-off may lead the system performance unacceptable under fault-free conditions, which will significantly limit the fault-tolerance capability of the system. This stimulates a new control strategy that incorporates adaptive control scheme into SMC to accommodate actuator faults and parametric uncertainties without knowing the exact uncertainty bounds and affecting system performance in fault-free conditions [39, 47, 48]. In [39], with the proposed adaptive SMC, it shows a good tracking performance when actuator fault occurs in the system. Nevertheless, as fault becomes larger, a big tracking error occurs, and the system performance cannot be maintained anymore. This is because the considered actuator fault is related to the uncertainty in the control effectiveness matrix, then after fault occurrence, the post-fault control effectiveness matrix needs to be changed correspondingly. The existing adaptive SMC strategies in the literature mainly incorporate adaptation parameter into the discontinuous control part which only use the discontinuous robust property of SMC for accommodating actuator faults. The overuse of the discontinuous control strategy will stimulate significant control chattering. In

fact, since the control effectiveness matrix is also used to derive the equivalent continuous control part, if one can incorporate the adaptation parameter in the continuous control part as well, it will reduce the use of discontinuous strategy. In this case, control chattering will also be avoided and larger faults can be tolerated.

1.2.3 Control Allocation

Complete actuator failures in an aircraft could significantly reduce reliability and even cause catastrophic accidents. Despite the analytical redundancy, the hardware redundancy is also very important for a safety-critical system, such as passenger aircraft [49] and modern combat aircraft [50]. Over-actuation gives freedom for designing FTCS to maintain system stability and acceptable performance in the presence of actuator faults/failures which can also achieve fast system response in fault-free conditions. Since such a system has infinite number of solutions, the problem is to find at least one that satisfies control input constraints and some additional optimization criterion. The problem of control allocation is to assign each available control effector an appropriate amount of deflection to generate the commanded forces and moments [51]. The design of control algorithms for over-actuated mechanical systems is often divided into several levels. Firstly, a high-level motion control algorithm is designed to compute a vector of virtual control inputs to the mechanical system. The virtual control inputs are usually chosen as a number of forces and moments that equals the number of degrees of freedom which the motion control system wants to control, and such that the basic requirement of controllability can be met. Secondly, a low-level control allocation algorithm is designed in order to map the vector of commanded virtual control inputs into individual effector control inputs. This design is usually based on a static effector model. The general modular structure of the control algorithm is illustrated in Fig. 1.5. The modular design of the control algorithm by employing control allocation approach allows the design of high-level motion control algorithm to be independent of actuator configuration by introducing virtual control module and control allocation module, respectively. In addition to the allocation of virtual control signals to the individual effectors, important issues such as input saturation, rate

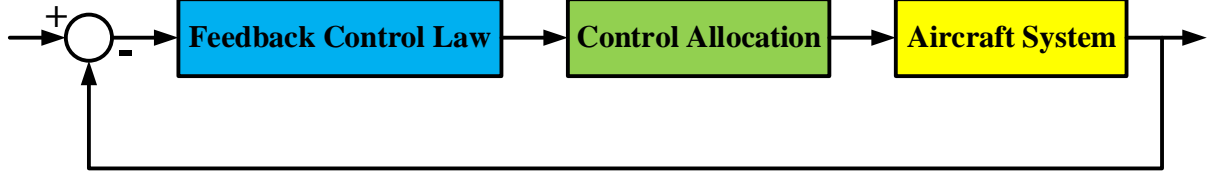


Figure 1.5: General modular structure of control allocation.

constraints, and actuator fault-tolerance are typically handled within the control allocation module.

The control allocation problem has been intensively studied following the work of Durham [52]. Different methods and approaches on control allocation are investigated in the literature [53–57]. The simplest control allocation methods are based on the unconstrained least-squares algorithm and modifications of the solution aimed at accounting for position and rate limits [58, 59]. More complex methods formulate control allocation as a constrained optimization problem [60, 61]. Because of the limited number of variables and the convexity of the constraint set, the optimization problems are simple from a modern computational perspective [62]. The redistributed pseudo-inverse is a very simple and effective approach to achieve control allocation [63]. However, it cannot guarantee full utilization of the actuators. The quadratic programming method seems to be favorable since the solution tends to combine the use of all control surfaces rather than just a few [64]. The fixed-point method can also provide an exact solution to the optimization problem, and it is guaranteed to converge [65]. Its drawback is that the convergence of the algorithm can be very slow and strongly depends on the problem [62]. Most of these methods assume that all the control surfaces are present, and the mechanical systems work under the normal operation. Due to its over-actuated feature, the control allocation approach has an inherent capability to tolerate certain level of actuator fault or even failure. In the presence of actuator fault, an effective re-allocation of the virtual control signals to the remaining healthy actuators is needed to maintain system stability and tracking performance, which is referred to as reconfigurable control allocation [66]. In the context of reconfigurable control, Zhang *et. al.* [66, 67] present the concept of control allocation and re-allocation for aircraft with redundant control effectors. For the sake of the closed-loop system

stability, a high-level motion controller is needed to provide the desired virtual control signals for the low-level control allocation module. Since the publication of the early works [66, 67] on the combination of a baseline control law with a reconfigurable control allocation scheme for achieving FTC, other baseline control laws combined with control allocation schemes have been developed in recent years [38, 68, 69]. In [38, 68], a sliding mode-based reconfigurable control allocation scheme is proposed to improve the system performance with single actuator fault for a fixed-wing aircraft benchmark model as used in [66] and [67], which presents a good example for making full use of the advantages of both high-level motion controller and low-level control allocation. However, most of the reconfigurable control allocation schemes in the literature only focus on the allocation of the virtual control signals over the available actuators and rarely concern about the stability of the closed-loop system in the context of FTC. If the control allocation module fails to meet the demanded virtual control signals from the high-level motion controller, the tracking performance of the closed-loop system will be degraded or even the stability of the closed-loop system cannot be maintained anymore.

1.3 Fault Detection and Diagnosis

The control allocation algorithm assumes that it has access to various parameters that define the moment generation capability of the control effectors, such as control effector position limits and control effectiveness. This information can be provided by look-up tables if the aircraft is assumed to be fault-free. However, if it is assumed that an actuator fault or failure is possible in an aircraft system, then the aforementioned parameters need to be updated in real time. Therefore, there has been research into approaches to estimate these parameters online [70, 71]. This adds fault diagnosis capabilities to the reconfigurable control system, creating a fault detection, isolation, identification, and reconfigurable control system, or more generally an AFTCS.

FDD is used to detect faults and diagnose their location and magnitude in a system. It has the

following tasks: fault detection, fault isolation, and fault identification [72]. Fault detection indicates that something is wrong in the system, for example, the occurrence of a fault and the time of the fault occurrence. Fault isolation determines the location and the type of a fault. Fault identification determines the magnitude of a fault. FDD addresses the challenge of real-time monitoring the occurrence of fault in a system. Due to real-time requirements and the dynamic nature of the mechanical system, there is usually only a very limited amount of time available to carry out the post-fault model construction and control reconfiguration actions.

Fault diagnosis algorithms are generally classified into two types known as model-based and data-driven methods. Model-based approaches are mostly based on analytical redundancy and require an analytical mathematical model of the system. The presence of faults is detected by means of the so-called residuals, which can be generated in different ways: parity equations, state estimation-based methods, and parameter estimation-based methods. The performance of model-based approaches depends strongly on the usefulness of the constructed model [73]. The constructed model must include all situations of the system under study. It must be able to handle changes at the operating point. If the constructed model fails, the whole diagnostic system will also fail. However, in practice, it is usually quite challenging and difficult to meet all the requirements of model-based approaches due to the inevitable unmodeled dynamics, uncertainties, model mismatches, noises, disturbances, and inherent nonlinearities [74]. The sensitivity to modeling errors has become the key problem in the application of model-based approaches. In contrast, data-driven diagnosis approaches, such as neural network-based intelligent methods, mostly rely on historical and current data from the sensors, and do not require a detailed mathematical model of the system but need representative training data. The idea is that the operation of the system is classified according to measurement data. Formally, this is a mapping from measurement space into decision space [73]. Therefore, data play a very important role in this kind of method. With application to UAVs, model-free neural network-based approaches are preferred due to the cost limitation and short period of development compared to conventional aircraft. The capabilities of neural networks for function approximation, classification, and their ability to deal with uncertainties and parameter

variations make them a viable choice for using in fault diagnosis problems [75].

The standard feed-forward neural networks or multilayer perceptron (MLP) are the best known members of the family of many types of neural networks. Feed-forward neural networks have been applied in tasks of FDD for many years [76–78]. Most recently, a new class of neural networks, namely dynamic neural networks, was introduced based on feed-forward neural networks to provide the static neural networks with dynamic properties, which means the behavior of the neural network depends not only on the current inputs (as in the feed-forward neural networks) but also on previous operations of the neural network. It can be grouped into two classes known as time-delay neural networks and recurrent neural networks (RNNs). Dynamic neural networks have been successfully used in many applications including the fault diagnosis of nonlinear dynamic systems. In [79], a dynamic neural network-based fault diagnosis scheme is proposed for gas turbine engines. The authors use a bank of dynamic neural networks to represent various operating modes of the healthy and faulty engine conditions. The fault diagnosis task is accomplished by using the residuals generated by measuring the difference between each network output and the measured engine output based on various criteria. In [80], a recurrent neural network (RNN) is proposed to carry out railway track circuit fault diagnosis based on the commonly available measurement signals. It can learn the dependences directly from the data and correctly classify 99.7% of the test input sequences without false positive fault detections.

In terms of fault diagnosis for aircraft, most of the studies in the literature are model-based [14, 81–83]. In fact, model uncertainties widely exist in practical engineering systems. Most of the model-based approaches do not take into consideration the model uncertainties. Moreover, the model-based fault diagnosis approaches are founded on the fact that a fault will cause changes in certain physical parameters which in turn will lead to changes in certain model parameters or states. However, in the case of closed-loop system, small changes in the system can be covered by control actions, therefore, the feedback control system in a UAV can hinder the early detection of system faults, which further challenges model-based approaches. With the rapid development of UAVs, it is hard to obtain accurate mathematical models in a short development period. Therefore, in order

to achieve fault detection, isolation, and identification in the presence of model uncertainties in a UAV system with consideration of feedback control system, a new and effective fault diagnosis scheme needs to be designed.

1.4 Active Disturbance Rejection

Disturbances widely exist in modern mechanical systems and bring adverse effects on the performance of the control systems. Moreover, UAVs are inevitably influenced by environmental disturbances when employed for practical applications, and the small-scale UAVs in particular are more sensitive to environmental disturbances due to their low inertia and small size. In this thesis, the disturbances refer to not only the disturbances from the external environment of a UAV but also disturbances from the controlled UAV including unmodeled dynamics which is difficult to handle. The existence of disturbance forces and torques caused by external winds and unmodeled dynamics will severely influence the flight control performance in the aeronautic and astronautic engineering community [84, 85]. The problem of disturbance rejection is an everlasting research topic since the appearance of control theory and applications [86].

Since the traditional control methods, such as proportional-integral-derivative (PID) and linear quadratic regulator (LQR) controller, do not explicitly take into account disturbance and uncertainty attenuation performance when the controllers are designed, they may be unable to achieve high-precision control performance in the presence of severe disturbances and uncertainties [87]. Therefore, the development of advanced control algorithms with strong disturbance rejection property has great importance to improve the control accuracy. With this consideration, many elegant advanced control approaches, such as adaptive control and robust control, have been proposed to handle the undesirable effects caused by unknown disturbances and uncertainties since 1950s [88–92]. However, these control approaches generally achieve the goal of disturbance rejection via feedback regulation based on tracking errors between the measured outputs and the reference signals rather than feedforward compensation control. Therefore, it is difficult for the

designed controllers to react directly and fast enough to strong disturbances, although they can finally suppress the disturbances through feedback regulation in a relatively slow way [93]. Due to this property, these control approaches are generally recognized as passive disturbance rejection control approaches.

In order to overcome the limitations of passive disturbance rejection control approaches in handling disturbances, researchers are motivated to investigate the so-called active disturbance rejection control approach. Generally speaking, the idea of active disturbance rejection control is to directly counteract disturbances through feedforward compensation control design based on disturbance measurements or estimations. Feedforward control is one of the most direct and active disturbance rejection control methods [86]. However, in most of the practical applications, the disturbances are unmeasurable or measurable but the sensors are excessively expensive, which limits the applications of feedforward control. In order to take advantages of the feedforward control in disturbance rejection and also overcome its disadvantages as mentioned before, the exploration of disturbance estimation techniques has attracted a lot of interest.

Since 1970s, many effective disturbance estimation techniques have been developed, such as unknown input observer [94], perturbation observer [95], equivalent input disturbance-based estimator [96], extended state observer [97], and disturbance observer [98, 99]. Among these different disturbance estimation approaches, the extended state observer and disturbance observer are most extensively investigated in terms of theory and applications. The extended state observer is generally regarded as a fundamental part of the so-called active disturbance rejection control, which is often employed to estimate the lumped disturbances consisting of unknown uncertainties and external disturbances. The disturbance observer was firstly proposed by Ohishi *et. al.* in the late 1980s [100]. The analysis and design method for disturbance observer has achieved significant progress during the past three decades.

Besides the disturbance estimation techniques, the composite control design and analysis based on disturbance observer is another important but challenging topic. Since disturbance observer is

one of the most effective and popular disturbance estimation techniques, the corresponding disturbance observer-based control (DOBC) has received a great deal of attention in both control theory and control engineering fields [101–105]. However, it should be pointed out that DOBC is still a model-based control approach, and it is difficult for a designed DOBC to achieve good control performance in the presence of severe model uncertainties. Due to this limitation, the introduction of advanced feedback control to DOBC becomes another research focus, which formulates the so-called composite hierarchical disturbance rejection control. The basic idea of composite hierarchical disturbance rejection control can be summarized as follows: the disturbances are feedforward compensated by DOBC while the model uncertainties are attenuated by advanced feedback control.

Most of the existing DOBC approaches are generally confined to uncertain systems with lumped disturbances. In this context, lumped disturbances refer to both the external disturbances and internal model uncertainties. However, multiple different types of disturbances widely exist in practical mechanical systems, and treating multiple disturbances as a single equivalent disturbance may result in conservativeness in disturbance rejection in the presence of multiple disturbances [101, 104, 106, 107]. Therefore, in order to make the designed controller more practical for real engineering applications, the multiple disturbances need to be considered and compensated separately by combining disturbance observer and adaptive control.

1.5 Objectives of The Dissertation

The main goal of the dissertation is to design and develop novel control schemes with application to UAVs to improve safety and reliability of such safety-critical systems. This dissertation in particular is organized around the following objectives:

- 1) Design and develop an adaptive SMC strategy for accommodating actuator faults which can show an advantage of tolerating larger actuator faults without stimulating control chattering. Then, based on this developed adaptive strategy, a fuzzy logic-based boundary layer is

designed to make a trade-off between tracking accuracy and system stability, which means much larger actuator faults can be compensated with acceptable tracking accuracy within this control scheme.

- 2) Develop an adaptive sliding mode-based control allocation scheme which has the capability to tolerate complete actuator failures and multiple actuator faults. The stability of the overall closed-loop system is theoretically proven.
- 3) Design and develop a model-based disturbance observer which can effectively estimate environmental disturbances from wind and unstructured model disturbances. The designed disturbance observer is expected to be incorporated with SMC to alleviate control chattering effect of SMC.
- 4) Develop an effective adaptive scheme to estimate model uncertainties, and then combine it with the former designed FTC scheme and disturbance observer to construct a complete reliable control scheme for UAVs.
- 5) Design and develop a RNN-based fault estimation scheme which can not only set up a cost-effective monitoring framework, but also can be used for integration with FTC strategies in active fault-tolerant architectures.

In summary, the conducted research works in this dissertation are expected to consider all the uncertain factors to design and develop advanced control schemes for UAVs to significantly improve their reliability and survivability and also to satisfy strict safety and reliability demands by US Federal Aviation Administration (FAA) or other country's licensing & certificating authorities to further broad the commercial uses of developed UAVs. The developed control schemes and strategies from this research dissertation will be verified by both simulation and experiment on an unmanned multirotor helicopter in the presence of actuator faults, model uncertainties, environmental disturbances, and different realistic fault scenarios.

1.6 Contributions of The Dissertation

Although tremendous efforts have been dedicated to the control of UAVs, there still exist significant challenges to improve the performance of the onboard controllers to further ensure the safety and reliability of UAVs. Many technical issues must be solved to increase the level of automation required for more sophisticated and hazardous applications. The main contributions of this dissertation can be summarized as follows:

- 1) An adaptive SMC is developed for a linear quadrotor helicopter with consideration of actuator faults. The developed control scheme can adaptively generate appropriate control inputs without the prior knowledge on uncertainty bound. It can effectively maintain system tracking performance in both fault-free and faulty conditions compared to a conventional uncertainty bound-based SMC.
- 2) An adaptive fuzzy FTC strategy is proposed for a nonlinear quadrotor helicopter against parametric uncertainties, actuator faults, and environmental disturbances based on an integral SMC, a fuzzy boundary layer, and a nonlinear disturbance observer. The proposed control strategy can adaptively generate appropriate control signals to compensate parametric uncertainties and actuator faults simultaneously without merely relying on the robust discontinuous control strategy. Since the proposed adaptive scheme is synthesized in both continuous and discontinuous control portions, the control effort is significantly reduced for accommodating the parametric uncertainties and actuator faults. Thus, larger uncertainties and actuator faults can be tolerated within this control scheme. Moreover, the fuzzy logic-based boundary layer can also help to maintain system stability and prevent overestimation of the adaptive control parameters. The designed nonlinear disturbance observer can accurately estimate the imposed disturbances, which will help to maintain system tracking performance while keeping the same discontinuous control gain and suppressing the control chattering effect.
- 3) An active FTC strategy is proposed for a quadrotor helicopter against actuator faults and

model uncertainties based on adaptive SMC and RNNs. Due to the fact that model-based fault estimation schemes may fail to correctly estimate faults in the presence of model uncertainties, a fault estimation scheme is proposed by designing a parallel bank of RNNs. With the trained RNNs, the severity of actuator faults can be precisely and reliably estimated. Finally, by synthesizing the proposed fault estimation scheme with the designed adaptive SMC, an active FTC mechanism is established. Moreover, the issue of actuator fault estimation error is explicitly considered and compensated by the proposed adaptive schemes.

- 4) A FTC scheme by combining adaptive SMC with control allocation is proposed, which can accommodate both single and simultaneous actuator faults and maintain the stability of the closed-loop system. In the presence of actuator faults, not only the control allocation/reallocation scheme needs to be triggered to redistribute more control signals to the less affected actuators, but also the synthesized adaptive scheme will be employed to adjust the control gains for the high-level SMC control module to compensate the virtual control error generated by the low-level control allocation/reallocation module. The stability of the entire control system is considered and proven theoretically.
- 5) The proposed and designed fault diagnosis and FTC schemes are validated and evaluated through numerical simulations and experimental tests and more practical for real applications.

1.7 Organization of The Dissertation

The rest of the dissertation is organized as follows:

- Chapter 2 mainly introduces the dynamic modeling of an unmanned multirotor helicopter. Moreover, some preliminary knowledges, such as actuator fault and environmental disturbance formulation are also presented in this chapter.
- Chapter 3 addresses the problem of FTC for linear systems. In this chapter, two types of

SMC schemes are designed. Due to the need of uncertainty bound during the design stage, the conventional robust SMC cannot handle large actuator faults with consideration of tracking performances in both fault-free and faulty conditions. On the contrary, the proposed adaptive SMC is able to automatically provide robustness and maintain good tracking performance for an unmanned quadrotor helicopter in the presence of actuator faults with even large fault magnitudes.

- Chapter 4 presents an adaptive control strategy for a nonlinear quadrotor helicopter against parametric uncertainties, actuator faults, and environmental disturbances based on an integral SMC, a fuzzy boundary layer, and a nonlinear disturbance observer. Within the proposed control scheme, both uncertain model parameters and actuator faults can be compensated without the knowledge of the uncertainty bounds and fault information. The designed nonlinear disturbance observer can accurately estimate the imposed disturbances, which will help to maintain system tracking performance while keeping the same discontinuous control gain.
- Chapter 5 proposes an active FTC strategy for a quadrotor helicopter with model uncertainties. The proposed fault estimation scheme is designed with a parallel bank of RNNs that are free from influences of model uncertainties. The corresponding weighting parameters are updated by using a back-propagation-through-time-based extended Kalman filter, which significantly improves the reliability and accuracy of severity estimation. The synthesized adaptive SMC can compensate both model uncertainties and fault estimation error to guarantee the desired tracking performance.
- Chapter 6 illustrates an adaptive sliding mode-based control allocation scheme to accommodate simultaneous actuator faults for a modified octorotor helicopter. By virtue of the modular design of the proposed control scheme, both single and simultaneous actuator faults can be effectively accommodated. Moreover, the stability of the closed-loop system is guaranteed theoretically in the presence of simultaneous actuator faults.

- Chapter 7 presents the conclusions of the conducted research works and important findings, and summarizes several predominant ideas for the future development of the dissertation's outcomes.

Chapter 2

Aircraft Model

This research work focuses on the study of multirotor helicopters. As an example of multirotor helicopters, a quadrotor helicopter is a relatively simple and easy-to-fly system [108]. Indeed, the quadrotor helicopter, as shown in Fig.2.1, is a small-scale UAV with four propellers placed around a main body. The main body includes power source, sensors, and control hardware. The vehicle is controlled by the four propellers and their rotational speeds are independent which makes it possible to control the roll, pitch, and yaw angle of the vehicle. And, its displacement is produced by the total thrust of the four propellers.

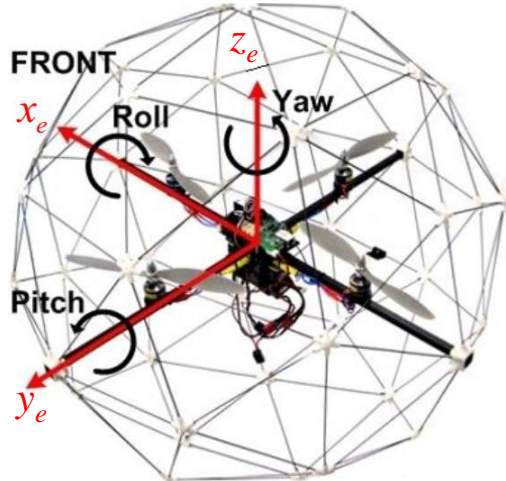


Figure 2.1: Illustration of the studied quadrotor helicopter.

2.1 Modeling of a Quadrotor Helicopter

In this section, the mathematical model of a quadrotor helicopter is presented. The considered quadrotor helicopter is mounted with four motors in a cross configuration, as shown in Figs. 2.1 and 2.2. All the propellers' axes of rotation are fixed and parallel. Moreover, they have fixed-pitch propellers and their air flows point downwards. These considerations reveal that the structure of the quadrotor helicopter is quite rigid and the only thing that can vary is the speed of the propeller. Each pair of the opposite propellers turns the same way. The front and rear propellers rotate clockwise, while the left and right ones spin counter-clockwise. In this configuration, each two opposite propellers contribute to the motion along x_e - and y_e -axis, respectively.

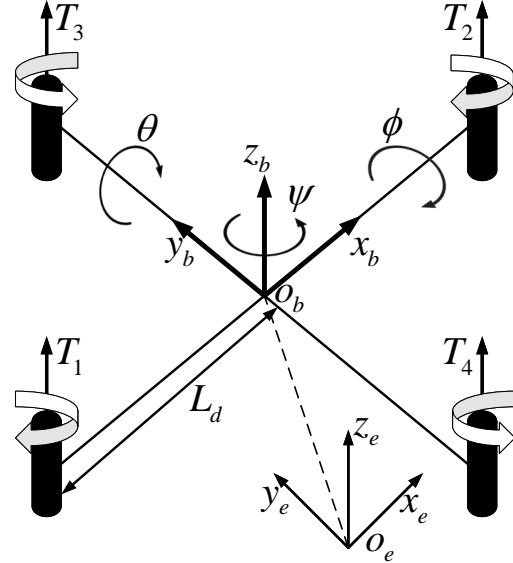


Figure 2.2: Configuration of the quadrotor helicopter.

2.1.1 Kinematic Equations

In order to model the quadrotor helicopter, we first discuss the coordinate systems used in this section. Two coordinate systems are employed: the local navigation frame and the body-fixed frame. The axes of the body-fixed frame are denoted as (o_b, x_b, y_b, z_b) , and the axes of the local navigation frame are denoted as (o_e, x_e, y_e, z_e) . The position $X^I = [x_e, y_e, z_e]^T$ and attitude

$\Theta^I = [\phi, \theta, \psi]^T$ of the quadrotor helicopter are defined in the local navigation frame which is regarded as the inertial reference frame. The translational velocity $V^B = [u, v, w]^T$ and rotational velocity $\omega^B = [p, q, r]^T$ are defined in the body-fixed frame.

To derive the equations of motion, the Newton-Euler formulation is employed in this work. However, Newton's equations of motion are usually derived relative to a fixed inertial reference frame, whereas the motion of object is most easily described in a body-fixed frame and onboard sensors collect data with respect to the body-fixed frame. Therefore, a transformation matrix from the body-fixed frame to the inertial reference frame is required to help model the quadrotor helicopter. In this work, the transformation matrix is obtained by premultiplying the three basic rotation matrices in the order of roll-pitch-yaw as follows:

$$\begin{aligned}
R_B^I &= R(\psi, z)R(\theta, y)R(\phi, x) \\
&= \begin{bmatrix} \cos \psi & -\sin \psi & 0 \\ \sin \psi & \cos \psi & 0 \\ 0 & 0 & 1 \end{bmatrix} \begin{bmatrix} \cos \theta & 0 & \sin \theta \\ 0 & 1 & 0 \\ -\sin \theta & 0 & \cos \theta \end{bmatrix} \begin{bmatrix} 1 & 0 & 0 \\ 0 & \cos \phi & -\sin \phi \\ 0 & \sin \phi & \cos \phi \end{bmatrix} \\
&= \begin{bmatrix} \cos \theta \cos \psi & \sin \phi \sin \theta \cos \psi - \cos \phi \sin \psi & \cos \phi \sin \theta \cos \psi + \sin \phi \sin \psi \\ \cos \theta \sin \psi & \sin \psi \sin \theta \sin \psi + \cos \phi \cos \psi & \cos \phi \sin \theta \sin \psi - \sin \phi \cos \psi \\ -\sin \theta & \sin \phi \cos \theta & \cos \phi \cos \theta \end{bmatrix}. \tag{2-1}
\end{aligned}$$

Then, another transformation matrix T_B^I can be determined by resolving the Euler angle rates into rotational velocities defined in the body-fixed frame as follows:

$$\begin{bmatrix} p \\ q \\ r \end{bmatrix} = \begin{bmatrix} \dot{\phi} \\ 0 \\ 0 \end{bmatrix} + R(\phi, x) \begin{bmatrix} 0 \\ \dot{\theta} \\ 0 \end{bmatrix} + R(\phi, x)R(\theta, y) \begin{bmatrix} 0 \\ 0 \\ \dot{\psi} \end{bmatrix} = (T_B^I)^{-1} \begin{bmatrix} \dot{\phi} \\ \dot{\theta} \\ \dot{\psi} \end{bmatrix} \tag{2-2}$$

$$T_B^I = \begin{bmatrix} 1 & \sin \phi \tan \theta & \cos \phi \tan \theta \\ 0 & \cos \phi & -\sin \phi \\ 0 & \sin \phi \sec \theta & \cos \phi \sec \theta \end{bmatrix}. \quad (2-3)$$

According to the above-mentioned transformation matrices, it is possible to describe the kinematic equations in the following matrix manner:

$$\dot{\xi}^I = \begin{bmatrix} \dot{X}^I \\ \dot{\Theta}^I \end{bmatrix} = \begin{bmatrix} R_B^I & 0_{3 \times 3} \\ 0_{3 \times 3} & T_B^I \end{bmatrix} \begin{bmatrix} V^B \\ \omega^B \end{bmatrix} = J_B^I \nu^B. \quad (2-4)$$

2.1.2 Dynamic Equations

In order to derive the dynamic equations of the quadrotor helicopter, two assumptions need to be addressed firstly [109]:

- 1) The origin of the body-fixed frame coincides with the center of mass (COM) of the quadrotor helicopter.
- 2) The axes of the body-fixed frame are coincident with the principal axes of inertia of the quadrotor helicopter.

With the above-mentioned assumptions, the inertial matrix becomes diagonal, and there is no need to take another point, COM, into account for deriving the dynamic equations.

By employing the Newton-Euler formulation, the forces and moments equations can be expressed as follows [108]:

$$\begin{bmatrix} F^I \\ \tau^B \end{bmatrix} = \begin{bmatrix} m & 0_{3 \times 3} \\ 0_{3 \times 3} & I \end{bmatrix} \begin{bmatrix} \ddot{X}^I \\ \dot{\omega}^B \end{bmatrix} + \begin{bmatrix} 0 \\ \omega^B \times I \omega^B \end{bmatrix} \quad (2-5)$$

where $F^I = [F_x, F_y, F_z]^T$ and $\tau^B = [\tau_x, \tau_y, \tau_z]^T$ are the force and moment vectors with respect to the inertial reference frame and the body-fixed frame, respectively. m is the total mass of the

quadrotor helicopter, and I is the diagonal inertial matrix defined as:

$$I = \begin{bmatrix} I_{xx} & 0 & 0 \\ 0 & I_{yy} & 0 \\ 0 & 0 & I_{zz} \end{bmatrix}. \quad (2-6)$$

The forces on the quadrotor helicopter are composed of three parts: gravitation (G), thrust (T), and the translational motion induced drag force (D), given by:

$$\begin{aligned} F^I &= G + R_B^I T + D \\ &= \begin{bmatrix} 0 \\ 0 \\ -mg \end{bmatrix} + R_B^I \begin{bmatrix} 0 \\ 0 \\ U_z \end{bmatrix} + \begin{bmatrix} -K_1 \dot{x}_e \\ -K_2 \dot{y}_e \\ -K_3 \dot{z}_e \end{bmatrix} \end{aligned} \quad (2-7)$$

where K_1 , K_2 , and K_3 are the drag coefficients, g is the acceleration of gravity, and U_z is the total thrust from the four propellers.

By substituting (2-7) into (2-5), we can obtain:

$$\begin{bmatrix} \ddot{x}_e \\ \ddot{y}_e \\ \ddot{z}_e \end{bmatrix} = \begin{bmatrix} 0 \\ 0 \\ -g \end{bmatrix} + \frac{1}{m} \begin{bmatrix} (\cos \phi \sin \theta \cos \psi + \sin \phi \sin \psi) U_z \\ (\cos \phi \sin \theta \sin \psi - \sin \phi \cos \psi) U_z \\ (\cos \phi \cos \theta) U_z \end{bmatrix} + \frac{1}{m} \begin{bmatrix} -K_1 \dot{x}_e \\ -K_2 \dot{y}_e \\ -K_3 \dot{z}_e \end{bmatrix}. \quad (2-8)$$

Similarly, the moments on the quadrotor helicopter are composed of gyroscopic torque (M_g),

the torque generated by the propellers (M_T), and the rotational motion induced torque (M_f), described as:

$$\begin{aligned}\tau^B &= M_g + M_T + M_f \\ &= - \sum_{i=1}^4 I_r \left(\omega^B \times \begin{bmatrix} 0 \\ 0 \\ 1 \end{bmatrix} \right) (-1)^{i+1} \Omega_i + \begin{bmatrix} U_\phi \\ U_\theta \\ U_\psi \end{bmatrix} + \begin{bmatrix} -K_4 L_d \dot{\phi} \\ -K_5 L_d \dot{\theta} \\ -K_6 \dot{\psi} \end{bmatrix} \quad (2-9)\end{aligned}$$

where I_r is the inertial moment of the propeller and Ω_i is the i th propeller's rotational speed. K_4 , K_5 , and K_6 are the drag coefficients, L_d is the distance between each motor and the COM of the quadrotor helicopter, and U_ϕ , U_θ , and U_ψ are the generated torques with respect to the body-fixed frame.

Then, by substituting (2-9) into (2-5), the following equation can be obtained:

$$\begin{bmatrix} \dot{p} \\ \dot{q} \\ \dot{r} \end{bmatrix} = I^{-1} \left(- \begin{bmatrix} 0 & I_{zz}r & -I_{yy}q \\ -I_{zz}r & 0 & I_{xx}p \\ I_{yy}q & -I_{xx}p & 0 \end{bmatrix} \begin{bmatrix} p \\ q \\ r \end{bmatrix} + I_r \begin{bmatrix} -q \\ p \\ 0 \end{bmatrix} \Omega \right. \\ \left. + \begin{bmatrix} U_\phi \\ U_\theta \\ U_\psi \end{bmatrix} + \begin{bmatrix} -K_4 L_d \dot{\phi} \\ -K_5 L_d \dot{\theta} \\ -K_6 \dot{\psi} \end{bmatrix} \right) \quad (2-10)$$

where $\Omega = \Omega_1 + \Omega_2 - \Omega_3 - \Omega_4$ is the residual of the overall propellers' speed.

2.1.3 Control Mixing

Due to the configuration of the quadrotor helicopter, the attitude (ϕ, θ) is coupled with the position (x_e, y_e), and a pitch or roll angle is required in order to move the quadrotor helicopter along x_e - or y_e -direction. The virtual control inputs ($U_z, U_\phi, U_\theta, U_\psi$) as shown in (2-8) and (2-10) for moving and stabilizing the quadrotor helicopter are mapped from the thrusts generated by the

four independent motors. The relationship between the generated thrust T_i and the i th motor's input is given as:

$$T_i = K_u \frac{\omega}{s + \omega} u_i \quad (2-11)$$

where K_u is a positive gain related to propeller generated thrust, ω is the actuator bandwidth, and u_i is the pulse-width modulation (PWM) input of the i th motor. In order to make it easy to model the actuator dynamics, a new variable u_i^* is defined to represent the dynamics of the i th motor as:

$$u_i^* = \frac{\omega}{s + \omega} u_i \quad (2-12)$$

Then, the corresponding torque τ_i generated by the i th propeller can be modeled as:

$$\tau_i = K_y u_i^* \quad (2-13)$$

where K_y is a positive gain related to propeller generated torque.

According to the configuration of the quadrotor helicopter as shown in Fig. 2.2, the total thrust U_z along z_b -direction is given by the sum of the thrusts from the four motors as:

$$U_z = T_1 + T_2 + T_3 + T_4. \quad (2-14)$$

The positive roll moment is generated by increasing the thrust in the left motor (T_3) and decreasing the thrust in the right motor (T_4) simultaneously as:

$$U_\phi = L_d(T_3 - T_4). \quad (2-15)$$

Similarly, the positive pitch moment is generated by increasing the thrust in the rear motor (T_1) and decreasing the thrust in the front motor (T_2) simultaneously as:

$$U_\theta = L_d(T_1 - T_2). \quad (2-16)$$

And, the positive yaw moment is caused by the difference between the torques exerted by the two clockwise and another two counter-clockwise rotating propellers as:

$$U_\psi = (\tau_1 + \tau_2 - \tau_3 - \tau_4). \quad (2-17)$$

Therefore, substituting (2-11)–(2-13) into the forces and moments equations (2-14)–(2-17), the relationship between the motor inputs and the intermediate virtual control inputs can be given in the following matrix fashion:

$$\begin{bmatrix} U_z \\ U_\phi \\ U_\theta \\ U_\psi \end{bmatrix} = \begin{bmatrix} K_u & K_u & K_u & K_u \\ 0 & 0 & K_u L_d & -K_u L_d \\ K_u L_d & -K_u L_d & 0 & 0 \\ K_y & K_y & -K_y & -K_y \end{bmatrix} \begin{bmatrix} u_1^* \\ u_2^* \\ u_3^* \\ u_4^* \end{bmatrix}. \quad (2-18)$$

Finally, the nonlinear dynamics of the quadrotor helicopter can be represented as:

$$\begin{aligned} \ddot{x}_e &= \frac{(\cos \phi \sin \theta \cos \psi + \sin \phi \sin \psi)(u_1^* + u_2^* + u_3^* + u_4^*)K_u}{m} - \frac{K_1 \dot{x}_e}{m} \\ \ddot{y}_e &= \frac{(\cos \phi \sin \theta \sin \psi - \sin \phi \cos \psi)(u_1^* + u_2^* + u_3^* + u_4^*)K_u}{m} - \frac{K_2 \dot{y}_e}{m} \\ \ddot{z}_e &= \frac{(\cos \phi \cos \theta)(u_1^* + u_2^* + u_3^* + u_4^*)K_u}{m} - \frac{K_3 \dot{z}_e}{m} - g \\ \dot{p} &= \frac{(I_{yy} - I_{zz})qr}{I_{xx}} + \frac{K_u L_d(u_3^* - u_4^*)}{I_{xx}} - \frac{I_r \Omega q}{I_{xx}} - \frac{K_4 L_d \dot{\phi}}{I_{xx}} \\ \dot{q} &= \frac{(I_{zz} - I_{xx})pr}{I_{yy}} + \frac{K_u L_d(u_1^* - u_2^*)}{I_{yy}} + \frac{I_r \Omega p}{I_{yy}} - \frac{K_5 L_d \dot{\theta}}{I_{yy}} \\ \dot{r} &= \frac{(I_{xx} - I_{yy})pq}{I_{zz}} + \frac{K_y(u_1^* + u_2^* - u_3^* - u_4^*)}{I_{zz}} - \frac{K_6 \dot{\psi}}{I_{zz}}. \end{aligned} \quad (2-19)$$

2.1.4 Model Linearization

In order to facilitate the controller design, the afore-derived nonlinear dynamics of the quadrotor helicopter can be simplified. Two assumptions are described as follows:

- 1) The motion of the quadrotor helicopter can be assumed close to the hovering condition ($U_z =$

mg), the yaw angle is fixed to zero ($\psi = 0$), and small angular changes occur to roll (ϕ) and pitch (θ) angles. Therefore, the transformation matrix T_B^I as shown in (2–3) is very close to an identity matrix and the rotational velocities can be replaced directly by Euler angle rates.

- 2) The angular components are quite complex because several variables have been taken into account. Most of them come from cross coupling of angular speeds (gyroscopic effects and Coriolis-centripetal form). Since the motion of the quadrotor helicopter can be assumed close to the hovering condition, and small angular changes occur, especially for roll and pitch motion. It follows that these terms can be simplified because they are much smaller than the main ones. Moreover, the drag effects can also be ignored due to the small values.

As a conclusion, the linearized dynamics of the quadrotor helicopter can be given as:

$$\begin{aligned}\ddot{x}_e &= g\theta \\ \ddot{y}_e &= -g\phi \\ \ddot{z}_e &= -g + \frac{U_z}{m} \\ \ddot{\phi} &= \frac{U_\phi}{I_{xx}} \\ \ddot{\theta} &= \frac{U_\theta}{I_{yy}} \\ \ddot{\psi} &= \frac{U_\psi}{I_{zz}}.\end{aligned}\tag{2-20}$$

Moreover, the linear dynamic equations of the quadrotor helicopter can be further described in

the following formal matrix manner:

$$\begin{bmatrix}
\dot{x}_e \\
\ddot{x}_e \\
\dot{y}_e \\
\ddot{y}_e \\
\dot{z}_e \\
\ddot{z}_e \\
\dot{\phi} \\
\ddot{\phi} \\
\dot{\theta} \\
\ddot{\theta} \\
\dot{\psi} \\
\ddot{\psi}
\end{bmatrix}
=
\begin{bmatrix}
0 & 1 & 0 & 0 & 0 & 0 & 0 & 0 & 0 & 0 & 0 & 0 \\
0 & 0 & 0 & 0 & 0 & 0 & 0 & g & 0 & 0 & 0 & 0 \\
0 & 0 & 0 & 1 & 0 & 0 & 0 & 0 & 0 & 0 & 0 & 0 \\
0 & 0 & 0 & 0 & 0 & 0 & -g & 0 & 0 & 0 & 0 & 0 \\
0 & 0 & 0 & 0 & 0 & 1 & 0 & 0 & 0 & 0 & 0 & 0 \\
0 & 0 & 0 & 0 & 0 & 0 & 0 & 0 & 0 & 0 & 0 & 0 \\
0 & 0 & 0 & 0 & 0 & 0 & 0 & 1 & 0 & 0 & 0 & 0 \\
0 & 0 & 0 & 0 & 0 & 0 & 0 & 0 & 0 & 0 & 0 & 0 \\
0 & 0 & 0 & 0 & 0 & 0 & 0 & 0 & 1 & 0 & 0 & 0 \\
0 & 0 & 0 & 0 & 0 & 0 & 0 & 0 & 0 & 0 & 0 & 0 \\
0 & 0 & 0 & 0 & 0 & 0 & 0 & 0 & 0 & 0 & 1 & 0 \\
0 & 0 & 0 & 0 & 0 & 0 & 0 & 0 & 0 & 0 & 0 & 0
\end{bmatrix}
\begin{bmatrix}
x_e \\
\dot{x}_e \\
y_e \\
\dot{y}_e \\
z_e \\
\dot{z}_e \\
\phi \\
\dot{\phi} \\
\theta \\
\dot{\theta} \\
\psi \\
\dot{\psi}
\end{bmatrix}
+
\begin{bmatrix}
0 \\
0 \\
0 \\
0 \\
-1 \\
g
\end{bmatrix}
\quad (2-21)$$

$$+
\begin{bmatrix}
0 & 0 & 0 & 0 \\
0 & 0 & 0 & 0 \\
0 & 0 & 0 & 0 \\
0 & 0 & 0 & 0 \\
0 & 0 & 0 & 0 \\
K_u/m & K_u/m & K_u/m & K_u/m \\
0 & 0 & 0 & 0 \\
0 & 0 & K_u L_d / I_{xx} & -K_u L_d / I_{xx} \\
0 & 0 & 0 & 0 \\
K_u L_d / I_{yy} & -K_u L_d / I_{yy} & 0 & 0 \\
0 & 0 & 0 & 0 \\
K_y / I_{zz} & K_y / I_{zz} & -K_y / I_{zz} & -K_y / I_{zz}
\end{bmatrix}
\begin{bmatrix}
u_1^* \\
u_2^* \\
u_3^* \\
u_4^*
\end{bmatrix}$$

$$\begin{bmatrix} y_1 \\ y_2 \\ y_3 \\ y_4 \\ y_5 \\ y_6 \end{bmatrix} = \begin{bmatrix} 1 & 0 & 0 & 0 & 0 & 0 & 0 & 0 & 0 & 0 & 0 & 0 \\ 0 & 0 & 1 & 0 & 0 & 0 & 0 & 0 & 0 & 0 & 0 & 0 \\ 0 & 0 & 0 & 0 & 1 & 0 & 0 & 0 & 0 & 0 & 0 & 0 \\ 0 & 0 & 0 & 0 & 0 & 0 & 1 & 0 & 0 & 0 & 0 & 0 \\ 0 & 0 & 0 & 0 & 0 & 0 & 0 & 0 & 1 & 0 & 0 & 0 \\ 0 & 0 & 0 & 0 & 0 & 0 & 0 & 0 & 0 & 0 & 1 & 0 \end{bmatrix} \begin{bmatrix} x_e \\ \dot{x}_e \\ y_e \\ \dot{y}_e \\ z_e \\ \dot{z}_e \\ \phi \\ \dot{\phi} \\ \theta \\ \dot{\theta} \\ \psi \\ \dot{\psi} \end{bmatrix}. \quad (2-22)$$

2.2 Actuator Fault Formulation

Actuator faults represent malfunctioning of the actuators in a system, which may be due to hydraulic leakages, broken wires, or stuck control surfaces in an aircraft. Such faults can be modeled as multiplicative faults as follows:

$$u_f(t) = (I_m - L_f(t))u(t) \quad (2-23)$$

where $u_f(t) = [u_{f1}(t), u_{f2}(t), \dots, u_{fm}(t)]^T$ is the faulty control input vector, $I_m \in \mathbb{R}^{m \times m}$ is an identity matrix, and $L_f(t) = \text{diag}([l_{f1}(t), l_{f2}(t), \dots, l_{fm}(t)])$ represents the loss of control effectiveness level of the actuators, where $l_{fi}(t)$ ($i = 1, 2, \dots, m$) is a scalar satisfying $0 \leq l_{fi}(t) \leq 1$. If $l_{fi}(t) = 0$, the i th actuator works perfectly, otherwise, the i th actuator suffers certain level of fault with a special case $l_{fi}(t) = 1$ denoting the complete failure of the i th actuator.

Note that although such multiplicative actuator faults do not directly affect the dynamics of the controlled system itself, they can significantly affect the dynamics of the closed-loop system, and

may even affect the controllability of the system [31].

2.3 Environmental Disturbance Formulation

Wind disturbance is regarded as the main factor of influencing aircraft performance. The wind vector can be characterized by two vectors as:

$$W(t) = W_0 + \Delta W(t) \quad (2-24)$$

where $W_0 = [w_{x0}, w_{y0}, w_{z0}]^T$ is the static wind vector that evolves slowly along the time and represents the mean value of the overall wind vector and $\Delta W(t)$ is the non-static vector featuring higher frequencies and smaller amplitudes in comparison with the static wind vector, that can be formulated as follows:

$$\Delta W(t) = \begin{bmatrix} \Delta w_x(t) \\ \Delta w_y(t) \\ \Delta w_z(t) \end{bmatrix} = \begin{bmatrix} a_x \sin(\omega_x t + \phi_x) \\ a_y \sin(\omega_y t + \phi_y) \\ a_z \sin(\omega_z t + \phi_z) \end{bmatrix} \quad (2-25)$$

with $[a_x, a_y, a_z]^T$, $[\omega_x, \omega_y, \omega_z]^T$, and $[\phi_x, \phi_y, \phi_z]^T$ denoting the amplitude, frequency, and phase of the non-static wind model.

Chapter 3

Adaptive Fault-Tolerant Control

In this chapter, a novel adaptive SMC scheme is proposed to accommodate system uncertainties caused by actuator faults. An integral SMC is employed as the baseline controller. When actuator faults occur, there is no need to know the exact bound of the uncertainties in the control effectiveness matrix. The post-fault control effectiveness matrix can be estimated by the proposed adaptive control scheme, and the control inputs will be changed accordingly. In such a way, the robustness of the controller to actuator faults is improved. With the help of adaptive change of both continuous and discontinuous control parts, a minimum value of the discontinuous control gain can be guaranteed. In this case, the resulting control effort is reduced accordingly to avoid control chattering problem. Owing to the minimized control effort to accommodate uncertainties compared to the conventional SMC, the proposed adaptive SMC can still maintain the system performance when severer faults occur. The effectiveness of the developed algorithm is demonstrated by the simulation results based on an unmanned quadrotor helicopter under various faulty conditions.

3.1 Introduction

UAVs are increasingly becoming a topic of interest, which is not only limited in military applications but also extended into civilian applications [5, 110–114]. In order to make wider use of UAVs and make them more intelligent for practical applications such as fire detecting and fighting,

power-line inspection, and city surveillance, safety is a big issue to be considered [3, 115]. More recently, the fault-tolerant capability of unmanned systems has begun to draw more and more attention in both industrial and academic communities, due to the increased demands for safety and reliability [14, 116, 117]. As argued in [11, 12], the increasing demands for safety, reliability, and high system performance have stimulated research in the area of FTC beneficial from the new developments in control theory, computer technology, actuator and sensor techniques. Fault-tolerant capability is an important feature for safety-critical systems, such as UAVs, chemical processing plants, nuclear power plants, etc. The main objective is to maintain the overall system stability and acceptable degree of performance in the presence of faults in the system [11]. From the point of view of fault occurrence location, fault can be classified into actuator fault, sensor fault, and other system component fault [11, 31]. Partial loss of control effectiveness of an actuator is a common fault occurring in aircraft systems. Since the actuator plays an important role of connecting control signals to physical movements of the system to accomplish specific objectives, actuator fault is considered in this chapter. One way to accommodate this kind of fault is to use the robustness of the control system which does not require on-line detection of fault as opposed to active fault-tolerant control system [11, 118, 119]. This so-called robust controller treats faults as uncertainties in the system, which can be incorporated in the design of a controller [120]. Therefore, a trade-off between system performance and robustness is unavoidable. Moreover, if a large fault is considered during the design stage, it will lead to unacceptable performance in normal (fault-free) conditions due to the big trade-off for taking such a large uncertainty into consideration. Since real systems mostly work under normal conditions and fault does not occur all the time, the consideration of fault during design stage will sacrifice certain degree of performance.

Therefore, in this chapter, a novel adaptive SMC with integral type sliding surface is introduced. An adaptive scheme is synthesized to estimate the post-fault control effectiveness matrix that has an effect on both continuous and discontinuous control parts. Like other adaptive SMC algorithms, the exact value of the uncertainty bound is not required to deal with the uncertainty caused by an actuator fault. Compared to the existing adaptive SMC schemes in the literature, the

main contributions of the proposed control scheme are listed below. Firstly, the proposed control scheme can adaptively generate appropriate control inputs without merely relying on the robustness generated from the discontinuous control strategy, i.e., the equivalent control part will also be changed adaptively to achieve a better tracking performance. Secondly, due to the less use of the discontinuous control strategy, the control effort is significantly reduced which means larger faults can be tolerated, and control chattering effect is also pacified.

The rest of this chapter is organized as follows. In Section 3.2, an adaptive SMC is proposed, and for comparison, a traditional SMC with bounded uncertainty in control effectiveness matrix is introduced as well. The modeling of an unmanned quadrotor helicopter is presented in Section 3.3. In Section 3.4, simulation results are presented to verify the effectiveness of the proposed algorithm. Finally, general conclusions of this chapter are summarized in Section 3.5.

3.2 Adaptive Fault-Tolerant Control Design

3.2.1 Problem Formulation

Consider a second-order uncertain linear system subject to actuator faults of the form:

$$\ddot{x}(t) = Ax(t) + B_0(I - L_f(t))u(t) \quad (3-1)$$

where $A \in \mathbb{R}^{n \times n}$ is the state matrix, $B_0 \in \mathbb{R}^{n \times m}$ is the control effectiveness matrix, and both of them are known. $u(t) \in \mathbb{R}^m$ is the control input vector and the diagonal matrix $L_f(t) = \text{diag}([l_{f1}(t), l_{f2}(t), \dots, l_{fm}(t)])$ represents the loss of control effectiveness level in the actuators, where $l_{fi}(t)$ is a scalar satisfying $0 \leq l_{fi}(t) < 1$. Thus, if $l_{fi}(t) = 0$, the i th actuator works perfectly, while if $l_{fi}(t) > 0$, the i th actuator suffers certain level of fault. Note that the state $x(t)$ is assumed measurable.

In order to make the faults clear and easy to be represented, one can define $\Delta B = -B_0L_f(t)$,

then (3–1) can be rewritten as:

$$\begin{aligned}\ddot{x}(t) &= Ax(t) + Bu(t) \\ B &= B_0 + \Delta B\end{aligned}\tag{3–2}$$

where B is the post-fault control effectiveness matrix.

Assumption 3.1 $\text{rank}B_0 = m$.

Assumption 3.2 *The pair (A, B_0) is controllable.*

Remark 3.1 *The actuator faults ΔB can be treated as a matched uncertainty and it satisfies the so-called matching condition:*

$$\Delta B \in \text{Im } B_0,$$

i.e., there exists a matrix $\gamma(t) \in \mathbb{R}^{m \times m}$, such that $\Delta B = B_0\gamma(t)$.

3.2.2 Integral-Type Sliding Surface Design

Typically, the design of a sliding mode controller is composed of two steps. The first step involves the design of a sliding surface, on which the system performance is maintained as expected. The second one is concerned with the selection of a control law that will make the sliding surface attractive to the system states. Once the sliding surface is reached, the states are kept in the close neighborhood of the designed sliding surface.

The integral sliding surface for the system is defined by the following set:

$$S = \{x(t) \in \mathbb{R}^n : \sigma(x(t), t) = 0\}.\tag{3–3}$$

The switching function $\sigma(x(t), t) \in \mathbb{R}^n$ is defined as:

$$\begin{aligned}\sigma(x(t), t) &= \sigma_0(x(t), t) + z \\ \sigma_0(x(t), t) &= C^T x(t)\end{aligned}\tag{3–4}$$

where $C \in \mathbb{R}^n$ and $\sigma_0(x(t), t)$ is the linear combination of the states, which is similar to the conventional SMC design. z includes the integral term and will be determined below.

First of all, assume that there is no fault, i.e., $\Delta B = 0$, then the ideal system can be given by the following equations:

$$\ddot{x}_0(t) = Ax_0(t) + B_0u_0(t) \quad (3-5)$$

$$x(t_0) = x_0(t_0) \quad (3-6)$$

where $x_0(t)$ denotes the state of the ideal system under control $u_0(t)$ and t_0 represents the initial time instant.

The choice of z is determined by the following equations which guarantee that $\sigma(x(t_0), t_0) = 0$.

$$\dot{z} = -C^T(Ax(t) + B_0u_0(t)) \quad (3-7)$$

$$z(t_0) = -C^T x(t_0) \quad (3-8)$$

i.e.,

$$z = -C^T \left[x(t_0) + \int_{t_0}^t (Ax(\tau) + B_0u_0(\tau)) d\tau \right]. \quad (3-9)$$

Remark 3.2 The term $x(t_0) + \int_{t_0}^t (Ax(\tau) + B_0u_0(\tau)) d\tau$ in (3-9) can be regarded as the trajectory of the ideal system under the nominal control u_0 . That is, the motion equation of the sliding mode coincides with that of the ideal system without perturbation.

Remark 3.3 With this definition of z , it is obtained that $\sigma(x(t_0), t_0) = \sigma_0(x(t_0), t_0) + z(0) = 0$. Thus, the system trajectory under integral SMC starts from the designed sliding surface and the reaching phase is eliminated accordingly in contrast with conventional SMC.

Now, the problem is to design a control law that, provided $x(t_0) = x_0(t_0)$, guarantees the identity $x(t) = x_0(t)$ for all the time $t \geq 0$. The control law can be formulated in the following form:

$$u(t) = u_0(t) + u_1(t) \quad (3-10)$$

where $u_0(t)$ is the continuous nominal control part to stabilize the ideal system, which is assumed to be fault-free and in absence of uncertainties as shown in (3–5), such that the ideal system follows a given trajectory with satisfactory accuracy. $u_1(t)$ is the discontinuous integral SMC part to compensate the perturbations that satisfy the matching condition in order to ensure the sliding motion.

Denoting $x_d(t)$ as the desired trajectory, another variable $\tilde{x}(t) = x(t) - x_d(t)$ can be defined. Then, the switching function is redefined as:

$$\sigma(\tilde{x}(t), t) = \sigma_0 + z \quad (3-11)$$

where

$$\sigma_0 = \tilde{x}(t) + \dot{\tilde{x}}(t) \quad (3-12)$$

$$\begin{aligned} \dot{z} &= -\dot{\tilde{x}}(t) + K_{c1}\dot{\tilde{x}}(t) + K_{c2}\tilde{x}(t) \\ z(t_0) &= -\tilde{x}(t_0) - \dot{\tilde{x}}(t_0) \end{aligned} \quad (3-13)$$

with diagonal matrices K_{c1} and K_{c2} denoting design parameters.

3.2.3 Fault-Tolerant Control with Bounded Uncertainty

In this section, the traditional SMC is introduced to make a comparison with the proposed adaptive SMC. Assume that the bound of the uncertainty is known during the design stage, and it is incorporated into the design of the discontinuous control gain. In this case, in order to compensate the presumed fault, the discontinuous control gain needs to be increased which will result in significant control effort.

Assumption 3.3 *The uncertainty in the control effectiveness matrix caused by an actuator fault is known within a certain margin and satisfies:*

$$\|\Delta B \cdot B_0^+\| < \beta < 1 \quad (3-14)$$

where B_0^+ is the pseudo inverse of B_0 defined by

$$B_0^+ = (B_0^T B_0)^{-1} B_0^T \quad (3-15)$$

and β is a positive constant representing the upper bound of the uncertainty induced by an actuator fault.

In order to analyze the sliding motion associated with the switching function in (3-11) in the presence of actuator fault, the time derivative of the sliding surface is computed as follows:

$$\dot{\sigma}(\tilde{x}(t), t) = \ddot{\tilde{x}}(t) + K_{c1}\dot{\tilde{x}}(t) + K_{c2}\tilde{x}(t). \quad (3-16)$$

Equalizing $\dot{\sigma}(\tilde{x}(t), t) = 0$ yields:

$$u_0 = B_0^+(\ddot{x}_d(t) - K_{c1}\dot{\tilde{x}}(t) - K_{c2}\tilde{x}(t) - Ax(t)). \quad (3-17)$$

Then, substituting (3-17) into (3-2) yields:

$$\ddot{x}(t) = Ax(t) + BB_0^+(\ddot{x}_d(t) - K_{c1}\dot{\tilde{x}}(t) - K_{c2}\tilde{x}(t) - Ax(t)). \quad (3-18)$$

Remark 3.4 Note that in the case of no fault in the system ($\Delta B = 0$), there exists $(B_0 + \Delta B)B_0^+ = I$. Then (3-18) becomes $\ddot{\tilde{x}}(t) + K_{c1}\dot{\tilde{x}}(t) + K_{c2}\tilde{x}(t) = 0$, thus the sliding motion is achieved for the ideal system.

In the presence of faults, in order to maintain the desired sliding motion, the discontinuous control part is added and designed as follows:

$$u_1 = -B_0^+ K_{c3} \text{sign}(\sigma) \quad (3-19)$$

where K_{c3} is a positive high gain matrix which makes the sliding surface attractive.

Theorem 3.1 For the system described in (3–1), assume that the uncertainty is bounded in (3–14).

Then, in a faulty condition for any $l_{fi}(t) > 0$, by employing the following feedback control:

$$u(t) = B_0^+(\ddot{x}_d(t) - K_{c1}\dot{\tilde{x}}(t) - K_{c2}\tilde{x}(t) - Ax(t)) - B_0^+K_{c3}sign(\sigma) \quad (3-20)$$

the sliding motion will be achieved and maintained if

$$K_{c3} \geq \frac{u^*\beta + \eta u^*/\|u^*\|}{1 + \beta} \quad (3-21)$$

where $u^* = \ddot{x}_d(t) - K_{c1}\dot{\tilde{x}}(t) - K_{c2}\tilde{x}(t) - Ax(t)$ and η is a small positive constant.

Proof 3.1 Substituting (3–20) into (3–16) gives:

$$\begin{aligned} \dot{\sigma}(\tilde{x}(t), t) = & Ax(t) + BB_0^+(\ddot{x}_d(t) - K_{c1}\dot{\tilde{x}}(t) - K_{c2}\tilde{x}(t) - Ax(t)) \\ & - BB_0^+K_{c3}sign(\sigma) - \ddot{x}_d(t) + K_{c1}\dot{\tilde{x}}(t) + K_{c2}\tilde{x}(t). \end{aligned} \quad (3-22)$$

Consider the candidate Lyapunov function as:

$$V_1(t) = \frac{1}{2}\sigma(\tilde{x}(t), t)^T\sigma(\tilde{x}(t), t). \quad (3-23)$$

The time derivative of the candidate Lyapunov function satisfies:

$$\begin{aligned} \dot{V}_1 = & \sigma Ax(t) + \sigma BB_0^+(\ddot{x}_d(t) - K_{c1}\dot{\tilde{x}}(t) - K_{c2}\tilde{x}(t) - Ax(t)) \\ & - \sigma BB_0^+K_{c3}sign(\sigma) - \sigma\ddot{x}_d(t) + \sigma K_{c1}\dot{\tilde{x}}(t) + \sigma K_{c2}\tilde{x}(t) \\ = & \sigma\Delta BB_0^+(\ddot{x}_d(t) - K_{c1}\dot{\tilde{x}}(t) - K_{c2}\tilde{x}(t) - Ax(t)) \\ & - \sigma K_{c3}sign(\sigma) - \sigma\Delta BB_0^+K_{c3}sign(\sigma). \end{aligned} \quad (3-24)$$

Since the loss of control effectiveness of actuator fault is considered here, the assumption $\|\Delta B\|$

$B_0^+ \| < \beta < 1$ holds. Therefore,

$$\begin{aligned} \dot{V}_1 &\leq \|\sigma\| \beta (\ddot{x}_d(t) - K_{c1}\dot{\tilde{x}}(t) - K_{c2}\tilde{x}(t) - Ax(t)) - \|\sigma\| K_{c3} - \|\sigma\| \beta K_{c3} \\ &= \|\sigma\| (u^* \beta - (1 + \beta) K_c) \\ &\leq \frac{-\eta u^* \|\sigma\|}{\|u^*\|}. \end{aligned} \quad (3-25)$$

Thus, the controlled system satisfies the standard η -reachability condition, which implies that the controlled system can asymptotically track the desired trajectory and the sliding motion is maintained all the time.

However, in order to account for control effectiveness matrix uncertainties, the control discontinuity is increased which may lead to control chattering. One can remove this condition by smoothing the control discontinuity in a thin boundary layer neighboring the designed sliding surface:

$$\bar{B} = \{\tilde{x}, \|\sigma(\tilde{x}, t)\| \leq \Phi\} \quad (3-26)$$

where Φ is the boundary layer thickness with positive value.

Accordingly, the feedback control law $u(t)$ becomes:

$$u(t) = B_0^+ (\ddot{x}_d(t) - K_{c1}\dot{\tilde{x}}(t) - K_{c2}\tilde{x}(t) - Ax(t) - K_{c3}\text{sat}(\sigma/\Phi)) \quad (3-27)$$

where the sat function is defined as follows:

$$\text{sat}(\sigma/\Phi) = \begin{cases} \text{sign}(\sigma) & \text{if } \|\sigma\| > \Phi \\ \sigma/\Phi & \text{if } \|\sigma\| < \Phi \end{cases}. \quad (3-28)$$

3.2.4 Adaptive Fault-Tolerant Control

As shown before, the integral SMC can achieve effective tracking performance in the presence of uncertainties in the control effectiveness matrix while avoiding exciting high-frequency dynamics. However, for some real applications, actuator faults can occur in the system at any time with

unknown magnitudes. It is hard to know the uncertainty bound in advance. This stimulates the author to investigate the adaptive approach combined with SMC to accommodate the unknown uncertainties and faults. For large actuator faults, which may cause significant control efforts, an adaptive SMC is also required to improve the control performance.

Intuitively, the actuator faults are related to the control effectiveness matrix. When actuator faults occur, the corresponding control gain will change accordingly. Therefore, in order to effectively accommodate the faults, merely increasing the discontinuous control gain is not enough. Because when the discontinuous control gain is increased, the related control effort will be increased, and the chattering phenomenon may be stimulated as well. Therefore, both continuous and discontinuous control parts need to be changed accordingly. In this section, instead of using the pre-fault control matrix B_0^+ , the post-fault control effectiveness matrix \hat{B}^+ is used for deriving the control law. The adaptive scheme is then employed to estimate the post-fault control effectiveness matrix. In this case, when actuator faults occur, both continuous and discontinuous control parts will be adaptively changed to compensate the faults more effectively (as shown in Fig. 3.1).

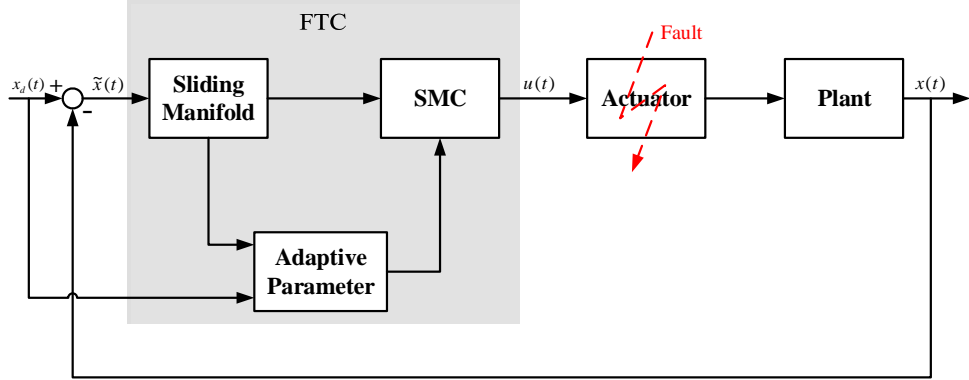


Figure 3.1: Schematic of the proposed adaptive SMC.

The sliding surface in (3–11) is employed, and the derivative of the sliding surface can be found in (3–16). Then the continuous control part is given by:

$$u_0 = \hat{B}^+(\ddot{x}_d(t) - K_{c1}\dot{\tilde{x}}(t) - K_{c2}\tilde{x}(t) - Ax(t)) \quad (3-29)$$

where \hat{B}^+ is the pseudo inverse of \hat{B} given by

$$\hat{B}^+ = (\hat{B}^T \hat{B})^{-1} \hat{B}^T \quad (3-30)$$

and \hat{B} is the available estimation of the post-fault control effectiveness matrix.

Theorem 3.2 Define the adaptive law for estimating the uncertain control effectiveness matrix as:

$$\dot{\hat{B}}^+ = [-\ddot{x}_d(t) + K_{c1}\dot{\tilde{x}}(t) + K_{c2}\tilde{x}(t) + Ax(t) + K_{c3}\text{sat}(\sigma/\Phi)]\sigma_\Delta \quad (3-31)$$

where $\sigma_\Delta = \sigma - \Phi\text{sat}(\sigma/\Phi)$ is the measurement of the algebraic distance between the current state and the boundary layer.

Assume that after fault occurrence, the control effectiveness matrix B is unknown but constant:

$$\Delta B = E \quad (3-32)$$

where E is a constant matrix.

Then, the system trajectory is guaranteed to remain on the sliding surface with the choice that,

$$K_{c3} \geq \frac{\eta u^*}{\|u^*\|}. \quad (3-33)$$

Remark 3.5 Compared to the discontinuous control gain K_{c3} in the traditional SMC with bounded uncertainty, the one in the proposed adaptive SMC is reduced due to the change of the continuous control part. In this case, the control chattering effect is suppressed.

Proof 3.2 In order to ensure the sliding motion converges to the boundary layer, a Lyapunov function is defined as follows:

$$V_2 = \frac{1}{2}[\sigma_\Delta^T \sigma_\Delta + B(\hat{B}^+ - B^+)^T(\hat{B}^+ - B^+)]. \quad (3-34)$$

When the sliding motion is inside the boundary layer; $\sigma_\Delta = 0$ holds, in this case the derivative of the Lyapunov function becomes:

$$\dot{V}_2 = 0. \quad (3-35)$$

When the sliding motion is outside the boundary layer, $\dot{\sigma}_\Delta = \dot{\sigma}$, and there exists:

$$\dot{V}_2 = \dot{\sigma}_\Delta \sigma_\Delta + B(\hat{B}^+ - B^+) \dot{\hat{B}}^+. \quad (3-36)$$

Substituting (3-29) and (3-31) into (3-36) gives:

$$\begin{aligned} \dot{V}_2 = & [Ax(t) + B\hat{B}^+(\ddot{x}_d(t) - K_{c1}\dot{\tilde{x}}(t) - K_{c2}\tilde{x}(t) - Ax(t)) \\ & - B\hat{B}^+K_{c3}\text{sat}(\sigma/\Phi) - \ddot{x}_d(t) + K_{c1}\dot{\tilde{x}}(t) + K_{c2}\tilde{x}(t)]\sigma_\Delta \\ & + B\hat{B}^+[-\ddot{x}_d(t) + K_{c1}\dot{\tilde{x}}(t) + K_{c2}\tilde{x}(t) + Ax(t)]\sigma_\Delta \\ & - BB^+[-\ddot{x}_d(t) + K_{c1}\dot{\tilde{x}}(t) + K_{c2}\tilde{x}(t) + Ax(t)]\sigma_\Delta \\ & + (B\hat{B}^+ - BB^+)K_{c3}\text{sat}(\sigma/\Phi)\sigma_\Delta. \end{aligned} \quad (3-37)$$

Furthermore, it can be obtained that,

$$\begin{aligned} \dot{V}_2 = & -K_{c3}\text{sat}(\sigma/\Phi)\sigma_\Delta \\ & \leq -K_{c3}\|\sigma_\Delta\|. \end{aligned} \quad (3-38)$$

Finally, with the physical control law obtained below:

$$u(t) = -\hat{B}^+[\ddot{x}_d(t) + K_{c1}\dot{\tilde{x}}(t) + K_{c2}\tilde{x}(t) + Ax(t) + K_{c3}\text{sat}(\sigma/\Phi)] \quad (3-39)$$

the sliding motion is maintained all the time.

Remark 3.6 Since the construction of the sliding surface is based on the tracking errors of the concerned state variables and their derivatives, and the desired sliding surface is defined as $\sigma = 0$, if the desired sliding surface can be achieved and maintained, it means that the tracking errors and

their derivatives converge to zero. In this case, the stability and original tracking performance of the system can be maintained.

3.3 Modeling of an Unmanned Quadrotor Helicopter

The mathematical model of an unmanned quadrotor helicopter is described in this section, which will be used as a testbed for demonstration of the developed algorithms. The quadrotor helicopter used in this paper is called Qball-X4, produced by Quanser as shown in Fig. 3.2.

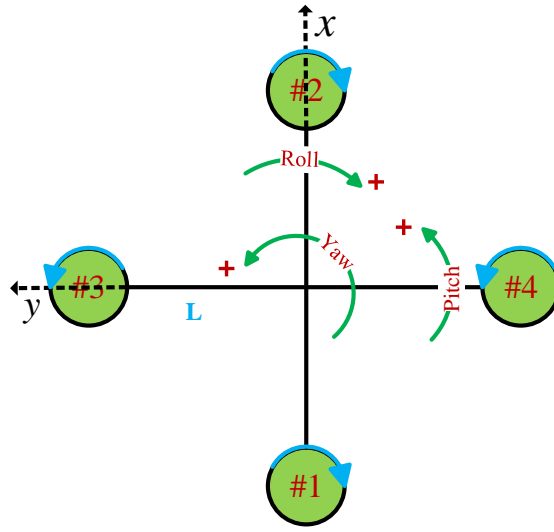


Figure 3.2: Configuration of the unmanned quadrotor helicopter.

In order to design the position and attitude controller of the quadrotor helicopter, the state vector is defined as $x = [x_e, y_e, z_e, \phi, \theta, \psi]^T$. By considering the linearized dynamics of the quadrotor

helicopter in (2–20), the matrices A and B_0 are calculated as follows:

$$A = \begin{bmatrix} 0 & 0 & 0 & 0 & g & 0 \\ 0 & 0 & 0 & -g & 0 & 0 \\ 0 & 0 & 0 & 0 & 0 & 0 \\ 0 & 0 & 0 & 0 & 0 & 0 \\ 0 & 0 & 0 & 0 & 0 & 0 \\ 0 & 0 & 0 & 0 & 0 & 0 \end{bmatrix} \quad (3-40)$$

$$B_0 = \begin{bmatrix} 0 & 0 & 0 & 0 \\ 0 & 0 & 0 & 0 \\ \frac{K_u}{m} & \frac{K_u}{m} & \frac{K_u}{m} & \frac{K_u}{m} \\ 0 & 0 & \frac{K_u L_d}{I_{xx}} & -\frac{K_u L_d}{I_{xx}} \\ \frac{K_u L_d}{I_{yy}} & -\frac{K_u L_d}{I_{yy}} & 0 & 0 \\ \frac{K_y}{I_{zz}} & \frac{K_y}{I_{zz}} & -\frac{K_y}{I_{zz}} & -\frac{K_y}{I_{zz}} \end{bmatrix}.$$

The associated parameters of the quadrotor helicopter used in the above equations are listed in Table 3.1.

Table 3.1: System Parameters

Parameter	Description	Value
K_u	Thrust gain	$120N$
ω	Motor bandwidth	$15rad/s$
m	Mass of the quadrotor helicopter	$1.4kg$
g	Acceleration of gravity	$9.8m/s^2$
L_d	Distance	$0.2m$
K_y	Torque gain	$4N \cdot m$
I_{xx}	Inertial moment along x -axis	$0.03kg \cdot m^2$
I_{yy}	Inertial moment along y -axis	$0.03kg \cdot m^2$
I_{zz}	Inertial moment along z -axis	$0.04kg \cdot m^2$

3.4 Simulation Results

In this section, in order to demonstrate the performance of the proposed adaptive SMC (named as ASMC), simulations based on the unmanned Qball-X4 quadrotor helicopter under different faulty scenarios are carried out. Firstly, the longitudinal motion of the quadrotor helicopter is considered to track a pitch angle command θ_d in the presence of actuator fault. In this case, it is assumed that the quadrotor helicopter is in a hover mode. The desired pitch command is generated from the following pre-filter:

$$\ddot{\theta}_d + 3\dot{\theta}_d + 4\theta_d = 4\theta^* \quad (3-41)$$

where θ^* changes from 0 to 5° at 5 s, and goes back to 0 at 10 s, then changes to -5° at 15 s, and goes back to 0 at 20 s, after that, remains on 0 for 10 s. Three different faulty cases are considered. In the first case, a 20% loss of control effectiveness fault occurs in actuator #1 at 14 s. In the second case, a 50% loss of control effectiveness fault occurs in actuator #1 at 14 s. Finally, the quadrotor helicopter is commanded to track a circular trajectory, and 50% loss of control effectiveness faults occur in two different actuators at 50 s and 70 s, respectively.

3.4.1 Case 1: 20% Loss of Control Effectiveness in One Actuator

For the nominal SMC (named as NSMC), parameters are chosen as $\eta = 0.1$, $\Phi = 0.1$, $K_{c1} = \text{diag}([4, 4, 10, 20, 20, 10])$, $K_{c2} = \text{diag}([4, 4, 25, 100, 100, 25])$, and $K_{c3} = [5, 5, 10, 12, 12, 10]^T$. For comparison, the same values of K_{c1} , K_{c2} , K_{c3} , η , and Φ are chosen for the proposed adaptive SMC.

Figures 3.3 and 3.5 show the tracking performance of pitch angle with the nominal SMC and the proposed adaptive SMC, respectively, with 20% loss of control effectiveness in actuator #1. Since the changed elements in matrix \hat{B} have the same absolute value, only the adaptive parameter with positive value is illustrated in Fig. 3.7, which stops changing when the trajectory of the sliding motion is inside the boundary layer. The simulation results show that, after occurrence of such a relatively small magnitude of the fault, both sliding mode controllers can make a quick

compensation to maintain good tracking performance. Moreover, the nominal SMC presents less tracking error than the proposed adaptive SMC. This is achieved by using more control efforts as can be observed from Figs. 3.4 and 3.6.

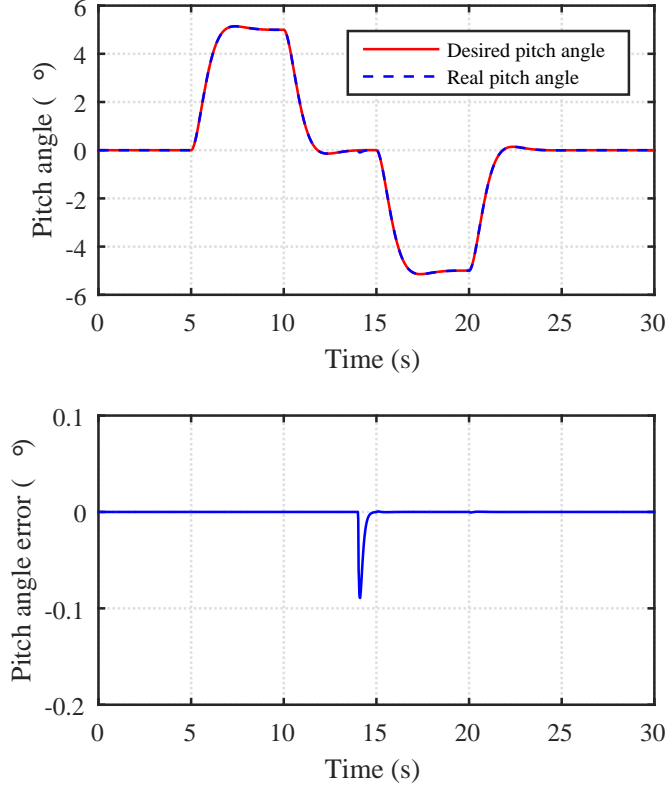


Figure 3.3: Tracking performance using nominal SMC with 20% loss of control effectiveness in actuator #1.

Remark 3.7 At the beginning, the actuator fault has been considered for designing the nominal SMC. If the fault is within the bound, the controller will have a quicker response to it and ensure less tracking error. But at the meantime, in order to accommodate the fault, it will sacrifice more control efforts than the adaptive SMC. This is because that, the nominal SMC uses the robustness of the discontinuous control strategy, and the control gain is chosen larger due to the consideration of the presumed fault.

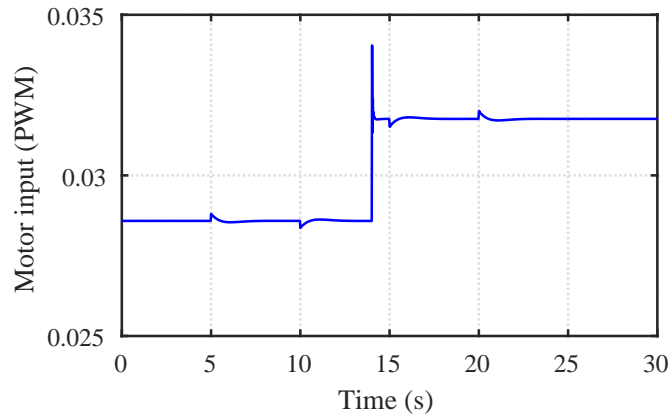


Figure 3.4: Control input of the faulty actuator using nominal SMC with 20% loss of control effectiveness in actuator #1.

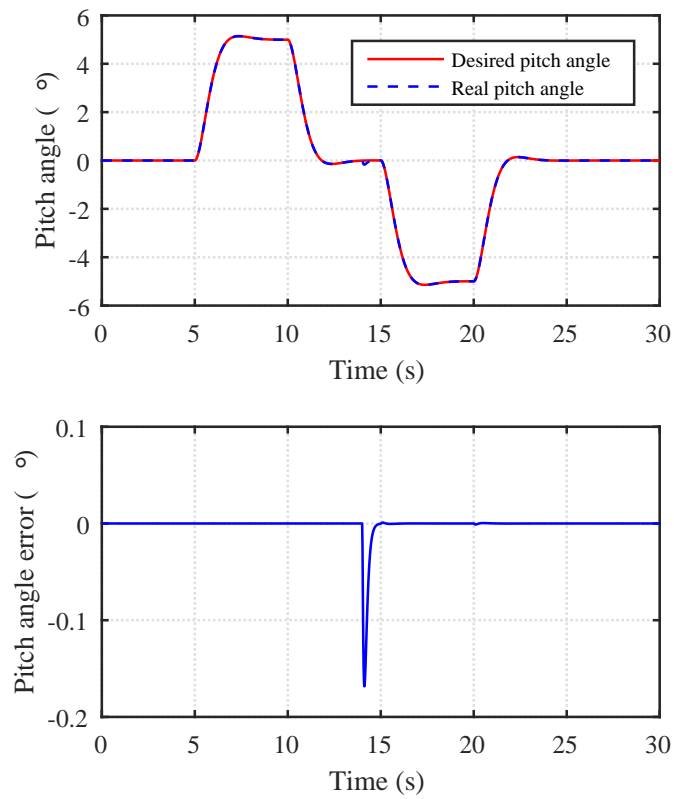


Figure 3.5: Tracking performance using adaptive SMC with 20% loss of control effectiveness in actuator #1.

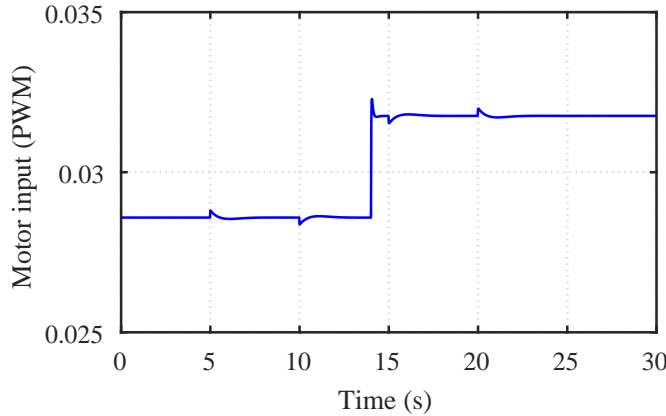


Figure 3.6: Control input of the faulty actuator using adaptive SMC with 20% loss of control effectiveness in actuator #1.

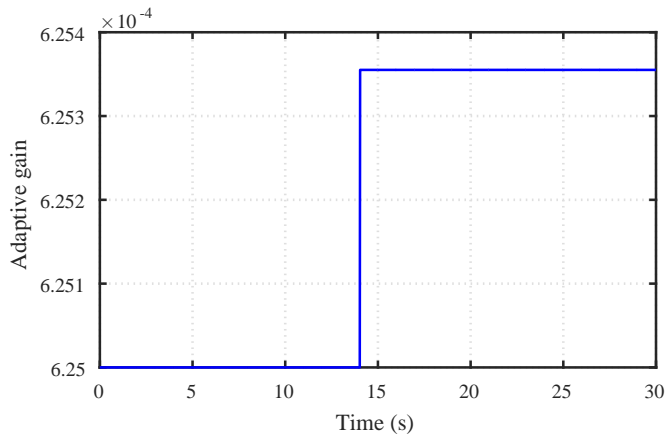


Figure 3.7: Adaptive control gain using adaptive SMC with 20% loss of control effectiveness in actuator #1.

3.4.2 Case 2: 50% Loss of Control Effectiveness in One Actuator

In this section, the performance of both controllers are demonstrated when a large fault occurs in actuator #1. In order to maintain the control performance in the fault-free condition, the discontinuous control gain cannot be enlarged ceaselessly. So the gains of both controllers are selected the same as the previous case. A 50% loss of control effectiveness fault is now injected at 14 s. As shown in Figs. 3.8 and 3.9, for the nominal SMC, when the actuator fault is increased to 50% loss of control effectiveness, the system still shows a quick response but it cannot track the desired

pitch command well with obvious tracking error. What is worse, the control chattering appears as shown in Fig. 3.9. This might stimulate other unmodeled dynamics and make the system performance worse. On the contrary, by using the proposed adaptive SMC, a good tracking performance is maintained and there is only one small overshoot at the initial stage after fault occurrence as shown in Fig. 3.10. The variation of one of the adaptive elements is shown in Fig. 3.12, which becomes bigger compared to the one dealing with 20% loss of control effectiveness fault to compensate the larger fault magnitude. As to the control inputs shown in Figs. 3.9 and 3.11, the one in the nominal SMC almost reaches the limit, while the one in the proposed adaptive SMC is maintained much lower. This feature of the proposed adaptive SMC shows its ability of making the system more robust to large uncertainties.

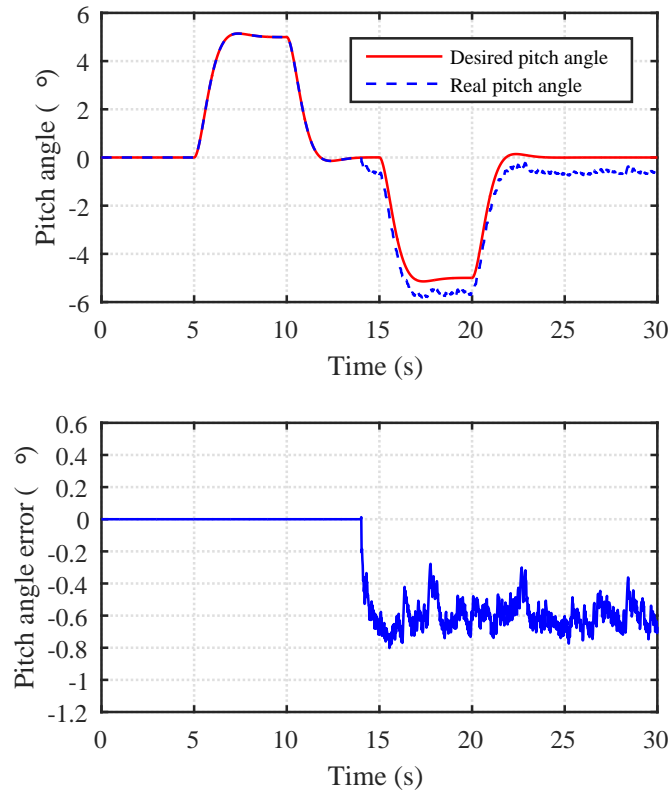


Figure 3.8: Tracking performance using nominal SMC with 50% loss of control effectiveness in actuator #1.

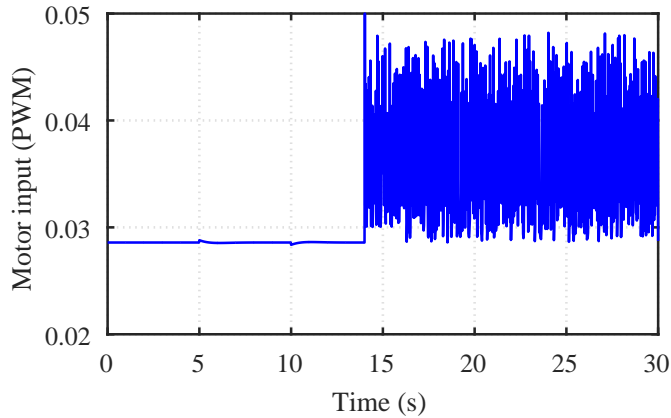


Figure 3.9: Control input of the faulty actuator using nominal SMC with 50% loss of control effectiveness in actuator #1.

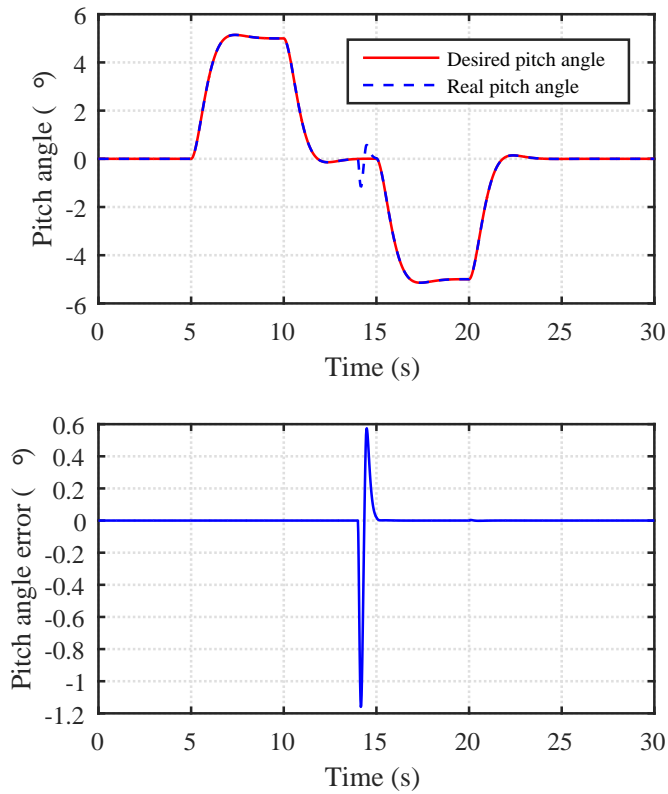


Figure 3.10: Tracking performance using adaptive SMC with 50% loss of control effectiveness in actuator #1.

Remark 3.8 During the design stage, if a large fault is considered for nominal SMC, the system performance cannot be guaranteed in fault-free conditions, although it can accommodate a large

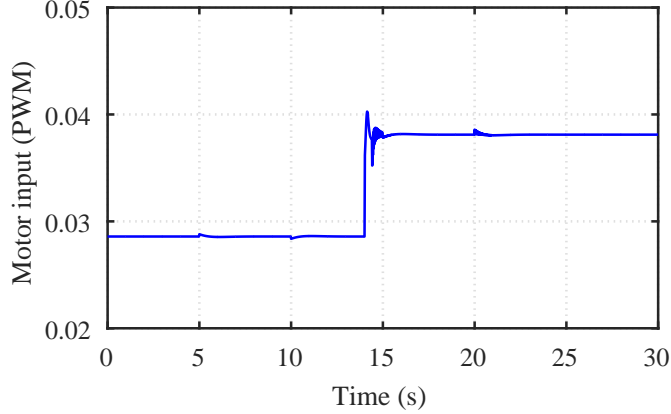


Figure 3.11: Control input of the faulty actuator using adaptive SMC with 50% loss of control effectiveness in actuator #1.

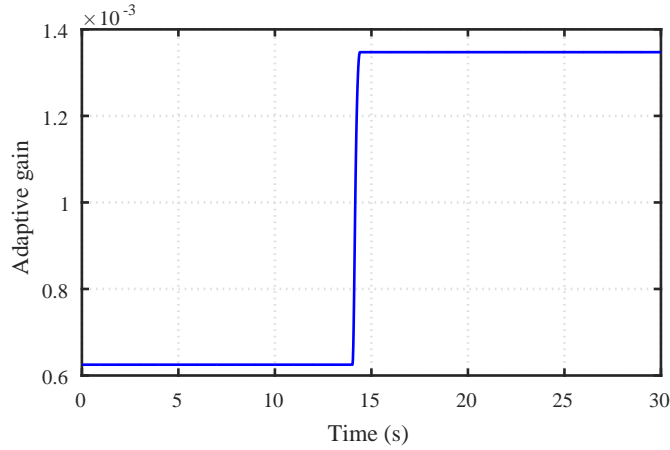


Figure 3.12: Adaptive control gain using adaptive SMC with 50% loss of control effectiveness in actuator #1.

fault. However, if only a small fault is considered for nominal SMC in order to maintain system performance in both fault-free and faulty conditions, when the uncertainty caused by fault exceeds the presumed bound, the system performance cannot be maintained anymore. On the contrary, there is no such a worry for the proposed adaptive SMC, and it shows the strong ability of maintaining system performance seamlessly in the presence of large actuator faults.

3.4.3 Case 3: 3D Trajectory Tracking with 50% Loss of Control Effectiveness in Two Different Actuators

In order to demonstrate the effectiveness of the proposed adaptive SMC in the case of multiple different actuator faults occurring in the system, a circular trajectory is commanded to the quadrotor helicopter as shown in Fig. 3.13. The tracking performance of the nominal SMC is also shown as comparison. The diameter of the circle is defined as 1 m. Firstly, the quadrotor helicopter is lifted up to 0.7 m, and then it is commanded to move along y -axis to the tip of the circle. After that, it follows a clock-wise circular trajectory. A 50% loss of control effectiveness fault occurs in actuators #1 and #4 at 50 s and 70 s, respectively. The detailed translational position tracking performance for each direction is shown in Figs. 3.14, 3.15, and 3.16, respectively, and the inner loop attitude control performance is shown in Figs. 3.17 and 3.18, respectively. From the simulation results, it can be seen that, after faults occurrence, the proposed adaptive SMC can make a quick compensation to maintain the inner loop attitude control, and then it results in less impact on the outer loop position tracking performance. The corresponding action of actuators are shown in Fig. 3.19.

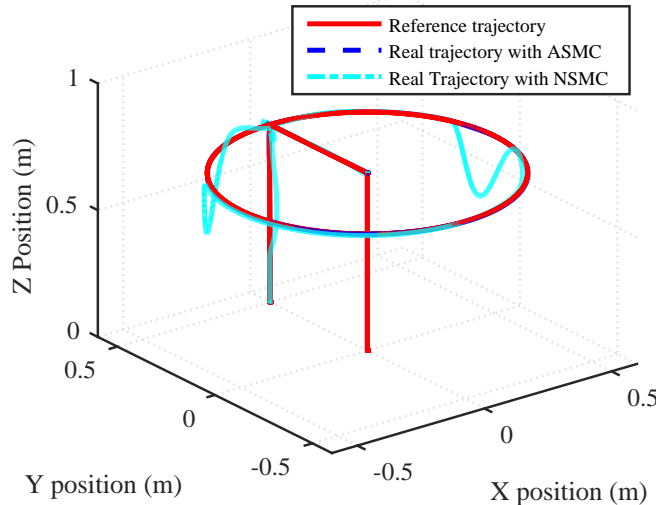


Figure 3.13: 3D trajectory tracking with 50% loss of control effectiveness in actuators #1 and #4 sequentially.

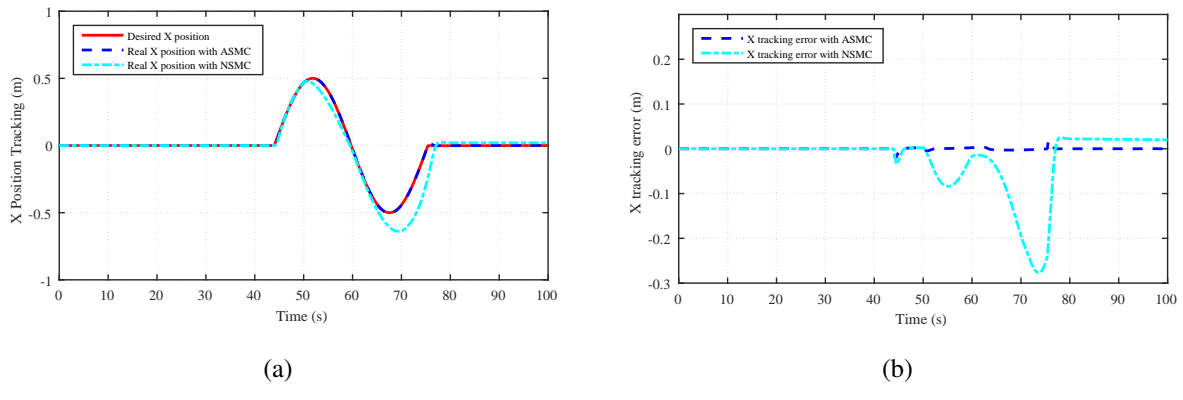


Figure 3.14: x position tracking and tracking error with 50% loss of control effectiveness in actuators #1 and #4 sequentially.

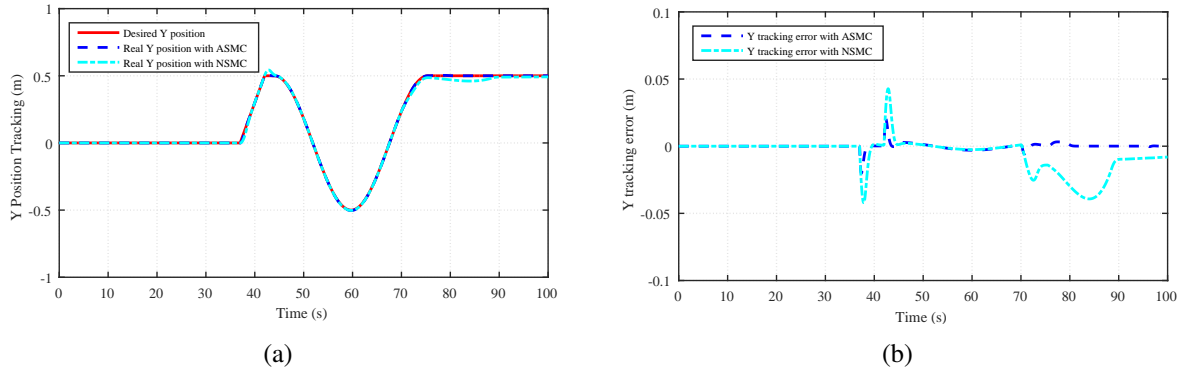


Figure 3.15: y position tracking and tracking error with 50% loss of control effectiveness in actuators #1 and #4 sequentially.

Remark 3.9 Since the output of the outer loop controller is the desired attitude angle, so there is no direct relationship between the position control and the actuators. Then, for x and y position control, when an actuator fault occurs, the most important is to maintain the inner loop attitude control performance. This is because, as long as the desired attitude angle is tracked, the performance of the whole system is guaranteed.

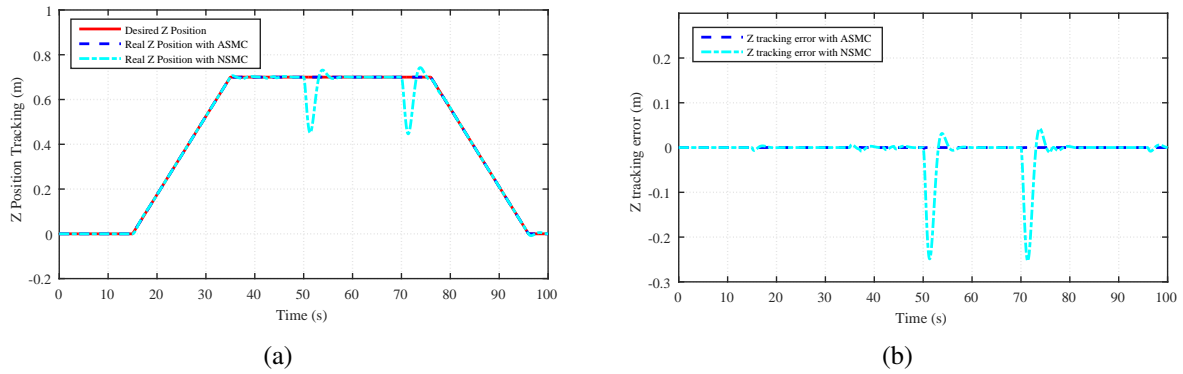


Figure 3.16: z position tracking and tracking error with 50% loss of control effectiveness in actuators #1 and #4 sequentially.

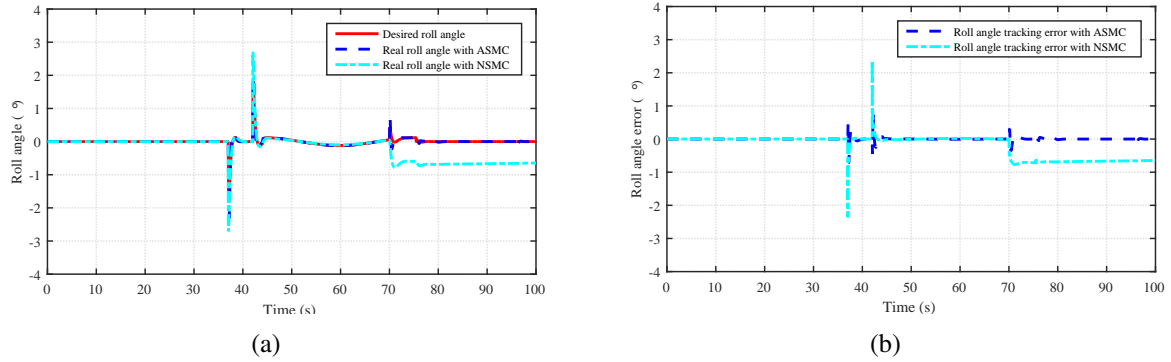


Figure 3.17: Roll angle tracking and tracking error with 50% loss of control effectiveness in actuators #1 and #4 sequentially.

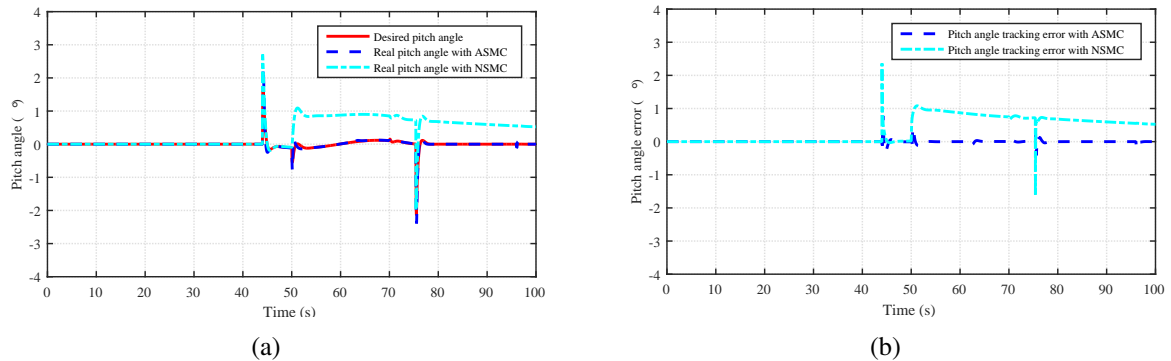


Figure 3.18: Pitch angle tracking and tracking error with 50% loss of control effectiveness in actuators #1 and #4 sequentially.

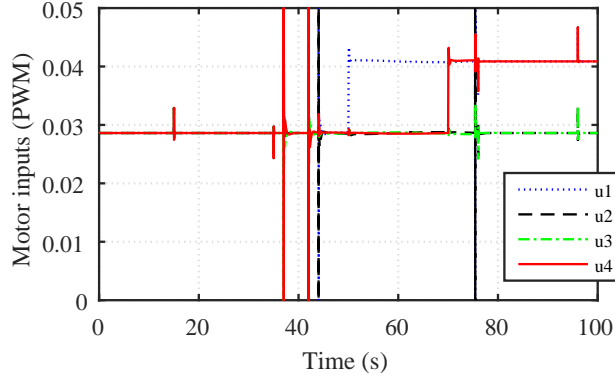


Figure 3.19: Control inputs of the four motors.

3.5 Conclusion

In this chapter, a novel adaptive SMC method is proposed to control an unmanned quadrotor helicopter in the presence of actuator faults. When actuator faults occur, the proposed adaptive SMC scheme is able to automatically provide robustness and maintain good tracking performance with even a large fault magnitude. The main contribution of the proposed method is that it does not require the bound of uncertainties to be known. Meanwhile, the control effort is reduced and the chattering phenomenon is eliminated especially when a large fault is considered with the help of the adaptive change of both continuous and discontinuous control parts. The control scheme is validated under different faulty scenarios. The simulation results show that the proposed adaptive SMC achieves good tracking performance in both fault-free and faulty conditions.

Chapter 4

Disturbance Observer-Based Adaptive Fuzzy Fault-Tolerant Control

This chapter presents an adaptive fuzzy control strategy for a quadrotor helicopter against parametric uncertainties, actuator faults, and environmental disturbances based on an integral SMC, a fuzzy boundary layer, and a nonlinear disturbance observer. Within the proposed control context, both uncertain model parameters and actuator faults can be compensated without the knowledge of the uncertainty bounds and fault information. By virtue of the designed adaptive schemes, the minimum discontinuous control gain is used in the developed control law, which significantly reduces the control chattering effect, as compared to the existing adaptive SMC schemes in the literature. Moreover, boundary layer is employed to smooth control discontinuity and further eliminate control chattering. However, the thickness of boundary layer is a trade-off between system tracking accuracy and system stability. By explicitly considering this fact, a fuzzy logic-based boundary layer is proposed together with the designed on-line adaptive control scheme to maintain system stability and tracking accuracy. When there is a trend to overestimate the control parameter, the fuzzy boundary layer can be switched in to appropriately adjust boundary layer thickness to avoid control parameter overestimation and ensure system stability. In such a way, larger parametric uncertainties and actuator faults can be accommodated within the proposed control scheme.

Moreover, by virtue of the designed nonlinear disturbance observer, external disturbances can be compensated without increasing discontinuous control gain which also helps to avoid control chattering. Simulation and experimental tests of a quadrotor helicopter are conducted to validate the effectiveness of the proposed control scheme in the presence of parametric uncertainties, actuator malfunctions and external disturbances. Its advantages are indicated in comparison with a conventional adaptive SMC.

4.1 Introduction

As a classical type of multirotor helicopters, the quadrotor helicopter is a relatively simple and easy-to-fly system with four propellers mounted around a main body. It can be lifted and controlled by the four propellers. In addition, the rotational speeds of the four propellers are independent, which makes it possible to control the roll, pitch, and yaw angle of the quadrotor helicopter. A variety of control strategies have been proposed to maintain good control performance of quadrotor helicopters, including LQR control [21], SMC [23, 121], model predictive control (MPC) [122], robust control [123] and adaptive control [124], to name a few. For many applications, in order to accomplish the specific task, different sensors need to be incorporated into the UAV to make it fully functional. Depending on different applications, the weights and locations of the configured sensors or payloads may vary, which brings a big challenge for the onboard flight controller. Moreover, UAVs are usually employed to work in complex and hazardous environments, such as urban surveillance, fire fighting, and special military actions. These situations may seriously threaten the safety of the UAVs and the expensive onboard instruments/payloads. For instance, considering the applications carried out in urban area, in-flight faults exposed on UAVs may endanger human life and property in addition to the loss of the UAV itself. Hence, it is highly desirable that a UAV is able to tolerate certain parametric uncertainties and system faults without imperiling itself and its surroundings.

SMC is an approach to design robust control systems handling large uncertainties with discontinuous control strategy which demonstrates invariance to so-called matched uncertainties while on a reduced order sliding surface [36, 40, 41]. To be more precise, one design parameter is synthesized in the discontinuous control portion to deal with uncertainties which leads to effective control performance. Recent studies on SMC-based fault-tolerant flight control can be found in [17, 39, 125, 126]. The property of insensitivity to system uncertainties and external disturbances makes SMC as one of the most promising control approaches in the field of FTC. In addition, fuzzy techniques have been proven successful in designing FTCS with application to safety-critical systems. Several research results in the literature are available to advance the development of FTCS by using fuzzy techniques [18, 28, 127–130].

In [128–130], the use of a Takagi-Sugeno (T-S) fuzzy model is established to describe the dynamics of a near space vehicle and an adaptive control approach is applied to alleviate the impacts of actuator faults. Moreover, in [46], SMC approach is intended to serve as an alternative to truly reconfigurable systems for maintaining the desired performance without requiring any fault information. However, this kind of traditional robust control approach makes trade-off between system performance and robustness in order to accommodate certain faults, and in order to effectively implement this conventional SMC, the bound of uncertainty is always needed at the design stage. In fact, at most time, real systems work under fault-free conditions. The consideration of faults at the system design stage will largely degrade system performance under fault-free conditions. If an excessive amount of faults are prescribed, the big trade-off may lead the system performance unacceptable under fault-free conditions which will significantly limit the fault-tolerant capability of the system. For many applications, uncertainties can be added to the system at any time with unknown magnitudes and actuator faults may also occur with unknown magnitudes. Therefore, it is difficult to obtain the exact uncertainty bounds in advance. This difficulty stimulates a new control strategy which incorporates an adaptive scheme into SMC to compensate uncertainties without knowing the exact uncertainty bounds. In [131], a self-constructing fuzzy neural network is designed and incorporated with SMC to obtain the bounds and accommodate actuator faults in

real time. Besides, some researchers are motivated to propose an adaptive sliding mode control (ASMC) to ensure system performance in both fault-free and faulty conditions [17, 39, 125].

Although extensive studies have been conducted for safe operation of aircraft, there are some difficulties that need to be addressed. 1) Most of the studies using SMC and fuzzy techniques to deal with actuator faults in the literature mainly focus on the adaptation of the discontinuous control portion, which may lead to control chattering effect if a severe fault occurs. 2) In order to avoid control chattering, one possible means is to use a thin boundary layer neighboring the designed sliding surface, which, however, will decrease the tracking accuracy. In some faulty conditions, in order to maintain system stability, one may sacrifice certain level of tracking accuracy. Whereas, in fault-free conditions, the boundary layer thickness should be chosen as small as possible to strive for good tracking accuracy. Therefore, the choice of boundary layer thickness is also a trade-off between tracking accuracy and fault-tolerance capability.

In an attempt to solve the aforementioned difficulties to improve the system fault-tolerance capability and robustness while suppressing control chattering, this chapter presents an adaptive fuzzy control strategy to simultaneously accommodate parametric uncertainties, actuator faults, and external disturbances for a quadrotor helicopter based on an integral SMC, a fuzzy boundary layer, and a nonlinear disturbance observer. The major contributions of this chapter are briefly summarized as follows:

- 1) The proposed control strategy can adaptively generate appropriate control signals to compensate parametric uncertainties and actuator faults simultaneously without merely relying on the robust discontinuous control strategy.
- 2) Since the proposed adaptive scheme is synthesized in both continuous and discontinuous control portions, the control effort is significantly reduced for accommodating parametric uncertainties and actuator faults. Thus, larger uncertainties and faults can be tolerated within this control scheme, and the control chattering effect is also suppressed.
- 3) Moreover, a fuzzy logic-based boundary layer is integrated to further eliminate control chattering effect. Based on specific rules, system tracking accuracy can be assured in fault-free and

mild faulty conditions. Whereas, in severe faulty conditions, the system stability can also be maintained with acceptable tracking performance, which further improves fault-tolerant capability of the proposed control strategy. Since the proposed adaptive scheme is also related to boundary layer thickness, the presented fuzzy logic-based boundary layer can also avoid overestimation of adaptive control parameter.

4) The synthesized nonlinear disturbance observer can give an accurate estimation of the external disturbances, which can help to reduce the discontinuous control gain and suppress control chattering.

The remainder of this chapter is organized as follows. The dynamic model of the quadrotor helicopter and problem statement are described in Section 4.2. Section 4.3 presents the detailed design procedure of the proposed integral sliding mode-based adaptive fuzzy control strategy. The simulation and experimental results are provided in Section 4.5 and 4.6, respectively, to demonstrate the effectiveness of the proposed control strategy. Finally, general conclusions of this chapter are summarized in Section 4.7.

4.2 Problem Formulation

4.2.1 Modeling of a Quadrotor Helicopter

The considered quadrotor helicopter is mounted with four motors in a cross configuration, as shown in Fig. 4.1. The front and rear propellers rotate clockwise, whereas the left and right ones spin counter-clockwise.

4.2.2 System Formulation

Focusing on the fault-tolerant attitude control of the quadrotor helicopter, define $x_1 = [\phi, \theta, \psi]^T$ and $x_2 = [p, q, r]^T$. With this state vector, the dynamic equations of the quadrotor helicopter can be resolved into the following equations [15]:

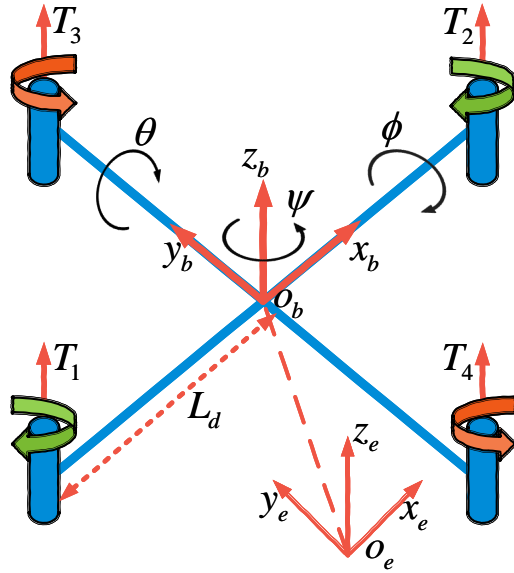


Figure 4.1: Configuration of the studied quadrotor helicopter.

$$\begin{cases} \dot{\phi} = p + q \sin \phi \tan \theta + r \cos \phi \tan \theta \\ \dot{\theta} = q \cos \phi - r \sin \phi \\ \dot{\psi} = q \sin \phi \sec \theta + r \cos \phi \sec \theta \end{cases} . \quad (4-1)$$

By recalling the definitions of x_1 and x_2 , (4–1) can be therefore expressed as:

$$\dot{x}_1 = f_1 + h_1 x_2 \quad (4-2)$$

where $f_1 = [0, 0, 0]^T$ and

$$h_1 = \begin{bmatrix} 1 & \sin \phi \tan \theta & \cos \phi \tan \theta \\ 0 & \cos \phi & -\sin \phi \\ 0 & \sin \phi \sec \theta & \cos \phi \sec \theta \end{bmatrix} . \quad (4-3)$$

Moreover, according to the moment equations of the quadrotor helicopter, one can obtain:

$$\begin{cases} \dot{p} = \frac{(I_{yy} - I_{zz})qr}{I_{xx}} - \frac{I_r\Omega q}{I_{xx}} + \frac{K_u L_d(u_3 - u_4)}{I_{xx}} - \frac{K_4 L_d p}{I_{xx}} \\ \dot{q} = \frac{(I_{zz} - I_{xx})pr}{I_{yy}} + \frac{I_r\Omega p}{I_{yy}} + \frac{K_u L_d(u_1 - u_2)}{I_{yy}} - \frac{K_5 L_d q}{I_{yy}} \\ \dot{r} = \frac{(I_{xx} - I_{yy})pq}{I_{zz}} + \frac{K_y(u_1 + u_2 - u_3 - u_4)}{I_{zz}} - \frac{K_6 r}{I_{zz}} \end{cases}. \quad (4-4)$$

Similarly, by recalling the definition of x_2 , (4-4) can be expressed as:

$$\dot{x}_2 = f_2 + h_2 B_u u + d \quad (4-5)$$

where $u = [u_1, u_2, u_3, u_4]^T$,

$$f_2 = \begin{bmatrix} (I_{yy} - I_{zz})qr/I_{xx} \\ (I_{zz} - I_{xx})pr/I_{yy} \\ (I_{xx} - I_{yy})pq/I_{zz} \end{bmatrix}, \quad (4-6)$$

$$h_2 = \begin{bmatrix} 1/I_{xx} & 0 & 0 \\ 0 & 1/I_{yy} & 0 \\ 0 & 0 & 1/I_{zz} \end{bmatrix}, \quad (4-7)$$

$$d = \begin{bmatrix} -(I_r\Omega q + K_4 L_d p)/I_{xx} \\ I_r\Omega p - K_5 L_d q/I_{yy} \\ -K_6 r/I_{zz} \end{bmatrix}, \quad (4-8)$$

and

$$B_u = \begin{bmatrix} 0 & 0 & K_u L_d & -K_u L_d \\ K_u L_d & -K_u L_d & 0 & 0 \\ K_y & K_y & -K_y & -K_y \end{bmatrix}. \quad (4-9)$$

Therefore, by differentiating (4-2) and recalling (4-5), it gives:

$$\ddot{x}_1 = \dot{f}_1 + \dot{h}_1 x_2 + h_1 f_2 + h_1 h_2 B_u u + d. \quad (4-10)$$

Equation (4–10) can be rewritten formally as:

$$\ddot{x}_1 = F(x_1, x_2) + H(x_1, x_2)B_u u + d \quad (4-11)$$

where $F(x_1, x_2) = \dot{h}_1 x_2 + h_1 f_2$ and $H(x_1, x_2) = h_1 h_2$.

The definition of the above-mentioned parameters can be found in Table 4.1.

Table 4.1: Nomenclature

Parameter	Definition
ϕ, θ, ψ	Roll, pitch, yaw angle
p, q, r	Angular velocity along x_b -, y_b -, z_b -axis
I_{xx}, I_{yy}, I_{zz}	Inertial moment along x_b -, y_b -, z_b -axis
I_r	Inertial moment of the propeller
m	Total mass of the quadrotor helicopter
L_d	The distance between each motor and the COM of the quadrotor helicopter
K_u	A positive gain related to propeller generated force
K_y	A positive gain related to propeller generated torque
K_i ($i = 4, 5, 6$)	Drag coefficients
u_i ($i = 1, 2, 3, 4$)	PWM input of the i th motor
Ω_i ($i = 1, 2, 3, 4$)	The i th propeller's rotational speed

4.2.3 Problem Statement

Consider a nonlinear affine system with parametric uncertainties and disturbances subject to actuator faults as follows:

$$\ddot{x}_1(t) = F(x_1(t), x_2(t)) + H(x_1(t), x_2(t))B_u L_c(t)u(t) + d(t) \quad (4-12)$$

where $x_1(t) \in \mathbb{R}^n$ and $x_2(t) \in \mathbb{R}^n$ are the state vectors, $u(t) \in \mathbb{R}^m$ is the control input vector, and $B_u \in \mathbb{R}^{n \times m}$ is the control effectiveness matrix. The vector $F(x_1(t), x_2(t)) \in \mathbb{R}^n$ is a nonlinear function containing parametric uncertainties, and the bounds of these uncertainties are unknown

a priori, $H(x_1(t), x_2(t)) \in \mathbb{R}^{n \times n}$. $d(t) \in \mathbb{R}^n$ represents unknown but bounded disturbances, i.e., $\|d(t)\| \leq D_d$. $L_c(t) = \text{diag}([l_{c1}(t), l_{c2}(t), \dots, l_{cm}(t)])$ represents the control effectiveness level of the actuators, where $l_{ci}(t)$ ($i = 1, 2, \dots, m$) is a scalar satisfying $0 \leq l_{ci}(t) \leq 1$. If $l_{ci}(t) = 1$, the i th actuator works well, otherwise, the i th actuator encounters certain level of fault with a special case $l_{ci}(t) = 0$ denoting the complete failure of the i th actuator.

With respect to the parametric uncertainties of the system, let $\hat{F}(x_1(t), x_2(t))$ denote the estimation of the vector $F(x_1(t), x_2(t))$. Therefore, the estimated error $\tilde{F}(x_1(t), x_2(t))$ can be obtained as follows:

$$\tilde{F}(x_1(t), x_2(t)) = \hat{F}(x_1(t), x_2(t)) - F(x_1(t), x_2(t)). \quad (4-13)$$

For the sake of simplicity, the notation t is omitted in the sequel, e.g., $x(t)$ is expressed as x .

4.3 Design of Adaptive Fuzzy Fault-Tolerant Flight Control

In this section, an integral SMC and fuzzy boundary layer-based adaptive fault-tolerant control strategy is designed with application to a quadrotor helicopter in the presence of parametric uncertainties and actuator malfunctions. The schematic of the proposed control strategy is illustrated in Fig. 4.2. There are two problems to be addressed. The first problem is to construct an integral sliding mode-based control law against parametric uncertainties and actuator faults. The second one is the problem of exploring the adaptive tuning method to determine the control parameters within the developed fault-tolerant flight control scheme.

4.3.1 Integral Sliding Mode Control

SMC design is typically composed of two steps. The first step features the construction of a sliding surface, on which the system performance can be maintained as expected. The second step is concerned with the selection of the control scheme to force the sliding variable reach the sliding surface, and hereafter keep the sliding motion within a vicinity of the designed sliding surface.

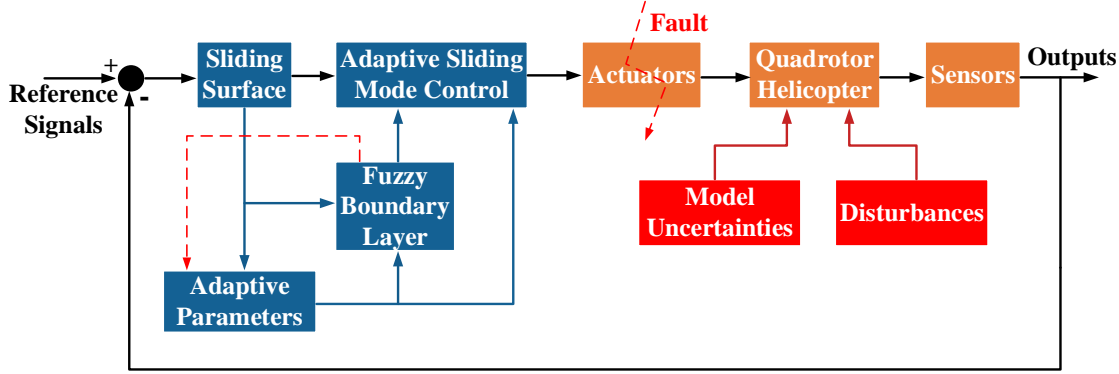


Figure 4.2: The schematic of the proposed control strategy.

By denoting x_1^d as the desired trajectory, the tracking error vector can be defined as:

$$\tilde{x}_1 = x_1 - x_1^d = \begin{bmatrix} \phi - \phi_d \\ \theta - \theta_d \\ \psi - \psi_d \end{bmatrix}. \quad (4-14)$$

With this tracking error vector, the integral sliding surface for the system can be defined by the following set:

$$S = \{\tilde{x}_1 \in \mathbb{R}^n : \sigma(\tilde{x}_1) = 0\}. \quad (4-15)$$

The switching function $\sigma(\tilde{x}_1)$ is defined as:

$$\sigma(\tilde{x}_1) = \sigma_0 + z \quad (4-16)$$

where

$$\sigma_0 = c\tilde{x}_1 + \dot{\tilde{x}}_1, \quad (4-17)$$

and

$$\begin{aligned} \dot{z} &= -c\dot{\tilde{x}}_1 + k_{c2}\dot{\tilde{x}}_1 + k_{c1}\tilde{x}_1 \\ z(0) &= -c\tilde{x}_1(t_0) - \dot{\tilde{x}}_1(t_0). \end{aligned} \quad (4-18)$$

From this definition, one can observe that σ_0 is the linear combination of the tracking errors,

which is similar to the conventional SMC design. Note that z includes the integral term which renders the sliding motion occurs at the initial time instant t_0 . Therefore, the system trajectory under integral SMC starts from the designed sliding surface and the reaching phase is eliminated accordingly. This feature sets the study apart from conventional SMC. By combining (4–17) and (4–18), (4–16) can be rewritten as:

$$\sigma = \dot{\tilde{x}}_1 + k_{c2}\tilde{x}_1 + k_{c1} \int_{t_0}^t \tilde{x}_1(\tau) d\tau - k_{c2}\tilde{x}_1(t_0) - \dot{\tilde{x}}_1(t_0) \quad (4-19)$$

where the diagonal matrices $k_{c1} \in \mathbb{R}^{n \times n}$ and $k_{c2} \in \mathbb{R}^{n \times n}$ represent the design parameters.

After obtaining the sliding surface, then, the next problem is to design an appropriate control law to make the sliding surface attractive. The design problem can be formulated as that, given $x_1(t_0) = x_1^0(t_0)$, the identity $x_1 = x_1^0$ should be guaranteed all the time $t \geq t_0$ with x_1^0 denoting the state of the ideal system without any parametric uncertainties, actuator faults and disturbances. According to this requirement, the corresponding control law can be constructed as:

$$u = u_0 + u_1 \quad (4-20)$$

where u_0 is the continuous nominal control portion to stabilize the ideal system, and u_1 is the discontinuous control portion for compensating the perturbations and disturbances in order to ensure the expected sliding motion.

The nominal control u_0 is designed by equalizing $\dot{\sigma} = 0$, and the disturbance d is omitted in this case as shown below:

$$u_0 = B_u^+ H^{-1} (\ddot{x}_1^d - k_{c2}\dot{\tilde{x}}_1 - k_{c1}\tilde{x}_1 - F) \quad (4-21)$$

where $B_u^+ = B_u^T (B_u B_u^T)^{-1}$.

The discontinuous control portion to reject the disturbance d is designed as:

$$u_1 = -B_u^+ H^{-1} k_{c3} \text{sign}(\sigma) \quad (4-22)$$

where $k_{c3} \in \mathbb{R}^{n \times n}$ is a diagonal matrix constructed by positive high gains which can make the designed sliding surface attractive.

In this way, the control law can be developed as:

$$u = B_u^+ H^{-1} (\ddot{x}_1^d - k_{c2}\dot{\tilde{x}}_1 - k_{c1}\tilde{x}_1 - F - k_{c3}\text{sign}(\sigma)). \quad (4-23)$$

Theorem 4.1 Consider the nonlinear system (4-12) with bounded disturbance, and the sliding variable dynamics (4-19). If the matrix k_{c3} is designed as $k_{c3} \geq \eta + D_d$ with $\eta > 0$, by employing the feedback control law (4-23), the sliding motion can be achieved at the initial time instant and maintained on the designed sliding surface thereafter.

Proof 4.1 Consider the Lyapunov candidate function as:

$$V_3 = \frac{1}{2} \sigma^T \sigma. \quad (4-24)$$

The time derivative of V_3 for $\sigma \neq 0$ is:

$$\begin{aligned} \dot{V}_3 &= \sigma^T \dot{\sigma} \\ &= \sigma^T (\ddot{\tilde{x}}_1 + k_{c2}\dot{\tilde{x}}_1 + k_{c1}\tilde{x}_1) \\ &= \sigma^T (F + H B_u B_u^+ H^{-1} (\ddot{x}_1^d - k_{c2}\dot{\tilde{x}}_1 - k_{c1}\tilde{x}_1 \\ &\quad - F - k_{c3}\text{sign}(\sigma)) + d - \dot{x}_1^d + k_{c2}\dot{\tilde{x}}_1 + k_{c1}\tilde{x}_1) \\ &= \sigma^T (-k_{c3}\text{sign}(\sigma) + d) \\ &\leq \sigma^T (-(\eta + D_d)\text{sign}(\sigma) + d) \\ &\leq -\eta \|\sigma\|. \end{aligned} \quad (4-25)$$

Thus, the system satisfies the standard η -reachability condition, and the disturbance is compensated by using the control law (4–23).

However, in order to account for perturbations and disturbances, the control discontinuity will be increased which may lead to control chattering. One can remove this condition by smoothing the control discontinuity in a thin boundary layer neighboring the designed sliding surface [132]. The boundary layer can be formulated as follows:

$$\bar{B} = \{\tilde{x}_1, \dot{\tilde{x}}_1, \|\sigma\| \leq \Phi\} \quad (4-26)$$

where the vector Φ is the boundary layer thickness with positive values.

Accordingly, the developed control law becomes:

$$u = B_u^+ H^{-1} (\ddot{x}_1^d - k_{c2} \dot{\tilde{x}}_1 - k_{c1} \tilde{x}_1 - F - k_{c3} \text{sat}(\sigma/\Phi)) \quad (4-27)$$

where the sat function is defined as:

$$\text{sat}(\sigma/\Phi) = \begin{cases} \text{sign}(\sigma) & \text{if } \|\sigma\| > \Phi \\ \sigma/\Phi & \text{if } \|\sigma\| \leq \Phi \end{cases}. \quad (4-28)$$

4.3.2 Adaptive Sliding Mode Control Design

With the consideration of actuator faults, the matrix L_c in (4–12) is not an identity matrix. If the control law is not changed accordingly, the overall tracking performance will be degraded. Let $\tilde{H}B_u = -HB_u(I - L_c)$, the following system dynamics can be obtained:

$$\ddot{x}_1 = F + (H + \tilde{H})B_u u + d. \quad (4-29)$$

Observing from (4–29), in order to maintain the closed-loop system tracking performance in the presence of actuator faults, the matrix H should be adjusted to eliminate the effect of actuator

faults. In this case, the estimated value of H can be expressed as $\hat{H} = H + \tilde{H}$. Moreover, in practice, there exist parametric uncertainties more or less in the system. By recalling (4–13), the estimation variables \hat{F} and \hat{H} should be employed to derive the corresponding control law instead of F and H .

By denoting $\hat{\Gamma} = H^{-1}\hat{F}$ and $\hat{\Psi} = \hat{h}_2^{-1}$, the control law (4–27) can be rearranged as:

$$u = B_u^+(-\hat{\Gamma} + \hat{\Psi}h_1^{-1}(\ddot{x}_1^d - k_{c2}\dot{x}_1 - k_{c1}\tilde{x}_1 - k_{c3}\text{sat}(\sigma/\Phi))). \quad (4-30)$$

With the purpose of compensating the parametric uncertainties and actuator faults, the estimations $\hat{\Gamma}$ and $\hat{\Psi}$ need to be updated on-line. The on-line adaptive laws for estimating the piecewise uncertain parameters are designed as:

$$\dot{\hat{\Gamma}}_i = \sigma_{\Delta i}, \quad i = 1, \dots, n \quad (4-31)$$

$$\begin{aligned} \dot{\hat{\Psi}}_{ij} &= (-\ddot{x}_{1i}^d + k_{ij}^{c2}\dot{x}_{1i} + k_{ij}^{c1}\tilde{x}_{1i} + k_{ij}^{c3}\text{sat}(\sigma_i/\Phi_i))\sigma_{\Delta j}^T \\ &\quad i = j = 1, \dots, n \end{aligned} \quad (4-32)$$

where σ_{Δ} is the measurement of the algebraic distance between the current sliding variable and the boundary layer defined as:

$$\sigma_{\Delta i} = \sigma_i - \Phi_i \text{sat}(\sigma_i/\Phi_i). \quad (4-33)$$

It features $\dot{\sigma}_{\Delta i} = \dot{\sigma}_i$ if the sliding variable is outside the boundary layer and $\dot{\sigma}_{\Delta i} = 0$ if the sliding variable is inside the boundary layer.

Remark 4.1 *With the help of the designed adaptive schemes, as long as the sliding variable is out of the boundary layer where the control performance is unacceptable, the adaptation will be triggered to bring the sliding variable back inside the defined boundary layer to maintain the prescribed system tracking performance. Moreover, when the sliding variable reaches or inside the boundary layer, the behavior of adaptation will be ceased. In such a way, the overestimation of the control parameters can be avoided compared to the adaptive approaches in the literature*

[16, 39, 47] where the adaptation is not easy to be stopped due to the use of sliding variable for constructing the adaptive scheme.

4.3.3 Fuzzy Boundary Layer Design

As described in the previous section, the boundary layer approach is exploited to avoid control chattering induced by control discontinuity. The thickness of the boundary layer is an important design parameter which determines system tracking accuracy. Moreover, it is of paramount importance to ensure system stability in the presence of parametric uncertainties and actuator faults. When parametric uncertainties and actuator faults become larger and severer, the afore-designed adaptive control law can no longer bring the sliding variable within the boundary layer, and the system stability cannot be maintained anymore due to the overestimation of adaptive control parameter. In this case, the thickness of boundary layer should be enlarged to degrade tracking performance and maintain system stability. This section presents a fuzzy logic-based approach for adjusting the boundary layer thickness to obtain a proper trade-off between tracking accuracy and system stability.

To this end, the thickness of the boundary layer Φ_i is the output of the fuzzy logic control scheme, which is determined by two parameters: the absolute value of the sliding variable $|\sigma_i|$ and the rate of adaptation parameter $\dot{\hat{\Psi}}_{ij}$, namely,

$$\Delta\Phi_i = f_{FSMC}(|\sigma_i|, \dot{\hat{\Psi}}_{ij}). \quad (4-34)$$

The main idea for constructing fuzzy rules used in this chapter can be summarized as follows:

- 1) When the rate of adaptation becomes increasing, the boundary layer thickness should be increased to smooth the actuator control input;

- 2) The boundary layer thickness should be decreased if the rate of adaptation is low or zero.

This is because, in order to strive for tracking accuracy, the thickness of the boundary layer is needed to be as small as possible;

- 3) When the absolute value of the sliding variable is high, the trajectory of sliding motion is far away from the nominal sliding surface. In this case, a steep saturation function is desired to decrease the duration of the reaching phase;
- 4) When the absolute value of the sliding variable is low, the trajectory of sliding motion is close to the nominal sliding surface, thus a steep saturation function is likely to introduce control chattering.

Implementation of the above four guidelines can naturally employ fuzzy logic rules to construct a tuning mechanism for the boundary layer thickness Φ_i . The designed fuzzy rules for online tuning of the boundary thickness are detailed in Table 4.2 and Fig. 4.3, where the subscript “PB” stands for positive big, “NB” is negative big, and “NS” is negative small. Finally, the boundary layer thickness is obtained by $\Phi_i(k) = \Phi_i(k - 1) + \Delta\Phi_i(k - 1)$ at every iteration.

Table 4.2: Fuzzy Rules

		$\dot{\Psi}_{ij}$	
		Small $\dot{\Psi}_{ij}$	Big $\dot{\Psi}_{ij}$
$ \sigma_i $	Small $ \sigma_i $	0	$\Delta\Phi_{iPB}$
	Big $ \sigma_i $	$\Delta\Phi_{iNB}$	$\Delta\Phi_{iNS}$

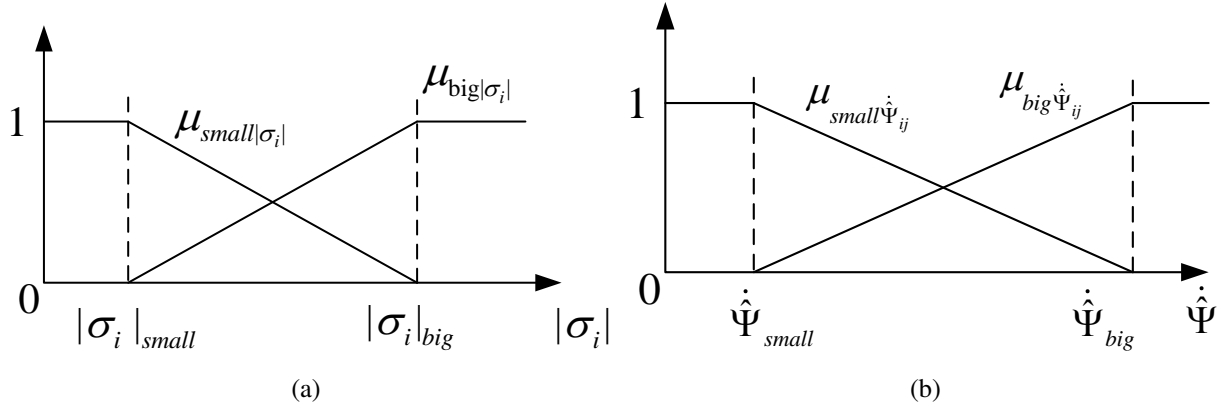


Figure 4.3: The membership functions.

Theorem 4.2 Consider a nonlinear affine system (4–12) with parametric uncertainties, actuator faults and bounded disturbances. Given the designed integral sliding surface (4–19), by employing the feedback control law (4–30), the adaptation laws (4–31)–(4–32), and the fuzzy boundary layer (4–34), the sliding motion can be achieved and maintained inside the boundary layer regardless of the parametric uncertainties, actuator faults and disturbances with the discontinuous control gain chosen as $k_{c3} \geq \eta + D_d$.

Proof 4.2 Consider the following Lyapunov candidate function:

$$V_4 = \sum_{i=j=1}^n \frac{1}{2} \left[\sigma_{\Delta i}^2 + \Psi_{ij}^{-1} (\hat{\Gamma}_i - \Gamma_i)^2 + \Psi_{ij}^{-1} (\hat{\Psi}_{ij} - \Psi_{ij})^2 \right]. \quad (4-35)$$

Then, the derivative of the selected Lyapunov candidate function is obtained as:

$$\begin{aligned} \dot{V}_4 &= \sum_{i=j=1}^n [\sigma_{\Delta i} \dot{\sigma}_{\Delta i} + \Psi_{ij}^{-1} (\hat{\Gamma}_i - \Gamma_i) \dot{\hat{\Gamma}}_i + \Psi_{ij}^{-1} (\hat{\Psi}_{ij} - \Psi_{ij}) \dot{\hat{\Psi}}_{ij}] \\ &= \sum_{i=j=1}^n [\sigma_{\Delta i} (\Psi_{ij}^{-1} \Gamma_i - \Psi_{ij}^{-1} \hat{\Gamma}_i + \Psi_{ij}^{-1} \hat{\Psi}_{ij} (\ddot{x}_{1i}^d - k_{ij}^{c2} \dot{\tilde{x}}_{1i} \\ &\quad - k_{ij}^{c1} \tilde{x}_{1i} - k_{ij}^{c3} \text{sat}(\sigma_i/\Phi_i)) + d_i - \ddot{x}_{1i}^d + k_{ij}^{c2} \dot{\tilde{x}}_{1i} \\ &\quad + k_{ij}^{c1} \tilde{x}_{1i}) + \Psi_{ij}^{-1} (\hat{\Gamma}_i - \Gamma_i) \dot{\hat{\Gamma}}_i + \Psi_{ij}^{-1} (\hat{\Psi}_{ij} - \Psi_{ij}) \dot{\hat{\Psi}}_{ij}] \\ &= \sum_{i=j=1}^n [\Psi_{ij}^{-1} (\hat{\Gamma}_i - \Gamma_i) (\dot{\hat{\Gamma}}_i - \sigma_{\Delta i}) + (\Psi_{ij}^{-1} \hat{\Psi}_{ij} - 1) (\ddot{x}_{1i}^d \\ &\quad - k_{ij}^{c2} \dot{\tilde{x}}_{1i} - k_{ij}^{c1} \tilde{x}_{1i}) \sigma_{\Delta i} + (\Psi_{ij}^{-1} \hat{\Psi}_{ij} - 1) \dot{\hat{\Psi}}_{ij} \\ &\quad + d_i \sigma_{\Delta i} - \Psi_{ij}^{-1} \hat{\Psi}_{ij} k_{ij}^{c3} \text{sat}(\sigma_i/\Phi_i) \sigma_{\Delta i}] \\ &= \sum_{i=j=1}^n [\Psi_{ij}^{-1} (\hat{\Gamma}_i - \Gamma_i) (\dot{\hat{\Gamma}}_i - \sigma_{\Delta i}) + (\Psi_{ij}^{-1} \hat{\Psi}_{ij} - 1) (\dot{\hat{\Psi}}_{ij} \\ &\quad + (\ddot{x}_{1i}^d - k_{ij}^{c2} \dot{\tilde{x}}_{1i} - k_{ij}^{c1} \tilde{x}_{1i} - k_{ij}^{c3} \text{sat}(\sigma_i/\Phi_i)) \sigma_{\Delta i}) \\ &\quad + d_i \sigma_{\Delta i} - k_{ij}^{c3} \text{sat}(\sigma_i/\Phi_i) \sigma_{\Delta i}]. \end{aligned} \quad (4-36)$$

Substituting (4–31) and (4–32) into (4–36) leads to:

$$\begin{aligned}
\dot{V}_4 &= \sum_{i=j=1}^n [-k_{ij}^{c3} \text{sat}(\sigma_i/\Phi_i) \sigma_{\Delta i} + d_i \sigma_{\Delta i}] \\
&\leq \sum_{i=j=1}^n [-(\eta_i + D_{di}) \text{sat}(\sigma_i/\Phi_i) \sigma_{\Delta i} + d_i \sigma_{\Delta i}] \\
&\leq \sum_{i=j=1}^n [-\eta_i |\sigma_{\Delta i}|].
\end{aligned} \tag{4–37}$$

Thus, the system satisfies the standard η –reachability condition, and the performance of the system is maintained with the proposed control law under parametric uncertainties, actuator faults, and bounded disturbances.

Remark 4.2 When large actuator fault occurs, if the chosen boundary layer thickness is not big enough, the sliding variable cannot be brought back into the defined boundary layer, which will result in the overestimation of adaptive control parameter. By employing the proposed fuzzy logic-based boundary layer, the overestimation of adaptive control parameter can be avoided and therefore system stability is maintained.

4.4 Active Disturbance Rejection

It should be pointed out that the invariance property against the so-called matched uncertainties and disturbances is accomplished by incorporating a discontinuous term in the controller, which results in the high-frequency chattering behavior of the control input and the designed switching function. To reduce or even eliminate the chattering effect, the simple and attractive approach is to soften the discontinuous control term by its continuous approximation at the cost of a slight deterioration of control performance. Moreover, the choice of the discontinuous control gain is usually based on the boundary assumption of disturbance, which will significantly affect system performance in normal condition due to the use of large discontinuous control gain. Therefore, a disturbance estimation-based feedforward compensation scheme is combined with the developed

adaptive fuzzy SMC feedback control law to relax the boundary assumption of disturbance and extend the applicability of the disturbance observer technique. The schematic of the proposed disturbance observer-based control strategy is depicted in Fig. 4.4. By incorporating the nonlinear disturbance observer, the use of the discontinuous control strategy will be reduced significantly. Moreover, it can leave more room for tolerating larger parametric uncertainties and actuator faults due to the less use of discontinuous control gain for disturbance compensation.

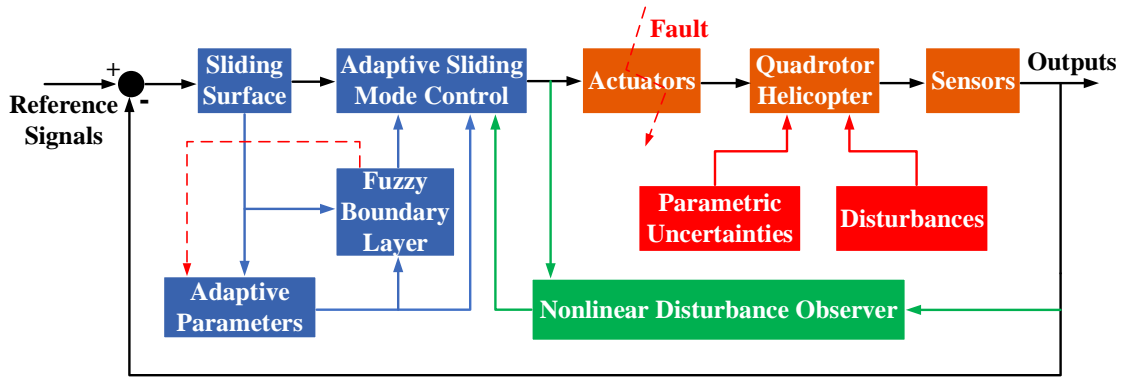


Figure 4.4: The schematic of the proposed disturbance observer-based control strategy.

4.4.1 Design of Disturbance Observer

Consider the nonlinear affine system depicted as follows:

$$\begin{cases} \dot{x}_1 = f_1 + h_1 x_2 \\ \dot{x}_2 = f_2 + h_2 B_u u + d \end{cases} . \quad (4-38)$$

Assumption 4.1 *The derivative of the disturbances in system (4-38) is bounded and satisfies*
 $\lim_{t \rightarrow \infty} \dot{d} = 0$.

To estimate the unknown disturbance d , a nonlinear disturbance observer is designed as:

$$\begin{aligned} \dot{z} &= -l z - l [p + F(x_1, x_2) + H(x_1, x_2) B_u u] \\ \hat{d} &= z + p \end{aligned} \quad (4-39)$$

where z is the internal state of the nonlinear observer, p is the nonlinear function to be designed, and l is the nonlinear disturbance observer gain which is determined by:

$$l = \frac{\partial p}{\partial x_2}. \quad (4-40)$$

With the estimated disturbance \hat{d} , the disturbance estimation error is defined as:

$$e_d = d - \hat{d}. \quad (4-41)$$

Combining (4-38), (4-39), (4-40), and (4-41), the dynamics of disturbance estimation error can be governed by:

$$\begin{aligned} \dot{e}_d &= \dot{d} - \dot{\hat{d}} \\ &= -\dot{z} - \frac{\partial p}{\partial x_2} \dot{x}_2 \\ &= lz + l[p + f_2 + h_2 B_u u] - l[f_2 + h_2 B_u u + d] \\ &= l(\hat{d} - p) + l[p + f_2 + h_2 B_u u] - l[f_2 + h_2 B_u u + d] \\ &= -le_d. \end{aligned} \quad (4-42)$$

Therefore, the nonlinear disturbance observer can estimate unknown constant disturbance if the observer gain l is chosen such that the disturbance estimation error dynamics is asymptotically stable.

4.4.2 Synthesize of Disturbance Observer

Assumption 4.2 *The disturbance estimation error e_d in (4-41) is bounded by $E_d = \sup_{t>0} |e_d|$.*

By recalling the designed control law (4-30) in the previous section and considering the disturbance estimation (4-39), the corresponding control law and adaptation law can be redesigned

as follows:

$$u = B_u^+(-\hat{\Gamma} + \hat{\Psi} h_1^{-1}(\ddot{x}_1^d - \hat{d} - k_{c2}\dot{\tilde{x}}_1 - k_{c1}\tilde{x}_1 - k_{c3}\text{sat}(\sigma/\Phi))) \quad (4-43)$$

$$\begin{aligned} \dot{\hat{\Psi}}_{ij} &= (-\ddot{x}_{1i}^d + \hat{d}_i + k_{ij}^{c2}\dot{\tilde{x}}_{1i} + k_{ij}^{c1}\tilde{x}_{1i} + k_{ij}^{c3}\text{sat}(\sigma_i/\Phi_i))\sigma_{\Delta j}^T. \\ i &= j = 1, \dots, n \end{aligned} \quad (4-44)$$

Theorem 4.3 Consider a nonlinear affine system (4–38) with parametric uncertainties, actuator faults and unknown constant disturbances. Given the designed integral sliding surface (4–19), by employing the disturbance estimation (4–39), the feedback control law (4–43), the adaptation laws (4–31) and (4–44), and the fuzzy boundary layer (4–34), the sliding motion can be achieved and maintained inside the boundary layer regardless of the parametric uncertainties, actuator faults and disturbances with the discontinuous gain chosen as $k_{c3} \geq \eta + E_d$.

Proof 4.3 Consider the following Lyapunov candidate function:

$$V_5 = \sum_{i=j=1}^n \frac{1}{2} \left[\sigma_{\Delta i}^2 + \Psi_{ij}^{-1}(\hat{\Gamma}_i - \Gamma_i)^2 + \Psi_{ij}^{-1}(\hat{\Psi}_{ij} - \Psi_{ij})^2 \right]. \quad (4-45)$$

Then, the derivative of the selected Lyapunov candidate function is obtained as:

$$\begin{aligned} \dot{V}_5 &= \sum_{i=j=1}^n [\sigma_{\Delta i}\dot{\sigma}_{\Delta i} + \Psi_{ij}^{-1}(\hat{\Gamma}_i - \Gamma_i)\dot{\hat{\Gamma}}_i + \Psi_{ij}^{-1}(\hat{\Psi}_{ij} - \Psi_{ij})\dot{\hat{\Psi}}_{ij}] \\ &= \sum_{i=j=1}^n [\sigma_{\Delta i}(\Psi_{ij}^{-1}\Gamma_i - \Psi_{ij}^{-1}\hat{\Gamma}_i + \Psi_{ij}^{-1}\hat{\Psi}_{ij}(\ddot{x}_{1i}^d - \hat{d}_i - k_{ij}^{c2}\dot{\tilde{x}}_{1i} \\ &\quad - k_{ij}^{c1}\tilde{x}_{1i} - k_{ij}^{c3}\text{sat}(\sigma_i/\Phi_i)) + d_i - \ddot{x}_{1i}^d + k_{ij}^{c2}\dot{\tilde{x}}_{1i} \\ &\quad + k_{ij}^{c1}\tilde{x}_{1i}) + \Psi_{ij}^{-1}(\hat{\Gamma}_i - \Gamma_i)\dot{\hat{\Gamma}}_i + \Psi_{ij}^{-1}(\hat{\Psi}_{ij} - \Psi_{ij})\dot{\hat{\Psi}}_{ij}] \\ &= \sum_{i=j=1}^n [\Psi_{ij}^{-1}(\hat{\Gamma}_i - \Gamma_i)(\dot{\hat{\Gamma}}_i - \sigma_{\Delta i}) + (\Psi_{ij}^{-1}\hat{\Psi}_{ij} - 1)(\dot{\hat{\Psi}}_{ij} \\ &\quad + (\ddot{x}_{1i}^d - \hat{d}_i - k_{ij}^{c2}\dot{\tilde{x}}_{1i} - k_{ij}^{c1}\tilde{x}_{1i} - k_{ij}^{c3}\text{sat}(\sigma_i/\Phi_i))\sigma_{\Delta i}) \\ &\quad + e_{di}\sigma_{\Delta i} - k_{ij}^{c3}\text{sat}(\sigma_i/\Phi_i)\sigma_{\Delta i}]. \end{aligned} \quad (4-46)$$

Substituting (4–31) and (4–44) into (4–46) leads to:

$$\begin{aligned}
\dot{V}_5 &= \sum_{i=j=1}^n [-k_{ij}^{c3} \text{sat}(\sigma_i/\Phi_i) \sigma_{\Delta i} + e_{di} \sigma_{\Delta i}] \\
&\leq \sum_{i=j=1}^n [-(\eta_i + E_{di}) \text{sat}(\sigma_i/\Phi_i) \sigma_{\Delta i} + e_{di} \sigma_{\Delta i}] \\
&\leq \sum_{i=j=1}^n [-\eta_i |\sigma_{\Delta i}|].
\end{aligned} \tag{4–47}$$

Thus, the system satisfies the standard η –reachability condition, and the performance of the system is maintained with the proposed control law under parametric uncertainties, actuator faults, and unknown constant disturbances.

Remark 4.3 To guarantee stability, the discontinuous control gain of the disturbance observer-based adaptive fuzzy SMC is designed as $k_{c3} \geq \eta + \sup_{t>0} |d - \hat{d}|$. Compared to that of the proposed adaptive fuzzy SMC in the previous section which is $k_{c3} \geq \eta + \sup_{t>0} |d|$, the value of the discontinuous control gain is reduced significantly since the disturbance has been precisely estimated by disturbance observer, and the magnitude of estimation error can be kept much smaller than the magnitude of disturbance. In this case, the chattering problem can be alleviated to some extent.

4.5 Simulation Results

In this section, in order to demonstrate the performance of the proposed control strategy, a series of numerical simulations based on the studied quadrotor helicopter is carried out. In the first scenario, the quadrotor helicopter is firstly lifted to 0.8 m to pick up a payload with 0.6 kg. With this payload, it is then lifted to 2 m and commanded to follow a set of pre-designed trajectory. During this phase, an actuator fault is injected to actuator #1 at 50 s. At the end, the payload is dropped from the air to the target area. During the whole flight phase, the mass of the payload and the level of actuator fault are both unknown to the onboard controller. With the synthesized adaptive schemes, it should have the capability to estimate the uncertain parameters adaptively and

maintain the tracking performance of the quadrotor helicopter throughout the entire mission.

The tracking performances of height and pitch motion are shown in Figs. 4.5 and 4.6. Compared to the commonly used LQR controller [21], the proposed adaptive fuzzy SMC shows a better tracking performance with the capability to estimate the total mass of the quadrotor helicopter and to compensate the actuator fault. Whereas, when the payload is added to and released from the quadrotor helicopter, the height tracking performance using LQR has a big fluctuation. Moreover, when actuator fault occurs, the compared LQR controller cannot maintain the original tracking performance anymore. The estimation of the total mass of the quadrotor helicopter is shown in Fig. 4.7, from which it can be seen that when the payload is added and released, the proposed adaptive scheme can accurately estimate the total mass of the quadrotor helicopter.

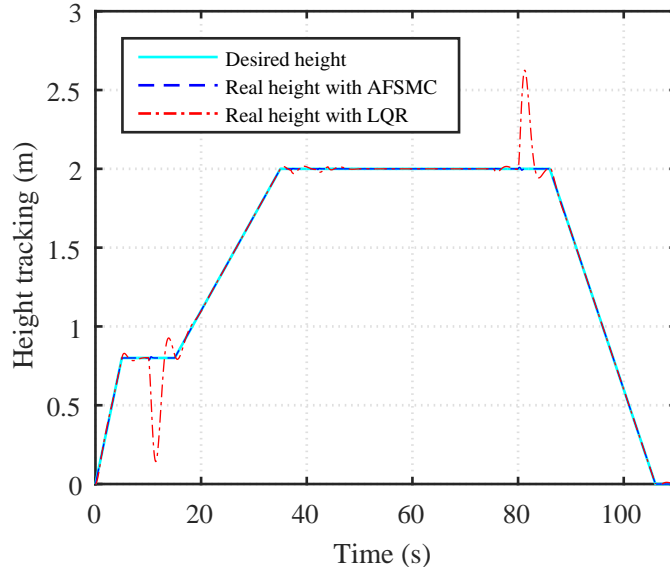


Figure 4.5: Tracking performances of height motion with different control approaches.

The second scenario aims to verify the effectiveness of the proposed active disturbance rejection control scheme. In order to show the advantage of the disturbance observer-based control strategy, a step external disturbance $d = 0.5$ is imposed on the quadrotor helicopter at 10 s. It can be observed from Figs. 4.8 and 4.9, by using the designed nonlinear disturbance observer, the tracking performance of pitch motion can be maintained as the original one after disturbance is injected. Whereas, if the disturbance observer is not incorporated with control law design, after

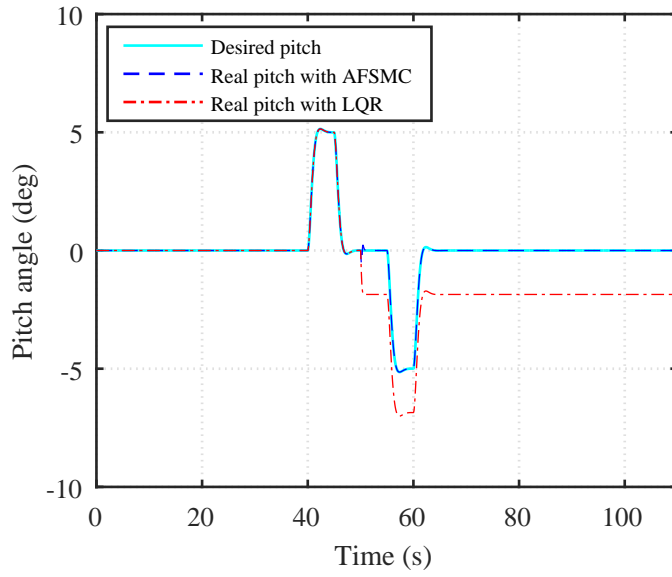


Figure 4.6: Tracking performances of pitch motion with different control approaches.

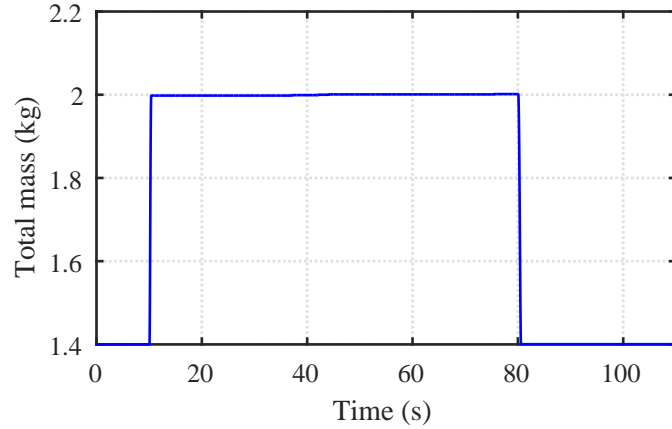


Figure 4.7: Estimation of the total mass of the quadrotor helicopter.

disturbance is injected, by using the same control parameters, there exists a constant tracking error compared to the one with disturbance observer-based control strategy. Moreover, as shown in Fig. 4.10, the imposed disturbance can be accurately estimated by the designed disturbance observer.

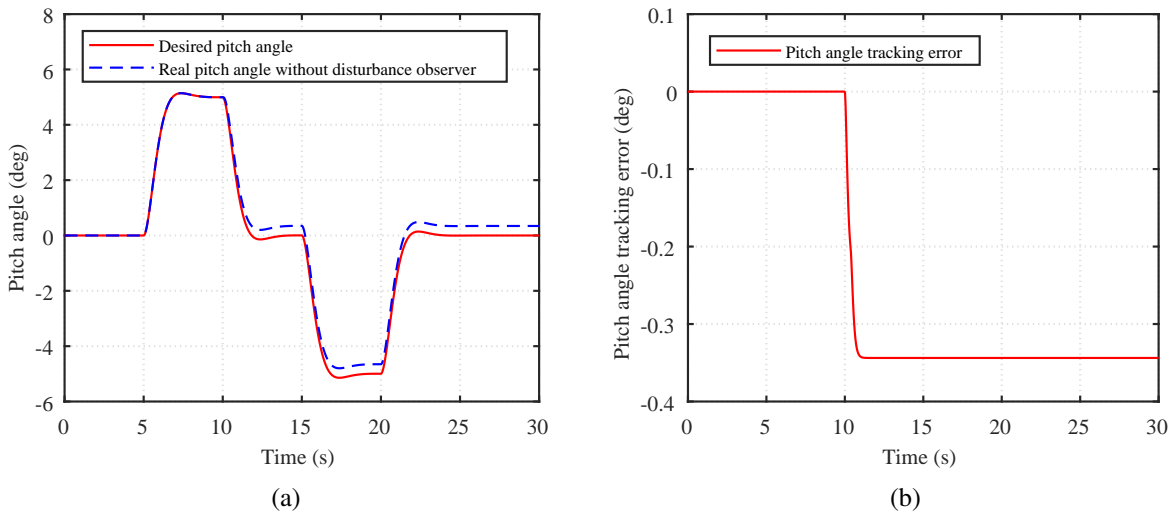


Figure 4.8: Tracking performance of pitch motion without disturbance observer.

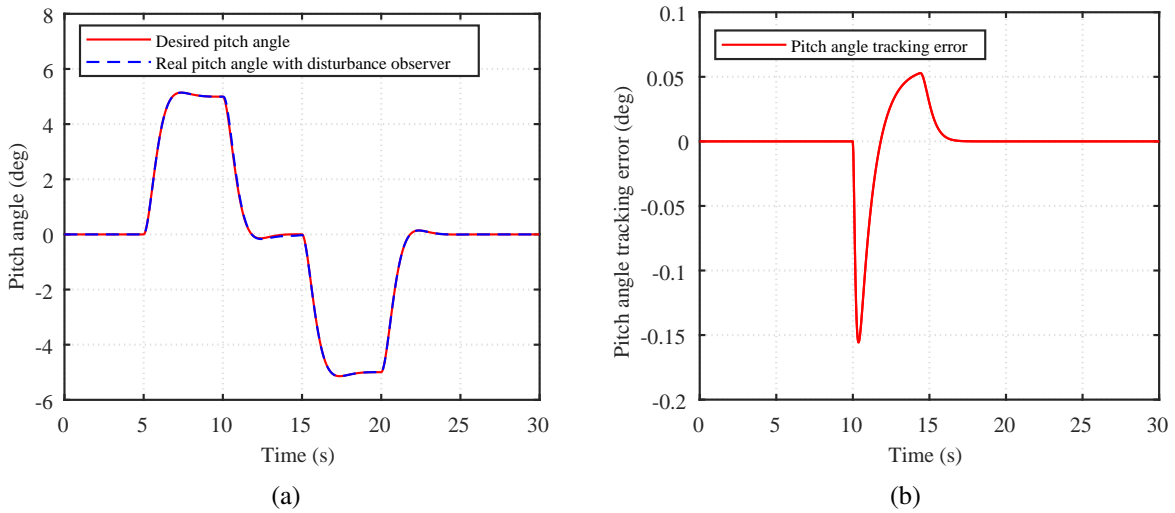


Figure 4.9: Tracking performance of pitch motion with disturbance observer.

4.6 Experimental Results

In order to validate the performance of the proposed adaptive fuzzy control strategy for accommodating parametric uncertainties and actuator faults, experimental tests based on the quadrotor helicopter have been carried out. Moreover, the comparative study between the developed control scheme and the adaptive SMC scheme presented in [39] is conducted.

The uncertainties corresponding to the roll, pitch and yaw moment of inertia (I_{xx} , I_{yy} , I_{zz})

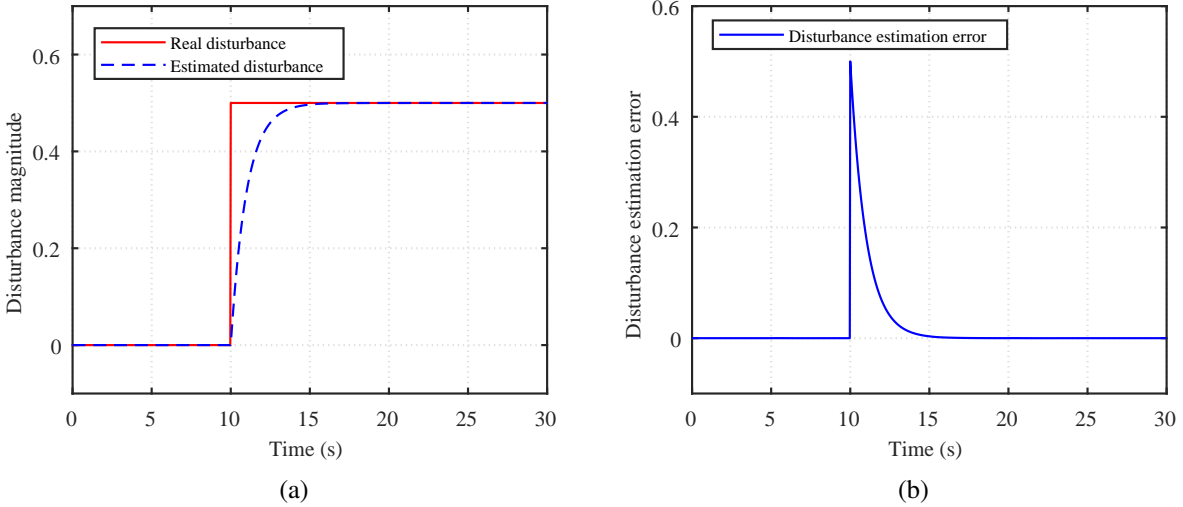


Figure 4.10: Estimation of the imposed disturbance.

are set as 10% of the nominal values. Focusing on the fault pattern of the actuators, two different faulty scenarios are considered which are listed in Table 4.3. In Scenario 1, a 30% loss of control effectiveness fault is injected to actuator #1 at 25 s. A severer faulty case of 50% loss of control effectiveness is examined in Scenario 2. The control parameters are chosen as $k_{c1} = \text{diag}([20, 20, 10])$, $k_{c2} = \text{diag}([100, 100, 25])$, $k_{c3} = \text{diag}([12, 12, 10])$, $\eta = \text{diag}([0.1, 0.1, 0.1])$, and $\Phi = [0.2, 0.2, 0.15]^T$. Based on the aforementioned rules, the fuzzy surface for pitch motion is shown in Fig. 4.11. Furthermore, in order to quantitatively evaluate the tracking performance, define:

$$e_{RMSE} = \sqrt{\frac{1}{t_1 - t_0} \int_{t_0}^{t_1} |x_1 - x_1^d|^2 d\tau} \quad (4-48)$$

where $[t_0, t_1]$ covers the time frame of the overall experiment test.

Table 4.3: Fault Scenarios Considered in Real Flight Experiment

Fault Scenario	Type & Magnitude	Position	Time Period (s)
1	30% loss of control effectiveness	Actuator #1	25–60
2	50% loss of control effectiveness	Actuator #1	25–60

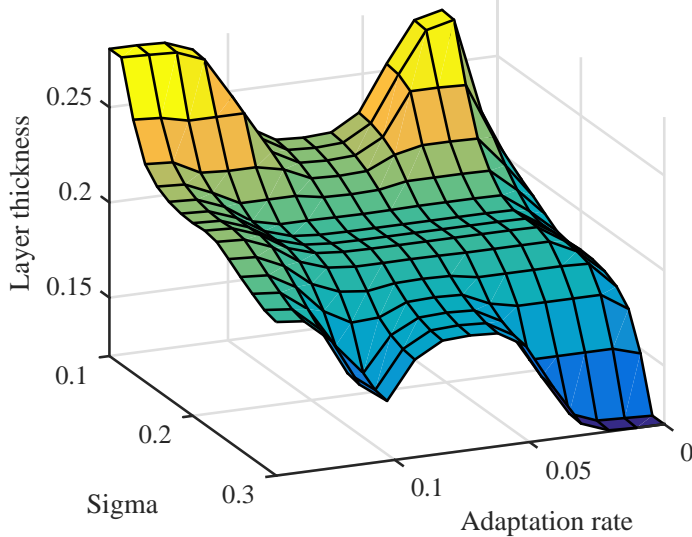


Figure 4.11: Fuzzy surface for pitch motion.

4.6.1 Experiment Setup

As shown in Fig. 4.12, the overall experimental platform consists of two subsystems. The ground station runs Windows 7 and MATLAB/Simulink. The indoor positioning system includes twenty-four cameras to provide the attitude of the quadrotor helicopter. The designed control algorithm can be compiled to C-code with the help of an integrated real-time control software, namely QuaRC. The compiled code runs on the embedded Linux-based system, Gumstix which uses an ARM Cortex-M4 single-chip computer, in real-time. The desired inputs and measured outputs are given from the ground station to the onboard processor of the quadrotor helicopter through Wi-Fi wireless communication.

4.6.2 Real Flight Test Results

Scenario 1: In this scenario, a 30% loss of control effectiveness fault is injected into actuator #1 at 25 s. The tracking performance of the pitch motion is shown in Fig. 4.13. After fault occurrence, the proposed adaptive scheme can instantly increase the corresponding control input as shown in Fig. 4.14 to make a prompt compensation and maintain the original system tracking

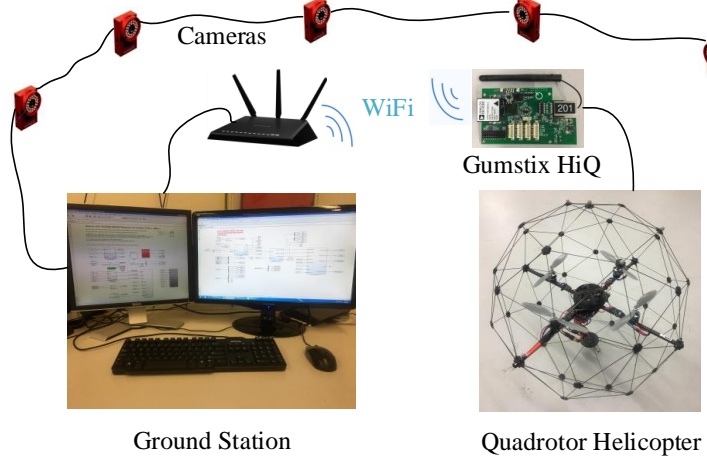


Figure 4.12: The schematic of the experiment setup.

performance. On the contrary, the compared adaptive SMC scheme stimulates the control chattering as shown in Fig. 4.15 and cannot maintain the original tracking performance although it has a smaller overshoot at the initial stage. Due to the synthesis of the adaptive parameter in both continuous and discontinuous control portions, the proposed adaptive scheme can significantly decrease control discontinuity during the course of fault accommodation. In such a way, control chattering is avoided.

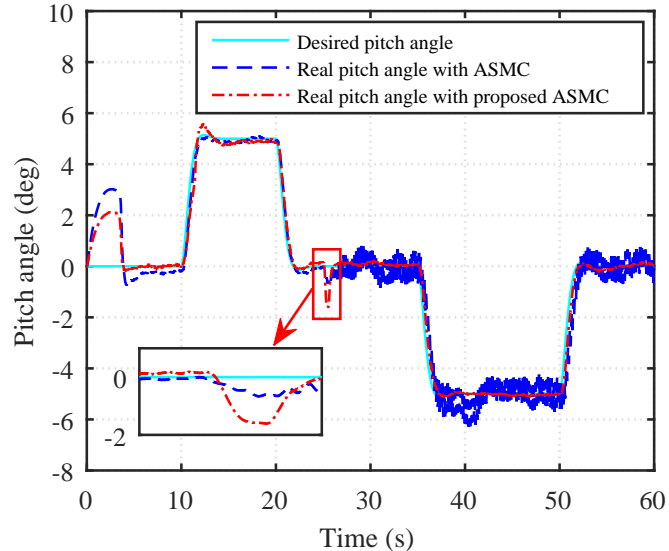


Figure 4.13: Tracking performance of pitch motion in the presence of 30% loss of control effectiveness fault in real flight test.

Scenario 2: As shown in Scenario 1, the proposed ASMC scheme has a good performance of

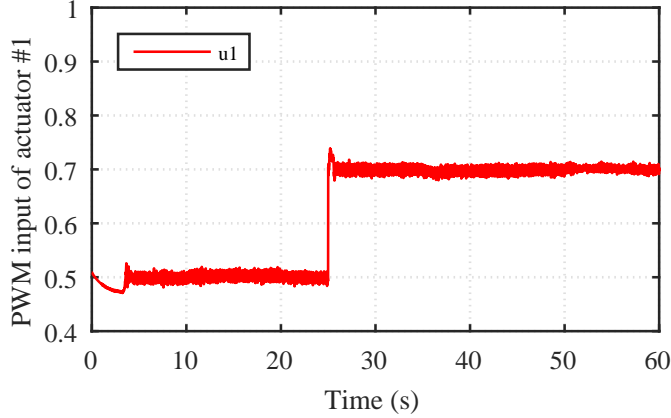


Figure 4.14: Control input of actuator #1 with proposed ASMC in the presence of 30% loss of control effectiveness fault in real flight test.

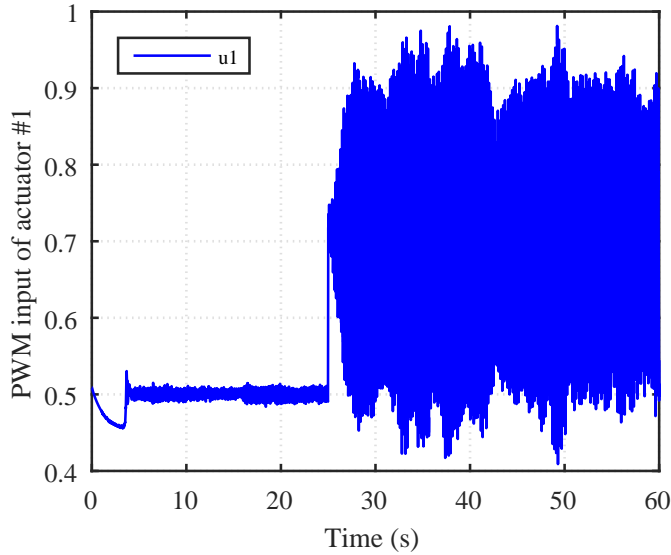


Figure 4.15: Control input of actuator #1 with compared ASMC in the presence of 30% loss of control effectiveness fault in real flight test.

dealing with large actuator fault. However, when actuator fault amplitude becomes larger (i.e., a 50% loss of control effectiveness fault is injected to the actuator), the adaptive control scheme fails to maintain the original system tracking performance and stability as can be observed from Fig. 4.16. This is because the adaptive scheme is intended to increase the corresponding adaptive control parameters to bring the sliding variable into the defined boundary layer, and if the defined boundary layer is too thin under such a fault condition, the sliding variable will be brought over the boundary layer and then oscillate around the boundary layer. This will result in the overestimation

of the adaptive control parameters and oscillatory control input of the system as shown in Fig. 4.17. In this case, the thickness of the boundary layer should be increased moderately by using the proposed rule-based fuzzy boundary layer. As depicted in Fig. 4.16, the system tracking performance can be very well maintained with the proposed adaptive fuzzy sliding mode control (AFSMC) under Scenario 2. It can be observed from Figs. 4.19 and 4.20 that, both adaptive control parameter and boundary layer thickness are changed in order to accommodate this kind of actuator fault and maintain system stability. Moreover, the change of boundary layer thickness is a little bit behind the change of adaptive control parameter. When comparing to the actuator control input in Scenario 1 as shown in Fig. 4.14, in order to accommodate larger fault, the actuator control input in this scenario is increased accordingly as shown in Fig. 4.18.

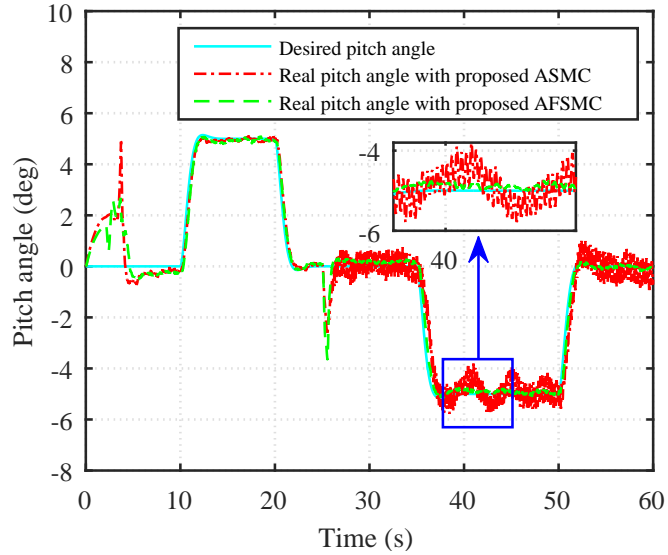


Figure 4.16: Tracking performance of pitch motion in the presence of 50% loss of control effectiveness fault in real flight test.

Moreover, the quantitative performance metrics are listed in Table 4.4. The quantitative analysis confirms that the presented control scheme can not only ensure a satisfactory tracking performance of the post-fault UAV but also preserve a low control input.

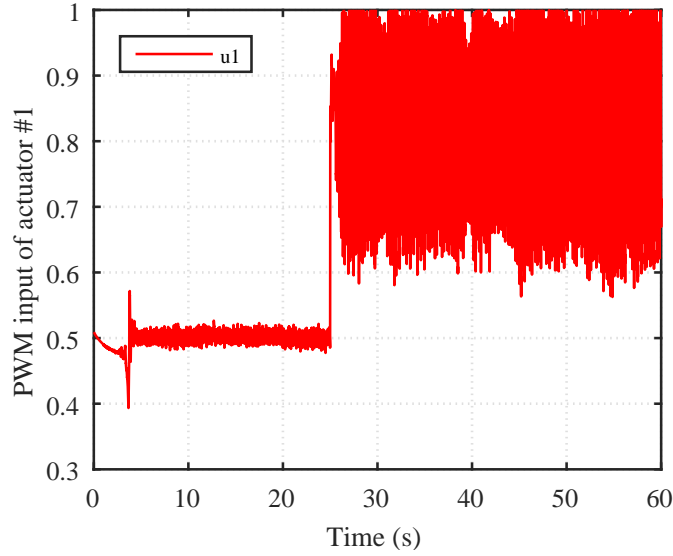


Figure 4.17: Control input of actuator #1 with proposed ASMC in the presence of 50% loss of control effectiveness fault in real flight test.

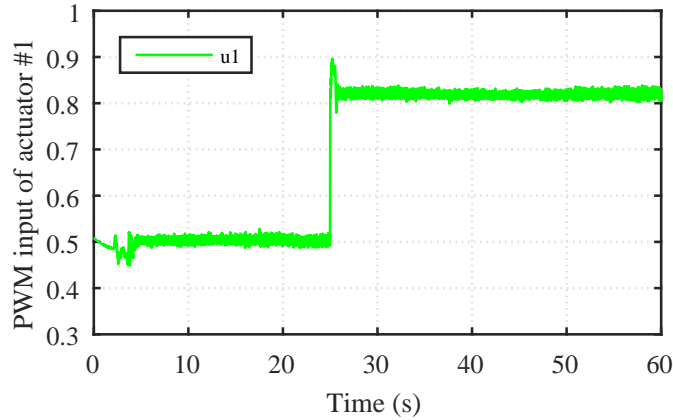


Figure 4.18: Control input of actuator #1 with proposed AFSMC in the presence of 50% loss of control effectiveness fault in real flight test.

Table 4.4: Performance Indices

Control Scheme	Fault Scenario	e_{RMSE}	Max Control Input
Compared ASMC	1	0.7754	0.9812
Proposed ASMC	1	0.5139	0.7387
Proposed ASMC	2	0.7190	1.0000
Proposed AFSMC	2	0.5628	0.8959

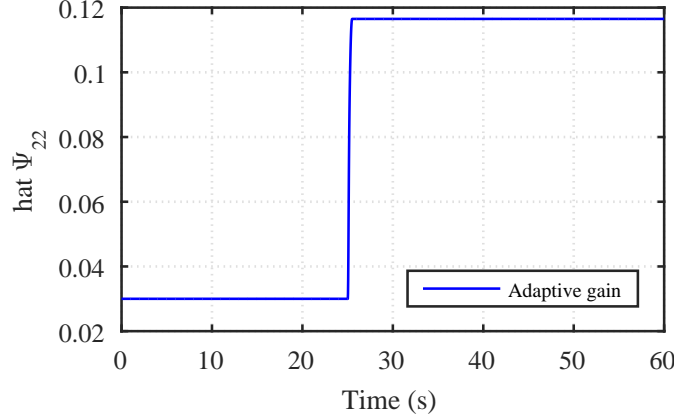


Figure 4.19: Adaptive control parameter related to pitch motion with proposed AFSMC in the presence of 50% loss of control effectiveness fault in real flight test.

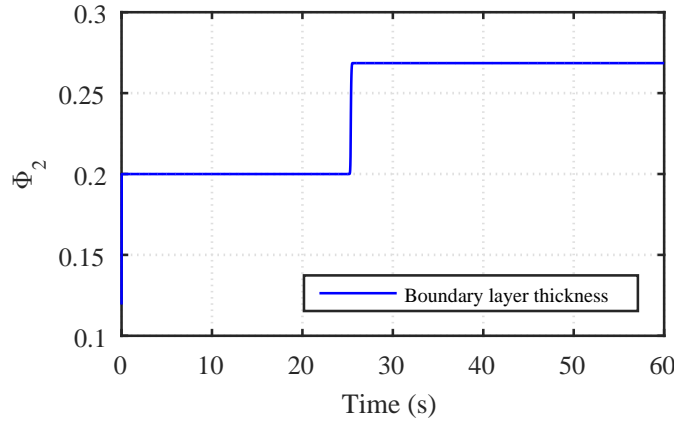


Figure 4.20: Boundary layer thickness related to pitch motion with proposed AFSMC in the presence of 50% loss of control effectiveness fault in real flight test.

4.7 Conclusion

In this chapter, an adaptive fuzzy control strategy based on an integral SMC, a fuzzy boundary layer, and a nonlinear disturbance observer is proposed to accommodate parametric uncertainties, actuator faults, and external disturbances for a quadrotor helicopter. By using the developed online adaptation laws, the corresponding parameters can be adaptively estimated without the knowledge of uncertainty bounds and actuator fault information to maintain tracking performance and stability of the quadrotor helicopter. By virtue of using the adaptive control parameters in both continuous and discontinuous control portions, the control discontinuity is significantly reduced in the presence of actuator faults, which helps the system avoid control chattering. Moreover, the fuzzy

logic-based boundary layer further helps to maintain system stability and prevent overestimation of the adaptive control parameters. The designed nonlinear disturbance observer can accurately estimate the imposed disturbances, which will help to maintain system tracking performance while keeping the smaller discontinuous control gain. The numerical simulation and experimental results of a quadrotor helicopter demonstrate the effectiveness and applicability of the proposed control strategy.

Chapter 5

Active Fault-Tolerant Control

In this chapter, an active FTC strategy is proposed for a quadrotor helicopter against actuator faults and model uncertainties based on adaptive SMC and RNNs. Firstly, a novel adaptive SMC is proposed. In virtue of the designed adaptive schemes, the system tracking performance can be guaranteed in the presence of model uncertainties and disturbances without stimulating control chattering. Then, due to the fact that model-based fault estimation schemes may fail to correctly estimate faults in the presence of model uncertainties, a fault estimation scheme is proposed by designing a parallel bank of RNNs. For constructing the RNNs, two hidden layers are employed, and the outputs of the first hidden layer are fed back to form a context layer with purposes of capturing more information and achieving better learning capability. The weighting parameters of the RNNs are updated by using back-propagation-through-time-based extended Kalman filter. With the trained RNNs, the severity of actuator faults can be precisely and reliably estimated. Finally, by synthesizing the proposed fault estimation scheme with the designed adaptive SMC, an active FTC mechanism is established. Moreover, the issue of actuator fault estimation error is explicitly considered and compensated by the proposed adaptive schemes. A number of numerical simulations and experimental tests are carried out to validate and demonstrate the effectiveness and advantages of the proposed control strategy. Various kinds of actuator faults can be accurately identified and compensated in the closed-loop system.

5.1 Introduction

With the development of microelectro-mechanical systems and onboard computers, more and more small-scale UAVs are available in the market. In order to accomplish specific tasks, different sensors and instruments are incorporated with UAVs, which are usually referred to as unmanned aerial systems (UASs) [10]. In this case, the cost of the onboard sensors and instruments can easily exceed the cost of the UAV itself. Moreover, UAVs are commonly employed in complex and dangerous environments, which will significantly threaten the safety and reliability of the UAVs [133]. Any failure occurs in a UAV can easily damage the UAV itself, the onboard sensors and instruments, and its surroundings. Therefore, the safety and reliability of UAVs are becoming imperative, and critical safety issues should be specially considered.

Among different types of UAVs, quadrotor helicopters draw more and more attention in both industrial and academic communities due to their simplicity and affordable price in recent years [15]. Partial loss of control effectiveness of actuator is a common fault occurring in a quadrotor helicopter system [23]. Unlike traditional manned aircraft and large-scale UAVs, due to hardware redundancy limitations, the design of a reliable control system plays an important role in ensuring acceptable and efficient performance for quadrotor helicopters. Moreover, quadrotor helicopters do not have the graceful degradation properties as fixed-wing aircraft in the case of failures [134]. A fault even in a component level may propagate to the overall system and deteriorate the performance of other components and eventually cause the whole system failure [18]. Therefore, if faults/failures are not properly detected and accounted for, quadrotor helicopters may encounter a catastrophic crash, which will also damage the expensive onboard instruments in addition to the loss of the UAV itself. A promising way for contributing to the aforementioned safety and reliability requirements is to apply a low-cost advanced fault detection, diagnosis, and accommodation scheme.

Fault diagnosis algorithms are generally classified into two types known as model-based and data-driven approaches. Model-based approaches are mostly based on analytical redundancy and require an analytical mathematical model of the system. The presence of faults is detected by

means of the so-called residuals, which can be generated in different ways: parity equations, state estimation-based methods, and parameter estimation-based methods. The performance of model-based methods depends strongly on the usefulness of the constructed model [73]. The constructed model must include all situations under study. It must be able to handle changes at the operating point. If the constructed model fails, the whole diagnostic system will also fail. However, in practice, it is usually quite challenging and difficult to meet all the requirements of model-based techniques due to the inevitable un-modeled dynamics, uncertainties, model mismatches, noises, disturbances, and inherent nonlinearities [74]. The sensitivity to modeling errors has become the key problem in the application of model-based methods. In contrast, data-driven diagnosis approaches, such as neural network-based intelligent methods, mostly rely on historical and current data from the sensors, and do not require a detailed mathematical model of the system but need representative training data. The idea is that the operation of the system is classified according to measurement data. Formally, this is a mapping from measurement space into decision space [73]. Therefore, data play a very important role in this kind of method. With application to UAVs, model-free neural network-based approaches are preferred due to the cost limitation and short period of development compared to conventional aircraft. The capabilities of neural networks for function approximation, classification, and their ability to deal with uncertainties and parameter variations make them a viable choice for using in FDD problems [75].

The standard feed-forward neural network or MLP are the best known members of the family of many types of neural networks. Feed-forward neural networks and their variations have been applied in tasks of FDD for many years [76–78, 135–137]. Most recently, a new class of neural networks, dynamic neural networks, was introduced based on feed-forward neural networks to provide the static neural networks with dynamic properties, which means the behavior of the neural network depends not only on the current inputs (as in the feed-forward neural networks) but also on previous operations of the neural network. It can be grouped into two classes known as time-delay neural networks and recurrent neural networks. Dynamic neural networks have been successfully used in many applications including the fault diagnosis of nonlinear dynamic systems. In [79], a

dynamic neural network-based fault diagnosis scheme is proposed for gas turbine engines. The authors use a bank of dynamic neural networks to represent various operating modes of the healthy and faulty engine conditions. The fault diagnosis task is accomplished by using the residuals generated by measuring the difference between each network output and the measured engine output based on various criteria. In [80], a RNN is proposed to carry out railway track circuit fault diagnosis based on the commonly available measurement signals. It can learn the dependences directly from the data and correctly classify 99.7% of the test input sequences without false positive fault detections.

Over the last decade, various FTC schemes have been proposed for quadrotor helicopters [14, 124, 138], that can be generally classified into two types known as passive FTC and active FTC. Passive FTC is designed to be robust against a class of presumed faults without requiring on-line detection of faults [25, 26]. However, it has limited fault-tolerance capability and may sacrifice nominal performance [11]. In contrast to passive FTC, an active FTC is designed based on controller reconfiguration or selection of pre-designed controllers with the help of fault diagnosis scheme that has the task of detecting and identifying faults in the system [24, 27]. In terms of fault diagnosis for quadrotor helicopters, most of the studies in the literature are model-based [14, 81–83]. A two-stage Kalman filter is designed in [81] to detect and identify actuator faults with experimental tests. In [83], a bank of nonlinear adaptive fault isolation estimators are designed for quadrotor actuator faults estimation. In the context of active FTC, a retrofit control mechanism with integration of an adaptive fault estimator and an adaptive fault compensator is devised in [139] against actuator faults for an unmanned quadrotor helicopter. In [17, 140, 141] sliding mode technique is employed to develop active FTC schemes to compensate actuator faults. In fact, model uncertainties widely exist in practical engineering systems. In the existing active FTC frameworks, most works on fault diagnosis and FTC do not take into consideration the model uncertainties and fault estimation errors that are inevitable in practical applications. Moreover, the model-based fault diagnosis approaches are founded on the fact that a fault will cause changes in certain physical parameters which in turn will lead to changes in certain model parameters or

states. However, in the case of closed-loop system, small changes in the system can be covered by control actions, therefore, the feedback control system in the quadrotor helicopter can hinder the early detection of system faults which further challenges model-based approaches. In contrast, data-driven diagnosis approaches, such as neural network-based intelligent methods, mostly rely on historical and current data from the sensors, and do not require a detailed mathematical model of the system but need representative training data. The idea is that the operation of the system is classified according to measurement data. Formally, this is a mapping from measurement space into decision space [73]. Therefore, data play a very important role in this kind of method. With application to UAVs, model-free neural network-based approaches are preferred due to the cost limitation and short period of development compared to conventional aircraft. The capabilities of neural networks for function approximation, classification, and their ability to deal with uncertainties and parameter variations make them a viable choice for using in fault diagnosis problems [75].

From the control point of view, SMC is an approach to design robust control systems dealing with large uncertainties with discontinuous control strategy which demonstrates invariance to so-called matched uncertainty while on a reduced order sliding surface [34, 41, 142]. To be more precise, one design parameter is synthesized in the discontinuous control part to deal with uncertainties which leads to effective control performance [36, 40]. The property of insensitivity to uncertainties and disturbances makes SMC as one of the most promising control approaches for applications in the field of flight control. However, this kind of traditional robust control algorithm makes trade-off between system performance and robustness in order to accommodate certain uncertainties. In this regard, some researchers are motivated to propose an adaptive SMC to ensure system performance in all conditions [39]. However, most of the studies in the literature mainly focus on the adaptation of the discontinuous control part, which may lead to control chattering effect if large uncertainties appear in the system.

Motivated by the aforementioned practical challenges, this study is intended to design an adaptive SMC and a fault severity estimator, that are then synthesized in an active FTC framework while explicitly considering model uncertainties and fault estimation error. The design procedures

of the proposed method can be illustrated as follows: 1) firstly, an adaptive SMC is developed as a baseline controller to compensate model uncertainties and ensure the stability and desired tracking performance of the quadrotor helicopter with healthy actuators; 2) then, a fault estimation scheme is proposed to accurately estimate actuator fault severity directly from the measurements without any modeling information; 3) finally, a fault compensator combined with the baseline controller is designed to counteract the adverse effects of actuator faults for the continuous operation of the quadrotor helicopter against actuator faults. The main contributions of this paper are summarized as follows:

- 1) With the synthesized adaptive schemes, the proposed adaptive SMC can adaptively generate appropriate control signals to compensate model uncertainties without merely relying on the robust discontinuous control strategy. Since the proposed adaptive schemes are synthesized in both continuous and discontinuous control parts, the control effort is significantly reduced for accommodating model uncertainties, which means larger uncertainties can be tolerated within this control scheme, and the chattering effect is also suppressed.
- 2) By designing a parallel bank of RNNs, the reliability and accuracy of actuator fault severity estimation is improved and free from influences of model uncertainties. An extended Kalman filter based on back-propagation-through-time is designed to effectively train the RNNs with fast convergence and avoidance of poor local minima. Various types of actuator faults can be accurately estimated in the closed-loop system.
- 3) The proposed active FTC scheme explicitly takes into account fault estimation error and is validated through experimental tests and more practical for real applications while most of the works in the literature do not consider fault estimation error and are evaluated through simulation results based on simplified nonlinear or linear models.

The remainder of this chapter is organized as follows. In Section 5.2, A brief description of the quadrotor helicopter model is presented. The detailed design procedures of the proposed active FTC are addressed in Section 5.3. In Section 5.4, numerical simulation results are illustrated to verify the effectiveness of the proposed fault estimation scheme. Corresponding experimental

results are followed in Section 5.5 to further validate the effectiveness of the proposed active FTC strategy. Finally, conclusions are summarized in Section 5.6.

5.2 Problem Formulation

5.2.1 Modeling of a Quadrotor Helicopter

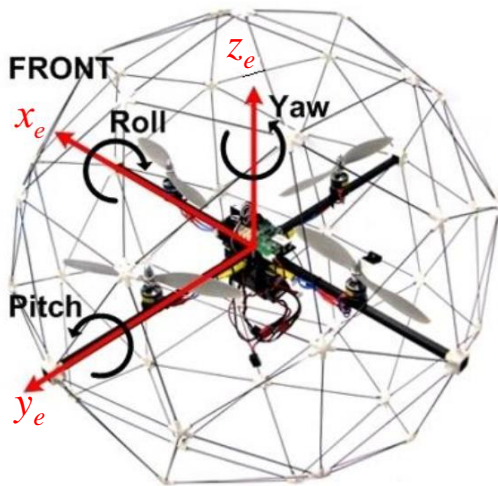


Figure 5.1: Configuration of the studied quadrotor helicopter.

The quadrotor helicopter studied in this chapter is produced by Quanser Inc., which is very well modeled with four motors in a cross configuration as shown in Fig. 5.1. In this configuration, each two opposite motors contribute to the motion along x_e - and y_e -axis, respectively. In order to obtain an accurate nonlinear model of the quadrotor helicopter, the gyroscopic effects produced by propeller rotations, the translational motion induced drag forces, and the rotational motion induced torques are all taken into account. The detailed nonlinear dynamics of the quadrotor helicopter can

be formulated as follows:

$$\begin{aligned}\ddot{\phi} &= \frac{(I_{yy} - I_{zz})\dot{\theta}\dot{\psi}}{I_{xx}} + \frac{K_u L_d(u_3 - u_4)}{I_{xx}} - \frac{K_4 L_d \dot{\phi}}{I_{xx}} \\ \ddot{\theta} &= \frac{(I_{zz} - I_{xx})\dot{\phi}\dot{\psi}}{I_{yy}} + \frac{K_u L_d(u_1 - u_2)}{I_{yy}} - \frac{K_5 L_d \dot{\theta}}{I_{yy}} \\ \ddot{\psi} &= \frac{(I_{xx} - I_{yy})\dot{\phi}\dot{\theta}}{I_{zz}} + \frac{K_y(u_1 + u_2 - u_3 - u_4)}{I_{zz}} - \frac{K_6 \dot{\psi}}{I_{zz}}.\end{aligned}\quad (5-1)$$

The definition of the above mentioned variables and parameters can be found in Table 5.1.

Table 5.1: Nomenclature

Parameter	Definition
ϕ, θ, ψ	Roll, pitch, yaw angle
I_{xx}, I_{yy}, I_{zz}	Inertial moment along x_e -, y_e -, z_e -direction
L_d	Distance between each motor and center of mass of the quadrotor helicopter
K_u	A positive gain related to force generation
K_y	A positive gain related to torque generation
K_i ($i = 4, 5, 6$)	Drag coefficients
u_i ($i = 1, 2, 3, 4$)	Pulse-width modulation input of the i th motor

5.2.2 Problem Statement

Consider an integral-chain nonlinear affine system with model uncertainties and disturbances subject to actuator faults:

$$\begin{aligned}\dot{x}_1(t) &= x_2(t) \\ \dot{x}_2(t) &= G(x_1(t), x_2(t)) + H B_u L_c(t) u(t) + d(t) \\ y(t) &= C x(t) + w(t)\end{aligned}\quad (5-2)$$

where $x(t) = [x_1(t), x_2(t)] \in \mathbb{R}^n$ is the state vector, $y(t) \in \mathbb{R}^q$ is the system output vector, $u(t) \in \mathbb{R}^m$ is the control input vector, and $B_u \in \mathbb{R}^{p \times m}$ is the control effectiveness matrix. The vector $G(x_1(t), x_2(t)) \in \mathbb{R}^p$ is a nonlinear function containing model uncertainties, and the bounds of

these uncertainties are unknown *a priori*. $d(t) \in \mathbb{R}^p$ represents disturbances and noises which are unknown but bounded, i.e. $\|d(t)\| \leq D_d$, and $w(t) \in \mathbb{R}^q$ represents sensor modeling uncertainties and noises. $L_c(t) = \text{diag}([l_{c1}(t), l_{c2}(t), \dots, l_{cm}(t)])$ represents the control effectiveness level of the actuators, where $l_{cj}(t)$ ($j = 1, 2, \dots, m$) is a scalar satisfying $0 \leq l_{cj}(t) \leq 1$. If $l_{cj}(t) = 1$, the j th actuator works perfectly, otherwise, the j th actuator suffers certain level of fault with a special case $l_{cj}(t) = 0$ denoting the complete failure of the j th actuator [27].

For simplicity of expression, the notation t is omitted in the following sections, e.g. $x(t)$ is expressed as x .

5.3 Design of Active FTC

In this section, an active FTC scheme is designed to accommodate actuator faults and model uncertainties for a quadrotor helicopter. The schematic of the proposed control strategy is illustrated in Fig. 5.2. There are two problems to be addressed in the following sections. The first problem is to construct an adaptive SMC against model uncertainties to guaranteed system tracking performance. The second one is the problem of exploring the real-time actuator fault severity estimation and accommodation with combination of the developed adaptive SMC to form an active FTC framework.

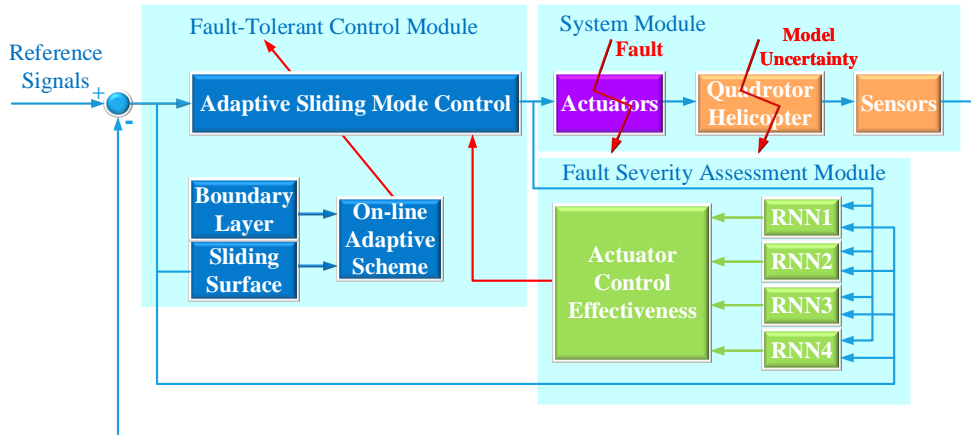


Figure 5.2: The schematic of the proposed active FTC strategy.

5.3.1 Adaptive Sliding Mode Control

In order to facilitate the state feedback control design, the nonlinear system described in (5–2) can be rewritten as:

$$\begin{aligned}\dot{x}_{2i-1} &= x_{2i} \\ \dot{x}_{2i} &= f_{1i}g_{1i}(x) + f_{2i}x_{2i-1} + h_i\nu_i + d_i \\ \nu_i &= B_{ui}L_c u\end{aligned}\tag{5-3}$$

where $i = 1, 2, 3$ represents each subsystem, $x_{2i-1} = [\phi, \theta, \psi]^T$, and $x_{2i} = [\dot{\phi}, \dot{\theta}, \dot{\psi}]^T$.

By denoting x_{2i-1}^d as the desired trajectory, the tracking error vector can be defined as:

$$\tilde{x}_{2i-1} = x_{2i-1} - x_{2i-1}^d = \begin{bmatrix} \phi - \phi_d \\ \theta - \theta_d \\ \psi - \psi_d \end{bmatrix}.\tag{5-4}$$

With this tracking error vector, the integral sliding surface for the system can be designed as:

$$\begin{aligned}\sigma_i &= \dot{\tilde{x}}_{2i-1} + k_{c2i}\tilde{x}_{2i-1} + k_{c1i} \int_{t_0}^t \tilde{x}_{2i-1}(\tau) d\tau \\ &\quad - k_{c2i}\tilde{x}_{2i-1}(t_0) - \dot{\tilde{x}}_{2i-1}(t_0)\end{aligned}\tag{5-5}$$

where t_0 is the initial time instant, k_{c1i} and k_{c2i} are the design parameters.

After designing the sliding surface, the next step is to design an appropriate control law to drive the sliding variable reach the designed sliding surface and thereafter keep it within the close neighborhood of the sliding surface. In this process, model uncertainties and actuator faults are not taken into account. The corresponding control law can be designed in the following form:

$$\nu_i = \nu_{i0} + \nu_{i1}\tag{5-6}$$

where ν_{i0} is the continuous nominal control part to stabilize the ideal system without uncertainties and disturbances, and ν_{i1} is the discontinuous control part for compensating the perturbations and

disturbances in order to ensure the sliding motion.

The nominal control ν_{i0} is designed by equalizing $\dot{\sigma}_i = 0$, and the disturbance d_i is omitted in this case as shown below:

$$\nu_{i0} = h_i^{-1}(\ddot{x}_{2i-1}^d - k_{c2i}\dot{\tilde{x}}_{2i-1} - k_{c1i}\tilde{x}_{2i-1} - f_{1i}g_{1i}(x) - f_{2i}x_{2i-1}). \quad (5-7)$$

The discontinuous control part which is synthesized to reject the disturbance d_i is accordingly designed as:

$$\nu_{i1} = -k_{c3i}\text{sat}(\sigma_i) \quad (5-8)$$

where k_{c3i} is a positive high gain that makes the sliding surface attractive, and the sat function is defined as [132]:

$$\text{sat}(\sigma_i) = \begin{cases} \text{sign}(\sigma_i) & \text{if } |\sigma_i| > \Phi_i \\ \sigma_i/\Phi_i & \text{if } |\sigma_i| \leq \Phi_i \end{cases} \quad (5-9)$$

with Φ_i denoting the boundary layer thickness with a positive value.

In this way, without considering actuator faults and model uncertainties, the control law can be developed as:

$$u = B_{ui}^+h_i^{-1}(\ddot{x}_{2i-1}^d - k_{c2i}\dot{\tilde{x}}_{2i-1} - k_{c1i}\tilde{x}_{2i-1} - f_{1i}g_{1i}(x) - f_{2i}x_{2i-1}) - B_{ui}^+k_{c3i}\text{sat}(\sigma_i) \quad (5-10)$$

where $B_{ui}^+ = B_{ui}^T(B_{ui}B_{ui}^T)^{-1}$.

With the consideration of model uncertainties, the estimated parameters \hat{f}_{1i} , \hat{f}_{2i} , and \hat{h}_i need to be employed to derive the corresponding control law. In order to fully use the discontinuous control strategy of SMC, instead of adaptively changing the value of k_{c3i} , the estimated parameter \hat{h}_i is synthesized with k_{c3i} to make change of the discontinuous control gain. Then, by denoting $\hat{\Gamma}_{1i} = \hat{h}_i^{-1}\hat{f}_{1i}$, $\hat{\Gamma}_{2i} = \hat{h}_i^{-1}\hat{f}_{2i}$, and $\hat{\Psi}_i = \hat{h}_i^{-1}$, the developed control law in (5-10) can be rearranged as:

$$u = B_{ui}^+\hat{\Psi}_i(\ddot{x}_{2i-1}^d - k_{c2i}\dot{\tilde{x}}_{2i-1} - k_{c1i}\tilde{x}_{2i-1} - k_{c3i}\text{sat}(\sigma_i)) - \hat{\Gamma}_{1i}g_{1i}(x) - \hat{\Gamma}_{2i}x_{2i-1}. \quad (5-11)$$

The corresponding on-line adaptive schemes for estimating the uncertain parameters are designed as:

$$\begin{aligned}\dot{\hat{\Gamma}}_{1i} &= g_{1i}(x)\sigma_{\Delta i} \\ \dot{\hat{\Gamma}}_{2i} &= x_{2i-1}\sigma_{\Delta i} \\ \dot{\hat{\Psi}}_i &= (-\ddot{x}_{2i-1}^d + k_{c2i}\dot{\hat{x}}_{2i-1} + k_{c1i}\tilde{x}_{2i-1} + k_{c3i}\text{sat}(\sigma_i))\sigma_{\Delta i}\end{aligned}\quad (5-12)$$

where $\sigma_{\Delta i}$ is the measurement of the algebraic distance between the current sliding variable and the boundary layer defined as:

$$\sigma_{\Delta i} = \sigma_i - \Phi_i \text{sat}(\sigma_i). \quad (5-13)$$

It features $\dot{\sigma}_{\Delta i} = \dot{\sigma}_i$ if the sliding variable is outside the boundary layer and $\dot{\sigma}_{\Delta i} = 0$ if the sliding variable is inside the boundary layer.

5.3.2 Construction of Reconfigurable Mechanism

After taking into account model uncertainties in controller design, the next problem is to carry out actuator fault estimation and construction of reconfigurable mechanism. In this section, the detailed procedures of designing an active FTC for a quadrotor helicopter are explained. In order to effectively estimate the fault severity for each actuator, a parallel bank of RNNs are employed as fault identifiers corresponding to the various but limited number of faulty modes that are of most interest or possible in a quadrotor helicopter. Since there are four actuators in the studied quadrotor helicopter, four RNNs are designed for each individual actuator in order to easily capture fault symptoms with extracted features. Therefore, the fault severity assessment and fault isolation tasks can be performed simultaneously. This proposed scheme makes the problem of fault severity assessment more reliable and yields significant improvement with comparison to a single neural network-based approach that may not remain valid given the occurrence of multiple faults in different actuators.

An appropriate feature extraction lays the foundation for a successful (accurate and reliable) diagnostic system. It is desirable that the features are not only computationally cheap but also

explainable in physical terms. These extracted features are supposed to be representative of the defined actuator faults. Considering the closed-loop quadrotor helicopter, after fault occurrence, the onboard control system will increase the corresponding control input to the actuator, and the system tracking error will be changed as well. Therefore, in this paper, the tracking errors between the reference command inputs and the quadrotor helicopter outputs, and the control inputs to the actuators can be served as the proper features and used as the inputs of the proposed RNNs. The output of each neural network is the estimated fault severity of the corresponding actuator which is represented by the control effectiveness level of the actuator.

RNNs are networks with one or more feedback loops [143]. Due to the introduction of feedbacks to the network structure, it is possible to accumulate previous information and use it later. Since these feedbacks can be either fully connected or partially connected, recurrent networks can be generally divided as fully recurrent networks [144] and partially recurrent networks [145, 146]. Due to the large structural complexity and slow convergence of fully recurrent networks, such kind of networks are generally too complex for practical applications. On the contrary to fully recurrent networks, the architecture of partially recurrent networks is based on a feed-forward multilayer perceptron consisting of an additional layer of units known as the context layer. The architecture of the employed recurrent network is depicted in Fig. 5.3, which has two hidden layers, and the outputs of the first hidden layer are fed back to form a context layer. Then, the general dynamic behavior of the RNN in response to an input vector $U(k) = [u_{n1}(k), u_{n2}(k), \dots, u_{nr}(k)]^T$ can be described as:

$$\begin{aligned} X_{h1}(k+1) &= \varphi_{h1}([X_{h1}(k), U(k)]^T, W_{h1}(k)) \\ X_{h2}(k+1) &= \varphi_{h2}(X_{h1}(k+1), W_{h2}(k)) \\ Y(k+1) &= W_O X_{h2}(k+1) \end{aligned} \tag{5-14}$$

where $U(k) \in \mathbb{R}^r$ is the input vector of the RNN, $X_{h1}(k+1) \in \mathbb{R}^{N1}$ is the output vector of the first hidden layer at time instant $k+1$, $X_{h2}(k+1) \in \mathbb{R}^{N2}$ is the output vector of the second hidden layer, and $Y(k+1) \in \mathbb{R}^q$ is the output vector of the RNN. $W_{h1}(k) \in \mathbb{R}^{N1 \times (r+N1)}$, $W_{h2}(k) \in \mathbb{R}^{N2 \times N1}$,

and $W_O(k) \in \mathbb{R}^{q \times N^2}$ represent the synaptic weighting matrix between the input layer and the first hidden layer, between the first hidden layer and the second hidden layer, and between the second hidden layer and the output layer, respectively. φ_{h1} and φ_{h2} represent the activation function for the first hidden layer and the second hidden layer, respectively.

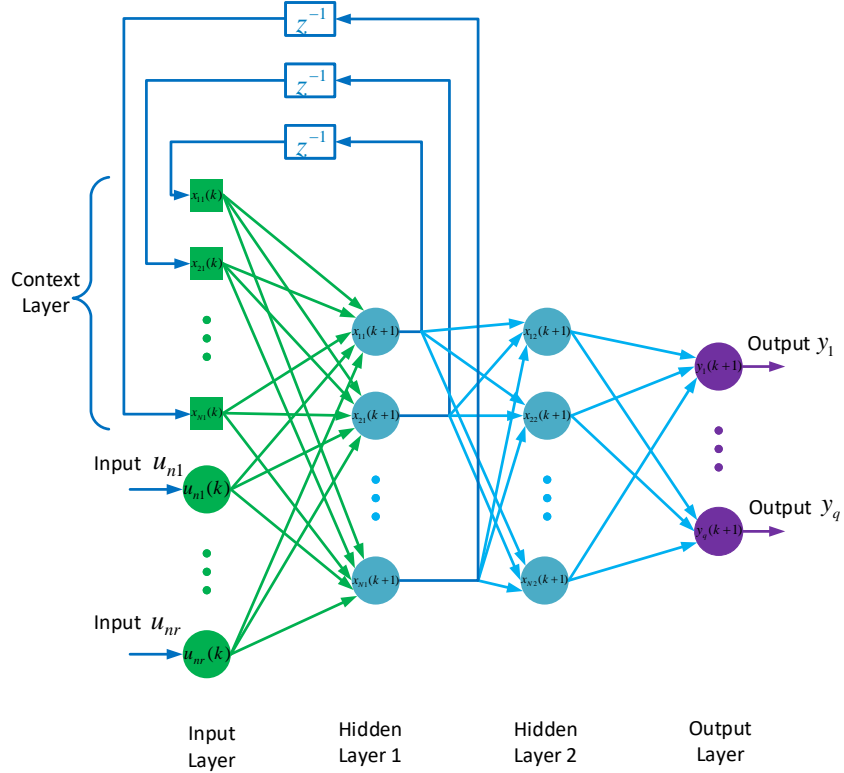


Figure 5.3: Architecture of the recurrent neural network.

Back-propagation is a common approach for training feed-forward neural networks. However, the feed-forward back-propagation training algorithm cannot be directly transferred to train RNNs because the error back-propagation pass presupposes that the connections between neurons induce a cycle-free order. In the case of training RNNs, an extension of the standard back-propagation, namely back-propagation-through-time, is used which is also based on gradient descent algorithm. The solution of back-propagation-through-time algorithm is derived by unfolding the recurrent network in time to obtain a layered feed-forward network which is amenable to the standard back-propagation algorithm.

Nevertheless, the gradient-descent-based training algorithms entirely rely on the first-order information, i.e., the Jacobian matrix, for their operation which therefore are inefficient in using the information of the training data. In order to improve the utilization of the information contained in the training data and overcome the vanishing-gradients problem, second-order optimization techniques, such as Levenberg-Marquardt, Quasi-Newton, and conjugate gradient algorithms, are proposed by many researchers to train RNNs. Although these nonlinear optimization algorithms have shown promising results, they often get stuck in poor local minima [147]. An alternative option is to use nonlinear sequential state estimation approaches [148]. The corresponding weights in the RNNs are updated in a sequential manner, and the second-order information in the training data is represented as a prediction error covariance matrix which is also evolved sequentially.

In this chapter, inspired by the early work [148] for training multilayer feed-forward neural networks with applications to nonlinear system modeling and identification, an extended Kalman filter based on back-propagation-through-time is employed to train the designed network. Consider the designed RNN in (5–14) with s synaptic weights and q output nodes. By denoting k as a time instant in the supervised training of the RNN, the entire set of synaptic weights in the RNN computed at time instant k is represented by the vector W_k . It is constructed by stacking the weights associated with the first neuron in the first hidden layer on top of each other, followed by those of the second neuron, and carrying on the same procedure until all the neurons in the first hidden layer are accounted for. Then, the same procedure will be applied to the second hidden layer and the output layer in the network to stack the weights into the vector W_k in the same orderly manner. Therefore, by choosing W_k as the state of the designed RNN, the state-space model of the network under training can be defined as:

$$\begin{aligned} W_{k+1} &= W_k + \omega_k \\ D_k &= f(W_k, V_k, U_k) + \nu_k \end{aligned} \tag{5-15}$$

where U_k is the vector of input signals applied to the network, and V_k is the internal state inside the network representing the network activities. The dynamic noise ω_k and measurement noise ν_k

are both uncorrelated Gaussian noises with zero mean and covariance matrices $Q_{\omega,k} \in \mathbb{R}^{s \times s}$ and $Q_{\nu,k} \in \mathbb{R}^{q \times q}$, respectively. f is the function denoting the overall nonlinearity of the RNN, and $D_k \in \mathbb{R}^q$ is the desired response.

The next problem is to carry out the supervised training process by using a sequential state estimator. Based on the designed RNN, a back-propagation-through-time-based extended Kalman filter is employed as the training algorithm with consideration of the nonlinear measurement model described in (5–15). The overall training process is illustrated in Algorithm 1. In order to implement the extended Kalman filter training algorithm, the measurement model should be linearized. By applying Taylor series expansion, (5–15) can be approximated as follows:

$$\begin{aligned} W_{k+1} &= W_k + \omega_k \\ \hat{D}_k &= F_k W_k + \nu_k \end{aligned} \tag{5–16}$$

where $F_k \in \mathbb{R}^{q \times s}$ is the measurement matrix of the linearized model which can be represented as:

$$F_k = \begin{bmatrix} \frac{\partial y_1}{\partial w_1} & \frac{\partial y_1}{\partial w_2} & \dots & \frac{\partial y_1}{\partial w_s} \\ \frac{\partial y_2}{\partial w_1} & \frac{\partial y_2}{\partial w_2} & \dots & \frac{\partial y_2}{\partial w_s} \\ \vdots & \vdots & \vdots & \vdots \\ \frac{\partial y_q}{\partial w_1} & \frac{\partial y_q}{\partial w_2} & \dots & \frac{\partial y_q}{\partial w_s} \end{bmatrix} \tag{5–17}$$

with q and s denoting the number of output neurons and synaptic weights, respectively, and $y_i (i = 1, 2, \dots, q)$ denoting the i th output neuron. The detailed calculation of matrix F_k can be found in Appendix 5.7.

Algorithm 1 Back-propagation-through-time-based extended Kalman filter training procedures

```
1: procedure TRAININGPROCEDURE
2:   initialize training epoch 1
3:   initialize weights with small random values
4:   loop1:
5:     if  $epoch < epoch_{max}$  then
6:       initialize training parameters and recurrent layer states  $P_{1|0} = 0.01^{-1}I^{s \times s}$   $W_{N1}^0 = 0^{N1 \times (N1+m)}$   $V_{1|0} = 0^{1 \times N1}$ 
7:       run the network twice to get the initial network states  $k = 3$ 
8:   loop2:
9:     if  $k \leq$  number of datasets then
10:      Forward run the network and calculate  $F_k$ 
11:       $\alpha_k = d_k - F_k(\hat{W}_{k|k-1}, V_k, U_k)$ 
12:       $G_k = P_{k|k-1}F_k^T[F_kP_{k|k-1}F_k^T + Q_{v,k}]$ 
13:      if  $\alpha_k > 0.05$  then
14:         $\hat{W}_{k+1|k} = \hat{W}_{k|k-1} + \eta_k G_k \alpha_k$ 
15:         $P_{k+1|k} = P_{k|k-1} - G_k F_k P_{k|k-1} + Q_{w,k}$ 
16:         $k \leftarrow k + 1$ 
17:        goto loop2
18:      close;
19:       $epoch \leftarrow epoch + 1$ 
20:      anneal covariance matrices and learning rate
21:      goto loop1
22:    close;
```

Given the training sample $\Gamma = \{U_k, D_k\}_{k=1}^N$, for $k = 1, 2, \dots, N$, the RNN weighting parameters are updated as follows:

$$\begin{aligned}
G_k &= P_{k|k-1} F_k^T [F_k P_{k|k-1} F_k^T + Q_{\nu,k}] \\
\alpha_k &= d_k - Y_k(\hat{W}_{k|k-1}, V_k, U_k) \\
\hat{W}_{k|k} &= \hat{W}_{k|k-1} + \eta_k G_k \alpha_k \\
\hat{W}_{k+1|k} &= \hat{W}_{k|k} \\
P_{k|k} &= P_{k|k-1} - G_k F_k P_{k|k-1} \\
P_{k+1|k} &= P_{k|k} + Q_{\omega,k}
\end{aligned} \tag{5-18}$$

which is initialized as:

$$\begin{aligned}
\hat{W}_{1|0} &= \mathbb{E}(W_1) \\
P_{1|0} &= \delta^{-1} I
\end{aligned} \tag{5-19}$$

where $\hat{W}_{k|k-1}$ is the predicted estimation of the weight vector W_k , $\hat{W}_{k|k}$ is the filtered estimation of the weight vector W_k , and $G_k \in \mathbb{R}^{s \times q}$ is the Kalman gain matrix. $P_{k|k-1} \in \mathbb{R}^{s \times s}$ is the prediction error covariance matrix, and $P_{k|k} \in \mathbb{R}^{s \times s}$ is the filtering error covariance matrix. η_k is the learning rate, δ is a constant with small positive value, and $I \in \mathbb{R}^{s \times s}$ is an identity matrix.

Remark 5.1 *The covariance matrix $Q_{\omega,k}$ is employed to anneal the supervised training of the RNN over time. At the early stages of training, the covariance matrix $Q_{\omega,k}$ is set to be large for avoiding the local minima. As training epoch increases, it is gradually reduced to a very small value.*

By employing the estimated value of actuator control effectiveness level \hat{L}_c , the ultimate control law can be developed as:

$$\begin{aligned}
u &= \hat{L}_c^{-1} B_{ui}^+ \hat{\Psi}_i (\ddot{x}_{2i-1}^d - k_{c2i} \dot{\tilde{x}}_{2i-1} - k_{c1i} \tilde{x}_{2i-1} - k_{c3i} \text{sat}(\sigma_i)) \\
&\quad - \hat{\Gamma}_{1i} g_{1i}(x) - \hat{\Gamma}_{2i} x_{2i-1}.
\end{aligned} \tag{5-20}$$

Consider the actuator fault estimation error and denote $\tilde{L}_c^{-1} = L_c^{-1} - \hat{L}_c^{-1}$, the actual generated virtual control input can be formulated as:

$$\nu_i = \nu_{id} - B_{ui}L_c\tilde{L}_c^{-1}B_{ui}^+\nu_{id} \quad (5-21)$$

where ν_{id} is the demanded virtual control input from the developed adaptive SMC.

Then, denoting $\tilde{\nu}_i = -B_{ui}L_c\tilde{L}_c^{-1}B_{ui}^+\nu_{id}$ and substituting (5-20) into (5-3), the following equation can be obtained:

$$\begin{aligned} \ddot{x}_{2i-1} &= f_{1i}g_{1i}(x) + f_{2i}x_{2i-1} + h_i\nu_{id} + h_i\tilde{\nu}_i + d_i \\ &= f_{1i}g_{1i}(x) + f_{2i}x_{2i-1} + (h_i + \tilde{h}_i)\nu_{id} + d_i \\ &= f_{1i}g_{1i}(x) + f_{2i}x_{2i-1} + \hat{h}_i\nu_{id} + d_i. \end{aligned} \quad (5-22)$$

Remark 5.2 *The actuator fault estimation error will firstly affect the generated virtual control input and then deteriorate the closed-loop system tracking performance. With the designed adaptive control schemes (5-12), the fault estimation error can be compensated by changing the parameter related to virtual control inputs without affecting system tracking performance.*

Theorem 5.1 *Consider an integral-chain nonlinear affine system in (5-3) with actuator faults, model uncertainties, and bounded disturbances. Given the designed integral sliding surface (5-5), by employing the fault severity estimation scheme (5-16) and the state feedback control law (5-20) that is updated by (5-12), the desired tracking performance can be guaranteed with the discontinuous gain chosen as $k_{c3i} \geq \eta_i + D_d$.*

Proof 5.1 *Consider the following Lyapunov candidate function:*

$$\begin{aligned} V_6 &= \sum_{i=1}^n \frac{1}{2} \left[\sigma_{\Delta i}^2 + \Psi_i^{-1}(\hat{\Gamma}_{1i} - \Gamma_{1i})^2 + \Psi_i^{-1}(\hat{\Gamma}_{2i} - \Gamma_{2i})^2 \right. \\ &\quad \left. + \Psi_i^{-1}(\hat{\Psi}_i - \Psi_i)^2 \right]. \end{aligned} \quad (5-23)$$

Then, the derivative of the selected Lyapunov candidate function can be calculated as:

$$\begin{aligned}
\dot{V}_6 &= \sum_{i=1}^n \left[\sigma_{\Delta i} \dot{\sigma}_{\Delta i} + \Psi_i^{-1} (\hat{\Gamma}_{1i} - \Gamma_{1i}) \dot{\hat{\Gamma}}_{1i} + \Psi_i^{-1} (\hat{\Gamma}_{2i} - \Gamma_{2i}) \dot{\hat{\Gamma}}_{2i} \right. \\
&\quad \left. + \Psi_i^{-1} (\hat{\Psi}_i - \Psi_i) \dot{\hat{\Psi}}_i \right] \\
&= \sum_{i=1}^n \left[\sigma_{\Delta i} (\Psi_i^{-1} \Gamma_{1i} g_1(x_2) + \Psi_i^{-1} \Gamma_{2i} g_2(x_2) + \Psi_i^{-1} \hat{\Psi}_i (\ddot{x}_{2i-1}^d \right. \\
&\quad \left. - k_{c2i} \dot{\tilde{x}}_{2i-1} - k_{c1i} \tilde{x}_{2i-1} - k_{c3i} \text{sat}(\sigma_i)) - \Psi_i^{-1} \hat{\Gamma}_{1i} g_1(x_2) \right. \\
&\quad \left. - \Psi_i^{-1} \hat{\Gamma}_{2i} g_2(x_2) + d_i - \ddot{x}_{2i-1}^d + k_{c2i} \dot{\tilde{x}}_{2i-1} + k_{c1i} \tilde{x}_{2i-1} \right) \\
&\quad + \Psi_i^{-1} (\hat{\Gamma}_{1i} - \Gamma_{1i}) \dot{\hat{\Gamma}}_{1i} + \Psi_i^{-1} (\hat{\Gamma}_{2i} - \Gamma_{2i}) \dot{\hat{\Gamma}}_{2i} + \Psi_i^{-1} (\hat{\Psi}_i - \Psi_i) \dot{\hat{\Psi}}_i \right] \quad (5-24) \\
&= \sum_{i=1}^n \left[\Psi_i^{-1} (\hat{\Gamma}_{1i} - \Gamma_{1i}) (\dot{\hat{\Gamma}}_{1i} - g_1(x_2) \sigma_{\Delta i}) + \Psi_i^{-1} (\hat{\Gamma}_{2i} - \Gamma_{2i}) (\dot{\hat{\Gamma}}_{2i} \right. \\
&\quad \left. - g_2(x_2) \sigma_{\Delta i}) + (\Psi_i^{-1} \hat{\Psi}_i - 1) \dot{\hat{\Psi}}_i + (\Psi_i^{-1} \hat{\Psi}_i - 1) (\ddot{x}_{2i-1}^d - \right. \\
&\quad \left. k_{c2i} \dot{\tilde{x}}_{2i-1} - k_{c1i} \tilde{x}_{2i-1}) \sigma_{\Delta i} + (d_i - \Psi_i^{-1} \hat{\Psi}_i k_{c3i} \text{sat}(\sigma_i)) \sigma_{\Delta i} \right] \\
&= \sum_{i=1}^n \left[\Psi_i^{-1} (\hat{\Gamma}_{1i} - \Gamma_{1i}) (\dot{\hat{\Gamma}}_{1i} - g_1(x_2) \sigma_{\Delta i}) + \Psi_i^{-1} (\hat{\Gamma}_{2i} - \Gamma_{2i}) (\dot{\hat{\Gamma}}_{2i} \right. \\
&\quad \left. - g_2(x_2) \sigma_{\Delta i}) + (\Psi_i^{-1} \hat{\Psi}_i - 1) (\dot{\hat{\Psi}}_i + (\ddot{x}_{2i-1}^d - k_{c2i} \dot{\tilde{x}}_{2i-1} \right. \\
&\quad \left. - k_{c1i} \tilde{x}_{2i-1} - k_{c3i} \text{sat}(\sigma_i)) \sigma_{\Delta i} + d_i \sigma_{\Delta i} - k_{c3i} \text{sat}(\sigma_i) \sigma_{\Delta i} \right].
\end{aligned}$$

Substituting (5-12) into (5-24) leads to:

$$\begin{aligned}
\dot{V}_6 &= \sum_{i=1}^n \left[-k_{c3i} \text{sat}(\sigma_i) \sigma_{\Delta i} + d_i \sigma_{\Delta i} \right] \\
&\leq \sum_{i=1}^n \left[-(\eta_i + D_d) \text{sat}(\sigma_i) \sigma_{\Delta i} + d_i \sigma_{\Delta i} \right] \quad (5-25) \\
&\leq \sum_{i=1}^n \left[-\eta_i |\sigma_{\Delta i}| \right].
\end{aligned}$$

Thus, the system satisfies the standard η -reachability condition, and the tracking performance of the considered system can be guaranteed with the proposed active FTC scheme in the presence of actuator faults, model uncertainties and disturbances.

5.4 Simulation Results

In order to verify the performance and capability of the proposed fault severity estimation scheme, simulations with respect to different scenarios are performed in this section.

5.4.1 Actuator Faults

In this chapter, actuator faults are modeled as loss of control effectiveness faults, which can be represented as $\gamma(t) = I - L(t)$. The term $h(x(t), t)B\gamma(t)u(t)$ in (5–2) represents the deviation in system dynamics due to actuator faults. Denoting t_f as fault occurrence time, the element $\gamma_j(t)$ in the diagonal matrix $\gamma(t)$ can be modeled as [149]:

$$\gamma_j(t) = \begin{cases} 0 & \text{if } t < t_f \\ 1 - e^{-\alpha_j(t-t_f)} & \text{if } t \geq t_f \end{cases} \quad (5-26)$$

where $\alpha_j > 0$ is a scalar denoting the unknown fault evolution rate.

Large values of α_j characterize fast faults development, which are also known as abrupt faults. Due to the fast changes, the ability to correctly detect these abrupt changes is a great challenge for most of the fault diagnosis algorithms [150]. Small values of α_j represent slow faults development, namely incipient faults. The difficulty in dealing with incipient faults is their small effects on system performance in a closed-loop system, which can be eliminated by the onboard control system. Moreover, in real applications, it is possible that faults occur in several actuators with different types and magnitudes.

Therefore, in order to make the proposed fault diagnosis strategy more general and practical, the aforementioned three types of fault modes are considered, i.e., abrupt, incipient, and multiple faults. An example of the injected abrupt and incipient fault is shown in Fig. 5.4. Beyond these faults, noises are added to actuators to make the diagnosis process more challenging and closer to practical cases for the proposed fault diagnosis scheme.

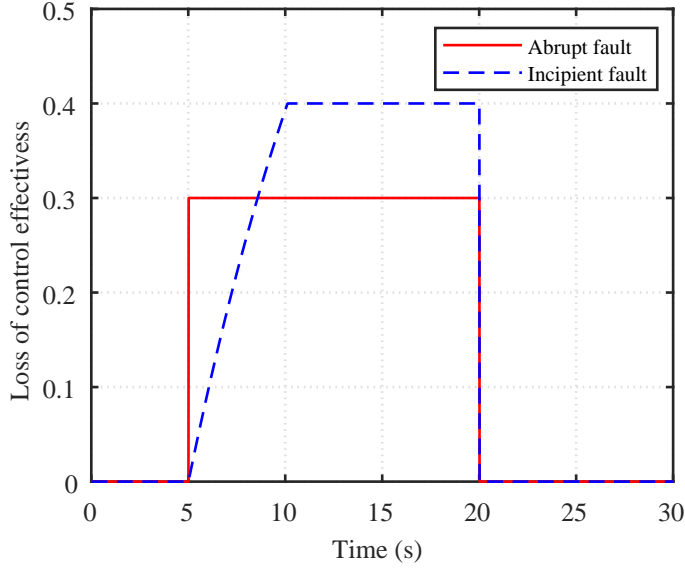


Figure 5.4: Two types of faults injected to actuators.

5.4.2 Construction of Recurrent Neural Networks

According to Fig. 5.2, four RNNs are employed for actuator faults diagnosis in the closed-loop quadrotor helicopter system. Each network has four layers where the input layer has 2 neurons, each of the two hidden layers has 10 neurons with sigmoidal activation functions, and the output layer has 1 neuron with linear function. The network weights are initialized with small random values to prevent early saturation of the hidden layer neurons. The inputs of the four networks are $[u_1, \tilde{\theta}]^T$, $[u_2, \tilde{\theta}]^T$, $[u_3, \tilde{\phi}]^T$, and $[u_4, \tilde{\phi}]^T$, respectively. u_i ($i = 1, 2, 3, 4$) is the pulse-width modulation input of the i th motor of the quadrotor helicopter as the control input to the system. $\tilde{\theta}$ and $\tilde{\phi}$ represent pitch angle tracking error and roll angle tracking error, respectively. The output of each network is the remaining control effectiveness level of the corresponding actuator which can be directly used by the control system to reconfigure the controller and accommodate actuator faults.

Table 5.2: Fault Scenarios Considered for Fault Diagnosis Problem in Simulation

Fault Scenario	Type & Magnitude	Position	Time Period (s)
1	Abrupt fault	Actuator #1	5–20
2	Incipient fault	Actuator #1	5–20
3	Abrupt fault	Actuator #1	5–20
	Incipient fault	Actuator #2	

5.4.3 Learning Phase

In order to train the designed neural networks, multiple faults with different types and magnitudes are considered and included in the training data. Due to physical limits for avoiding losing control of the quadrotor helicopter, complete actuator failure cases are not considered in this work. Thus, for generating the training samples, the loss of control effectiveness magnitude is set to be between 0 and 0.8. The neural networks are individually trained by using 8000 data points with 200 epochs. The learning rate changes from 1 to 1×10^{-5} , the covariance matrix of the dynamic noise changes from 1×10^{-2} to 1×10^{-6} , and the covariance matrix of the measurement noise changes from 100 to 5 with the change of training epoch.

5.4.4 Fault Diagnosis Case Studies

In this section, three fault scenarios are considered to demonstrate the performance of the proposed fault estimation scheme. The detailed scenario descriptions are summarized in Table 5.2 and explained as follows. In order to make the demonstrated results more clear, the shown outputs of the RNNs are only limited to the faulty actuators.

Fault scenario 1: An abrupt fault with 25% loss of control effectiveness is injected into actuator #1 between 5 and 20 s. In this case, the control input u_1 and pitch angle tracking error $\tilde{\theta}$ will be increased. By employing these two inputs, the fault estimation performance is shown in Fig. 5.5. After fault occurrence at 5 s, it can be precisely estimated by the proposed fault estimation strategy. Then, at 20 s when the actuator fault is recovered, the proposed fault estimation strategy can also

give a correct result.

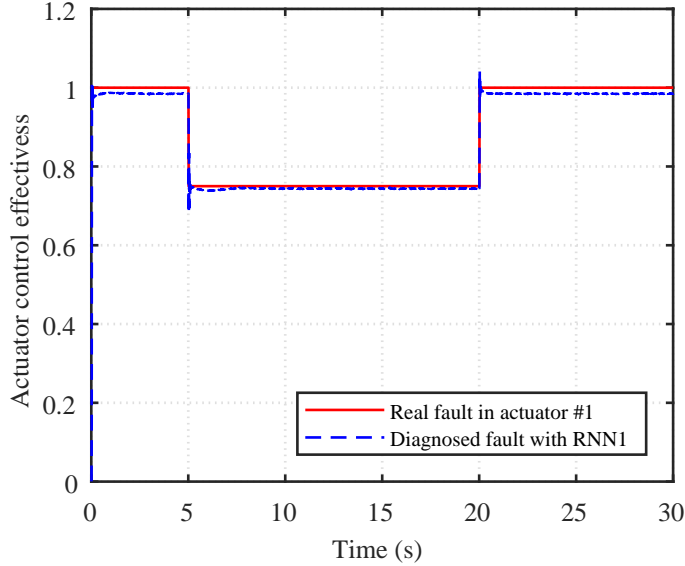


Figure 5.5: Fault estimation performance of RNN1 for actuator #1 in the presence of abrupt fault.

Fault scenario 2: An incipient fault with 25% loss of control effectiveness is introduced to actuator #1 between 5 and 20 s. The difficulty for estimating such kind of faults in the closed-loop system lies in that the feedback control system will help to maintain system tracking performance due to the low fault evolution rate. The fault severity assessment performance with the proposed fault diagnosis scheme is illustrated in Fig. 5.6. Similar to scenario 1, the proposed fault estimation scheme shows an accurate fault severity assessment result.

Fault scenario 3: Multiple actuator faults with different types and magnitudes are considered in this scenario where an abrupt fault with 30% loss of control effectiveness occurs in actuator #1 and an incipient fault with 40% loss of control effectiveness is introduced to actuator #2 at the same time. This brings more challenges for isolating the faults since both of them will affect the same system output which is difficult for most of the model-based fault diagnosis schemes [82, 150]. As shown in Fig. 5.7, the severity of both faults can be correctly and simultaneously estimated by taking advantage of the parallel structure in the proposed fault estimation scheme.

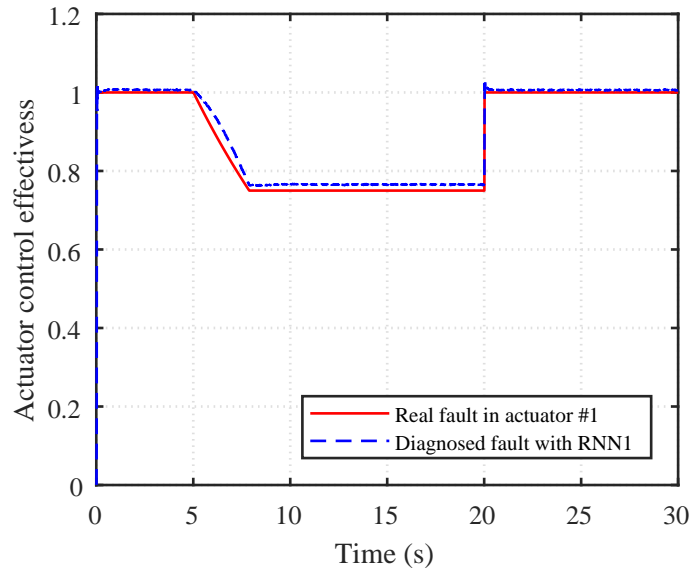


Figure 5.6: Fault estimation performance of RNN1 for actuator #1 in the presence of incipient fault.

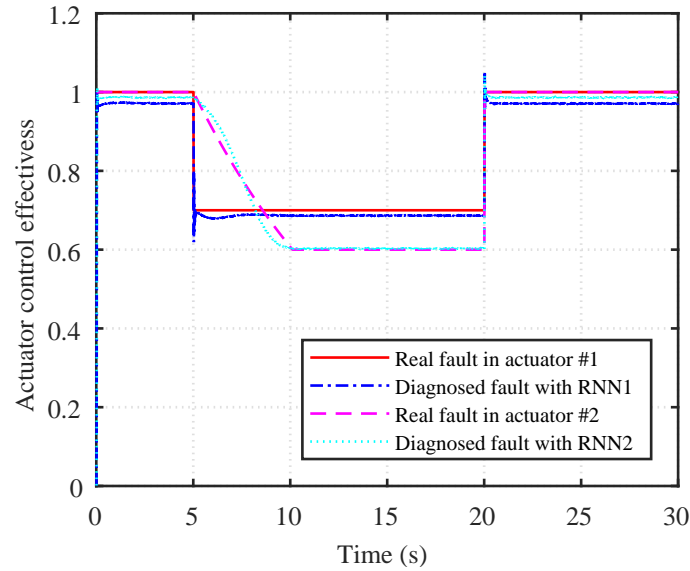


Figure 5.7: Fault estimation performance of RNN1 and RNN2 for actuator #1 and actuator #2, respectively, in the presence of multiple faults.

5.5 Experimental Results

In order to further validate the effectiveness of the proposed active FTC scheme for real applications, some real flight experiments have been carried out and are presented in this section.

5.5.1 Description of the Experiment Setup

The schematic of the experiment setup is demonstrated in Fig. 5.8. In the whole system, besides the quadrotor helicopter itself, there is another subsystem called OptiTrack, which includes twenty-four cameras as an indoor positioning system for providing the position and attitude of the quadrotor helicopter. For calculating the attitude of the quadrotor helicopter, the on-board IMU can also be used which is called HiQ. The control algorithm is compiled to C-code running on an embedded Linux-based system, namely Gumstix, that uses an ARM Cortex-M4 single-chip computer. Reference command inputs are given from the ground host computer to the on-board processor of the quadrotor helicopter through Wi-Fi wireless communication.

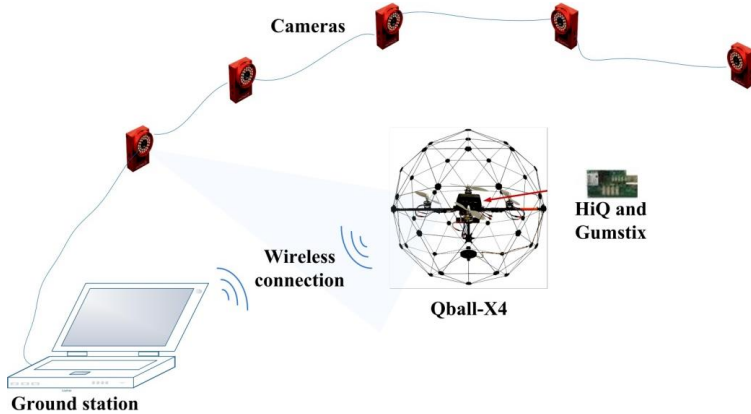


Figure 5.8: The schematic of the experiment setup.

5.5.2 Real Flight Fault Estimation and Accommodation Results

For generating training data, a set of faults with different types and magnitudes are injected into different actuators during the flight. In order to ensure the safety of the quadrotor helicopter during the experimental tests, the worst injected fault is a 50% loss of control effectiveness fault. The setup of the parameters for training the neural networks is the same as those in Section 5.4 except that the training epoch is set to be 500.

Two fault scenarios are considered in this section to test the fault estimation and accommodation effectiveness of the proposed active FTC, which are summarized in Table 5.3.

Table 5.3: Fault Scenarios Considered in Real Flight Experiment

Fault Scenario	Type & Magnitude	Position	Time Period (s)
1	Multiple abrupt faults	Actuator #1	5–15 & 15–30
2	Incipient and abrupt faults	Actuator #1	5–15 & 15–30

In the first scenario, multiple abrupt faults with different level of loss of control effectiveness in actuator #1 are considered. A 20% loss of control effectiveness fault occurs at 5 s and then it undergoes a severer trend up to 35% loss of control effectiveness at 15 s. The fault estimation result is shown in Fig. 5.9. After fault occurrence, the fault severity can be rapidly identified with only a small overshoot. Then, when the considered fault becomes severer, it can also be correctly identified by the proposed fault estimation scheme. Then, by employing the estimated fault severity, the tracking performance of the pitch motion is shown in Fig. 5.10. After fault occurrence, the proposed active FTC scheme can instantly reconfigure the corresponding control input to make a quick compensation and maintain the original system tracking performance and system stability in contrast to the conventional SMC without fault estimation scheme. Moreover, compared to the conventional SMC with the same fault estimation scheme, the proposed adaptive SMC has a better tracking performance in face of model uncertainties and can also help to reduce the tracking error at the initial stage of fault occurrence.

The second scenario corresponds to multiple different types of faults occurring in actuator #1 at different time instants, i.e., 5 s and 15 s, respectively. Due to the slow development of the incipient fault, it can be easily hidden by the onboard controller at the early stage which makes it hard to be identified. Moreover, the different system responses to abrupt fault and incipient fault will also bring more difficulty for the proposed fault estimation scheme. As shown in Fig. 5.11, the severity of both faults can be instantaneously and accurately identified once they occur despite the aforementioned difficulties. The corresponding tracking performance of the pitch motion is shown in Fig. 5.12. Due to the slow evolution of the incipient fault, it has a smaller adverse effect on system tracking performance compared to abrupt fault. The proposed active FTC scheme

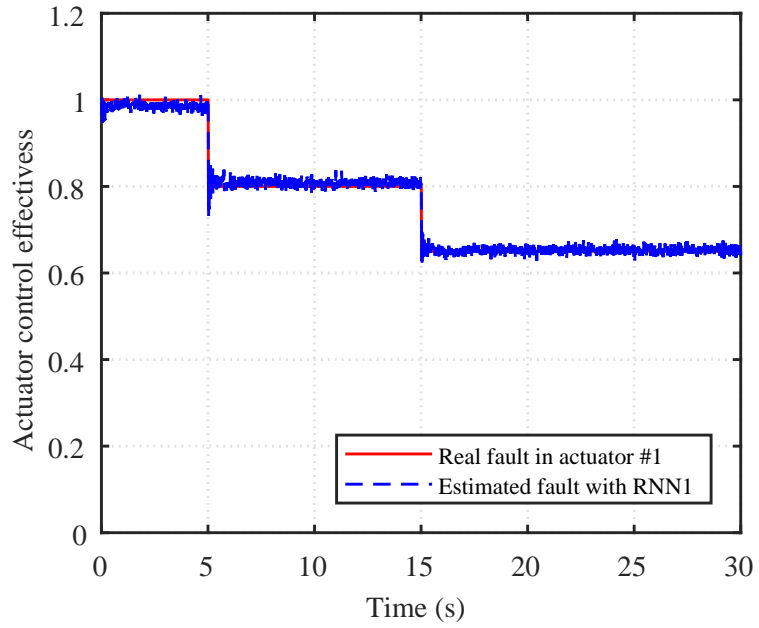


Figure 5.9: Fault estimation performance of RNN1 for actuator #1 in the presence of multiple abrupt faults in real flight test.

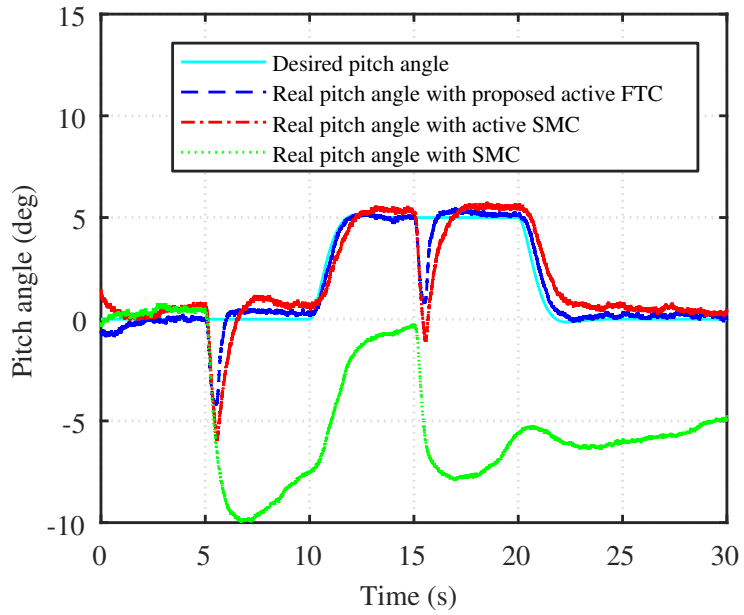


Figure 5.10: Tracking performance of pitch motion in the presence of multiple abrupt faults in real flight test.

shows a better system tracking performance compared to the other two control methods after fault occurrence.

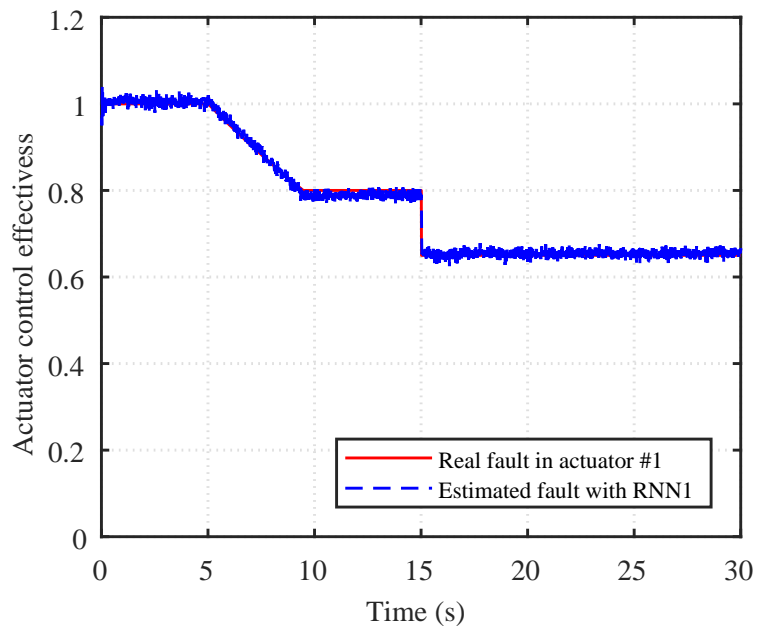


Figure 5.11: Fault estimation performance of RNN1 for actuator #1 in the presence of incipient and abrupt faults in real flight test.

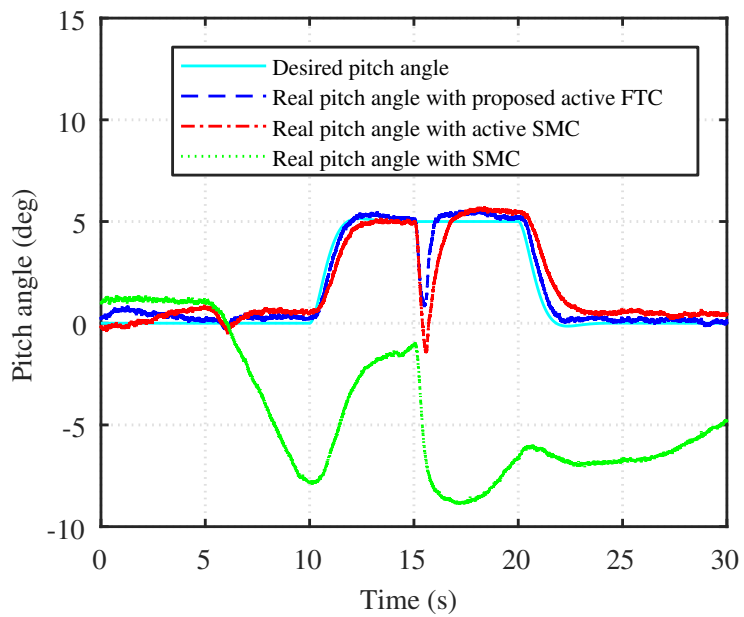


Figure 5.12: Tracking performance of pitch motion in the presence of incipient and abrupt faults in real flight test.

5.6 Conclusion

In this chapter, an active FTC strategy based on adaptive SMC and RNN is proposed to accommodate actuator faults and model uncertainties for a quadrotor helicopter. With the help of the developed online adaptive schemes, the proposed control strategy can adaptively generate appropriate control signals to compensate model uncertainties without the knowledge of uncertainty bounds to maintain tracking performance and stability of the quadrotor helicopter. Then, by designing a parallel bank of RNNs, the severity of the actuator faults can be precisely and reliably estimated, which is then synthesized with the proposed adaptive SMC to reconfigure the controller and accommodate actuator faults. Moreover, the actuator fault estimation error is explicitly considered, which can be compensated by the proposed adaptive control schemes. In this way, the robustness of the proposed active FTC strategy is improved. The simulation results show that the proposed scheme can effectively estimate the severity of various kinds of actuator faults in the closed-loop quadrotor helicopter system. Furthermore, the demonstrated experimental results confirm the effectiveness and superiority of the proposed active FTC strategy with comparison to a conventional SMC.

5.7 Appendix

The Jacobian matrix F_k is calculated by using the back-propagation-through-time algorithm that can be written as follows:

$$F_k = \begin{bmatrix} \frac{\partial Y}{\partial W_{N1}} & \frac{\partial Y}{\partial W_{N2}} & \frac{\partial Y}{\partial W_O} \end{bmatrix} \quad (5-27)$$

where the detailed formulations for $\frac{\partial Y}{\partial W_{N1}}$, $\frac{\partial Y}{\partial W_{N2}}$, and $\frac{\partial Y}{\partial W_O}$ can be found in (5-28)–(5-30).

$$\begin{aligned}
\frac{\partial Y}{\partial W_O} &= \left[\begin{array}{cccccc} \frac{\partial y_1}{\partial W_O(1,1)} & \cdots & \frac{\partial y_1}{\partial W_O(1,N2)} & \cdots & \frac{\partial y_1}{\partial W_O(q,1)} & \cdots & \frac{\partial y_1}{\partial W_O(q,N2)} \\ \frac{\partial y_2}{\partial W_O(1,1)} & \cdots & \frac{\partial y_2}{\partial W_O(1,N2)} & \cdots & \frac{\partial y_2}{\partial W_O(q,1)} & \cdots & \frac{\partial y_2}{\partial W_O(q,N2)} \\ \vdots & \vdots & \vdots & \vdots & \vdots & \vdots & \vdots \\ \frac{\partial y_q}{\partial W_O(1,1)} & \cdots & \frac{\partial y_q}{\partial W_O(1,N2)} & \cdots & \frac{\partial y_q}{\partial W_O(q,1)} & \cdots & \frac{\partial y_q}{\partial W_O(q,N2)} \end{array} \right] \\
&= \left[\begin{array}{ccccccccc} x_{2,1}(k) & \cdots & x_{2,N2}(k) & 0 & \cdots & 0 & 0 & \cdots & 0 \\ 0 & \cdots & 0 & x_{2,1}(k) & \cdots & x_{2,N2}(k) & 0 & \cdots & 0 \\ \vdots & \vdots & \vdots & \ddots & \ddots & \ddots & \vdots & \vdots & \vdots \\ 0 & \cdots & 0 & 0 & \cdots & 0 & x_{2,1}(k) & \cdots & x_{2,N2}(k) \end{array} \right] \quad (5-28) \\
&= \left[\begin{array}{ccc} x_2(k) & 0 & 0 \\ 0 & \ddots & 0 \\ 0 & 0 & x_2(k) \end{array} \right]
\end{aligned}$$

$$\begin{aligned}
\frac{\partial Y}{\partial W_{N2}} &= W_O(k-1) \left[\begin{array}{cccc} \frac{\partial x_{2,1}(k)}{\partial W_{N2}(1:)} & \frac{\partial x_{2,1}(k)}{\partial W_{N2}(2:)} & \cdots & \frac{\partial x_{2,1}(k)}{\partial W_{N2}(N2:)} \\ \frac{\partial x_{2,2}(k)}{\partial W_{N2}(1:)} & \frac{\partial x_{2,2}(k)}{\partial W_{N2}(2:)} & \cdots & \frac{\partial x_{2,2}(k)}{\partial W_{N2}(N2:)} \\ \vdots & \vdots & \vdots & \vdots \\ \frac{\partial x_{2,N2}(k)}{\partial W_{N2}(1:)} & \frac{\partial x_{2,N2}(k)}{\partial W_{N2}(2:)} & \cdots & \frac{\partial x_{2,N2}(k)}{\partial W_{N2}(N2:)} \end{array} \right] \\
&= W_O(k-1) \left[\begin{array}{ccc} \varphi'(W_{N2}(1:)(k-1), x_1) & 0 & 0 \\ 0 & \ddots & 0 \\ 0 & 0 & \varphi'(W_{N2}(N2:)(k-1), x_1) \end{array} \right] x_1(k) \quad (5-29)
\end{aligned}$$

$$\begin{aligned}
\frac{\partial Y}{\partial W_{N1}} &= W_O(k-1) \varphi'(W_{N2}(k-1), x_1(k)) W_{N2}(k-1) \\
&\quad \left[\begin{array}{cccc} \frac{\partial x_{1,1}(k)}{\partial W_{N1}(1 :)} & \frac{\partial x_{1,1}(k)}{\partial W_{N1}(2 :)} & \cdots & \frac{\partial x_{1,1}(k)}{\partial W_{N1}(N1 :)} \\ \frac{\partial x_{1,2}(k)}{\partial W_{N1}(1 :)} & \frac{\partial x_{1,2}(k)}{\partial W_{N1}(2 :)} & \cdots & \frac{\partial x_{1,2}(k)}{\partial W_{N1}(N1 :)} \\ \vdots & \vdots & \vdots & \vdots \\ \frac{\partial x_{1,N1}(k)}{\partial W_{N1}(1 :)} & \frac{\partial x_{1,N1}(k)}{\partial W_{N1}(2 :)} & \cdots & \frac{\partial x_{1,N1}(k)}{\partial W_{N1}(N1 :)} \end{array} \right] \\
&= W_O(k-1) \varphi'(W_{N2}(k-1), x_1(k)) W_{N2}(k-1) \\
&\quad \left[\begin{array}{ccccc} \varphi' \left(W_{N1}(1 :)(k-1), \begin{bmatrix} x_1(k-1) \\ u(k-1) \end{bmatrix} \right) & 0 & & & 0 \\ 0 & \ddots & & & 0 \\ 0 & & \varphi' \left(W_{N1}(N1 :)(k-1), \begin{bmatrix} x_1(k-1) \\ u(k-1) \end{bmatrix} \right) & & \\ \left(\begin{bmatrix} x_1(k-1) \\ u(k-1) \end{bmatrix} + W_{N1}(k-1) \right) & & & & \\ \varphi' \left(W_{N1}(1 :)(k-1), \begin{bmatrix} x_1(k-1) \\ u(k-1) \end{bmatrix} \right) & 0 & & & 0 \\ 0 & \ddots & & & 0 \\ 0 & & \varphi' \left(W_{N1}(N1 :)(k-1), \begin{bmatrix} x_1(k-1) \\ u(k-1) \end{bmatrix} \right) & & \\ \left(\begin{bmatrix} x_1(k-2) \\ u(k-2) \end{bmatrix} \right) & & & & \end{array} \right] \tag{5-30}
\end{aligned}$$

Chapter 6

Adaptive Fault-Tolerant Control Allocation

This chapter proposes a novel adaptive sliding mode-based control allocation scheme for accommodating simultaneous actuator faults. The proposed control scheme includes two separate control modules, which are the virtual control module and the control allocation module, respectively. As a low-level control module, the control allocation/re-allocation scheme is used to distribute/redistribute virtual control signals among the available actuators under fault-free and faulty cases, respectively. In the case of simultaneous actuator faults, the control allocation and re-allocation module may fail to meet the required virtual control signal which will degrade the overall system stability. The proposed on-line adaptive scheme can seamlessly adjust the control gains for the high-level sliding mode control module and reconfigure the distribution of control signals to eliminate the effect of the virtual control error and maintain stability of the closed-loop system. In addition, with the help of the boundary layer for constructing the adaptation law, the overestimation of control gains is avoided, and the adaptation ceases once the sliding variable is within the boundary layer. A significant feature of this study is that the stability of the closed-loop system is guaranteed theoretically in the presence of simultaneous actuator faults. The effectiveness of the proposed control scheme is demonstrated by experimental results based on a modified unmanned multirotor helicopter under both single and simultaneous actuator faults conditions with comparison to a conventional sliding mode controller and a linear quadratic regulator scheme.

6.1 Introduction

As argued in [11–13], the increasing demands for safety, reliability, and high system performance have stimulated research in the area of FTC with the development in control theory and computer technology. Fault-tolerant capability is an important feature for safety-critical systems [11], such as UAVs [14], spacecrafts [17], wind turbines [18] etc., which will help to minimize the effect of possible faults/failures in the system and preserve the performance of the entire system. In terms of developing and testing advanced FDD and FTC schemes on quadrotor helicopters, the work described in [14] represents the cutting edge research in this area. However, due to the configuration of quadrotor helicopter, it lacks available actuator redundancy which is critical for a safer operation. As a consequence, a failure of any one of the motors will result in a crash of the quadrotor helicopter. In this case, it will harm not only the UAV itself but also its surroundings, which is catastrophic especially for those applications carried out in urban areas. For this reason, FTC should be considered and embedded in flight control laws for UAVs to improve the reliability and safety of UAV systems.

Most studies about FTC on quadrotor helicopters only consider partial actuator fault in the literature due to the limited hardware redundancy available in such a system. Some researchers sacrifice the yaw motion control to maintain the pitch and roll motion control performance when one motor encounters big fault or even failure [151–153]. However, in this case, it is hard to continue the assigned mission, and emergency landing should be executed. An obvious alternative is to increase physical redundancy and embed FTC within the physical redundancy structure of the system [154]. In the case of a quadrotor helicopter, it could become a hexarotor or octorotor helicopter with the increased hardware redundancy, which can also increase system performance such as increased payload capability, etc. This will significantly improve the reliability and survivability of the system due to the redundant motors [155], which can be naturally used to develop and test advanced FTC schemes. In [156], Du *et al.* analyze the controllability for a class of hexarotor helicopters subject to motor failure. When one motor fails, the hexarotor helicopter

considered in [156] is uncontrollable, even though it is over-actuated compared to a quadrotor helicopter. Thus, in order to minimize flight performance degradation in the case of motor failure, an octorotor helicopter is a better choice for real applications. Motivated by this, the author mounted extra four motors under the original ones on an existing quadrotor helicopter available at the author's lab, respectively. Compared to the octorotor helicopter used in [157] and [158], the one used in this chapter is more compact, and more suitable for applications in urban and indoor environments. In fact, due to payload and better flight performance requirements for different engineering applications, more and more hexarotor and octorotor helicopters are available on the small UAVs market. Such a development and application trend also provides natural needs and platforms for developing and implementing FTC strategies on these UAVs towards satisfaction of strict safety and reliability demands by US Federal Aviation Administration (FAA) or other country's licensing & certificating authorities for practical and commercial uses of developed UAVs. With the increase of available redundant actuators, the problem of allocating them to achieve the desired forces and moments becomes non-unique and far more complex. Such redundancy has called for effective control allocation schemes to distribute the required control forces and moments over the available actuators. In particular, in the case of actuator fault/failure, an effective control re-allocation of the remaining healthy actuators is needed to achieve acceptable performance.

As one of the effective control techniques for controlling over-actuated systems, control allocation approach offers the advantage of modular design, where the design of the high-level control strategy is independent of the actuator configuration by introducing the virtual control module and control allocation module, respectively. The allocation of the virtual control signals to the individual actuators is accomplished within the control allocation module. Important issues such as input saturation, rate constraints, and actuator fault-tolerance can also be handled within this module. The control allocation problem without considering system fault/failure has been intensively studied following the work of Durham [52]. In the presence of actuator fault/failure, an effective re-allocation of the virtual control signals to the remaining healthy actuators is needed to maintain system performance, which is referred to as reconfigurable control allocation problem [66]. In the

context of reconfigurable FTC, Zhang *et al.* [66, 67] present the concept of control allocation and re-allocation for aircraft with redundant control effectors. Moreover, for the sake of the overall system performance and stability, a high-level virtual controller is needed to provide the desired virtual control signals for the low-level control allocation module.

SMC is known as a robust control approach to maintain system performance and keep the closed-loop system insensitive to uncertainties and disturbances [33]. Due to this advantage of SMC over the other nonlinear control approaches, it has been extensively employed in the FTC area [16, 23, 38, 39, 43, 47, 48]. However, only SMC itself cannot directly deal with complete actuator failure without any redundant actuators [159]. In particular, most studies of FTC using SMC technique on multirotor helicopters only deal with partial loss of control effectiveness fault in actuators [23, 43]. Since the publication of the early works [66, 67] on combination of a baseline control law with a reconfigurable control allocation scheme for achieving FTC, SMC and other baseline/virtual control laws combined with control allocation schemes have been developed in recent years [38, 68, 69, 159]. In this case, the virtual control signals will be re-allocated to the remaining healthy actuators in the presence of actuator fault/failure without reconfiguring the high-level SMC to inherit the original system performance. However, most of the reconfigurable control allocation schemes in the literature only focus on the allocation of the virtual control signals over the available actuators to minimize the designed performance function and rarely concern the stability of the overall system. If the control allocation module fails to meet the required virtual control signals, the performance of the overall system will be degraded or even the stability of the overall system cannot be maintained anymore.

In this chapter, a novel control scheme by combining adaptive SMC with control allocation is proposed, which can accommodate simultaneous actuator faults in the same grouped actuators and maintain the stability of the closed-loop system. Here, the grouped actuators stands for the actuators which have the same/similar control effects on the aircraft or specially on the octorotor helicopter platform developed in this work. The main contributions of this chapter are summarized as follows:

- 1) The stability of the entire control system is considered and proven theoretically. When control allocation module fails to meet the required virtual control signals, the tracking performance and stability of the closed-loop system can still be maintained with the proposed control scheme.
- 2) The proposed control scheme is able to tolerate both single actuator fault and simultaneous actuator faults, where not only the control re-allocation scheme needs to be triggered to redistribute more control signals to the less affected actuators, but also the synthesized adaptive scheme will be employed to adjust the control gains for the high-level control module to compensate the virtual control error generated by the low-level control allocation module.
- 3) The design of the adaptive control law can significantly reduce the use of discontinuous control strategy of SMC, which can help to suppress control chattering. Moreover, the over-estimation of control gains is avoided with the construction of adaptation law. The adaptation ceases once the sliding surface is within the defined boundary layer.

The remainder of this chapter is organized as follows. The modeling of the modified octorotor helicopter and problem formulation are described in Section 6.2. Then in Section 6.3, the detailed design procedure of the proposed adaptive FTC scheme is presented. The simulation and experimental results based on the modified octorotor helicopter are followed in Sections 6.4 and 6.5 to demonstrate the effectiveness of the proposed control scheme. Finally, general conclusions of this chapter are summarized in Section 6.6.

6.2 Problem Formulation

6.2.1 Modeling of an Octorotor Helicopter

In this section, the mathematical model of the octorotor helicopter is presented, which is modified based on a quadrotor helicopter produced by Quanser. In fact, in order to keep the compact structure of the modified octorotor helicopter, the extra four motors should be added just under the

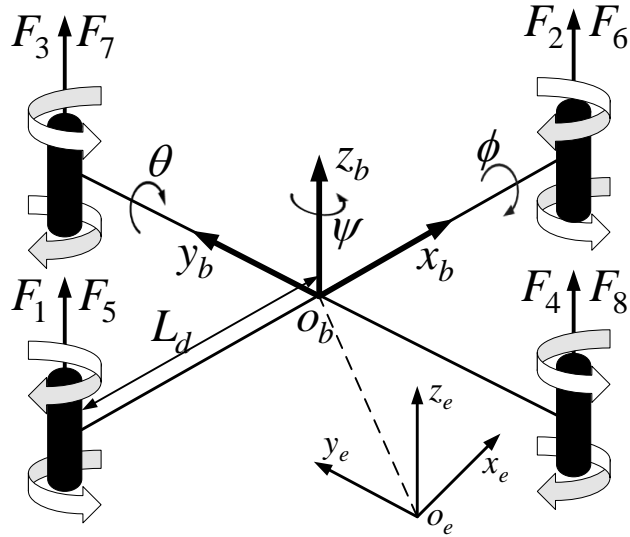


Figure 6.1: Configuration of the modified octorotor helicopter.

original ones, respectively. The rotational direction of each added motor is set opposite to the original one inspired by coaxial helicopters, which can counteract the yaw torque mutually as depicted in Fig. 6.1.

Assume that the changes of roll and pitch angles are very small, and therefore the nonlinear dynamics of the octorotor helicopter can be represented as:

$$\begin{aligned}
 \ddot{x}_e &= \frac{(\cos \phi \sin \theta \cos \psi + \sin \phi \sin \psi)U_z}{m} - \frac{K_1 \dot{x}_e}{m} \\
 \ddot{y}_e &= \frac{(\cos \phi \sin \theta \sin \psi - \sin \phi \cos \psi)U_z}{m} - \frac{K_2 \dot{y}_e}{m} \\
 \ddot{z}_e &= \frac{(\cos \phi \cos \theta)U_z}{m} - \frac{K_3 \dot{z}_e}{m} - g \\
 \ddot{\phi} &= \frac{(I_{yy} - I_{zz})\dot{\theta}\dot{\psi}}{I_{xx}} + \frac{U_\phi}{I_{xx}} - \frac{I_r \Omega \dot{\theta}}{I_{xx}} - \frac{K_4 L_d \dot{\phi}}{I_{xx}} \\
 \ddot{\theta} &= \frac{(I_{zz} - I_{xx})\dot{\phi}\dot{\psi}}{I_{yy}} + \frac{U_\theta}{I_{yy}} + \frac{I_r \Omega \dot{\phi}}{I_{yy}} - \frac{K_5 L_d \dot{\theta}}{I_{yy}} \\
 \ddot{\psi} &= \frac{(I_{xx} - I_{yy})\dot{\phi}\dot{\theta}}{I_{zz}} + \frac{U_\psi}{I_{zz}} - \frac{K_6 \dot{\psi}}{I_{zz}}.
 \end{aligned} \tag{6-1}$$

Due to the configuration of the octorotor helicopter, the attitude (ϕ, θ) is coupled with the position (x_e, y_e) , and a pitch or roll angle is required in order to move the octorotor helicopter along the x_e - or y_e -direction. The virtual control inputs as shown in (6-1) for moving and stabilizing the

octorotor helicopter are mapped from the thrusts generated by the eight independent motors, which can be represented as:

$$\begin{bmatrix} U_z \\ U_\phi \\ U_\theta \\ U_\psi \end{bmatrix} = \begin{bmatrix} K_u & K_u \\ 0 & 0 & K_u L_d & -K_u L_d & 0 & 0 & K_u L_d & -K_u L_d \\ K_u L_d & -K_u L_d & 0 & 0 & K_u L_d & -K_u L_d & 0 & 0 \\ K_y & K_y & -K_y & -K_y & -K_y & -K_y & K_y & K_y \end{bmatrix} \begin{bmatrix} u_1 \\ u_2 \\ u_3 \\ u_4 \\ u_5 \\ u_6 \\ u_7 \\ u_8 \end{bmatrix}. \quad (6-2)$$

6.2.2 Problem Statement

Consider a nonlinear affine system:

$$\dot{x}(t) = f(x(t), t) + h(x(t), t)\nu(t) + d(t) \quad (6-3)$$

$$\nu(t) = B_u L_c(t)u(t) \quad (6-4)$$

where (6-4) represents the relationship between the virtual control inputs and the actual control inputs [160]. $u(t) \in \mathbb{R}^m$ is the control input vector, $\nu(t) \in \mathbb{R}^n$ is the virtual control input vector, and $x(t) \in \mathbb{R}^n$ is the state vector. The vector $f(x(t), t) \in \mathbb{R}^n$ is a nonlinear function and $h(x(t), t) \in \mathbb{R}^{n \times n}$ is a diagonal matrix. $d(t) \in \mathbb{R}^n$ represents disturbance which is assumed to be unknown but bounded, $\|d(t)\| \leq D$. $B_u \in \mathbb{R}^{n \times m}$ is the control effectiveness matrix. $L_c(t) = \text{diag}([l_{c1}(t), l_{c2}(t), \dots, l_{cm}(t)])$ represents the control effectiveness level of the actuators, where $l_{cj}(t)$ ($j = 1, 2, \dots, m$) is a scalar satisfying $0 \leq l_{cj}(t) \leq 1$. If $l_{cj}(t) = 1$, the j th actuator works perfectly, otherwise, the j th actuator suffers certain level of fault with a special case $l_{cj}(t) = 0$ denoting the complete failure of the j th actuator.

In this chapter, control allocation problem refers to the distribution of the virtual control signals over the available actuators. In a faulty condition where $l_{cj}(t) < 1$, given the desired virtual control signal $\nu_d(t)$, the solution $u(t)$ is searched such that $\nu_d(t) = B_u L_c(t)u(t)$ is satisfied. To facilitate the controller development, the following assumptions with respect to the nonlinear affine system (6–3)–(6–4) are made.

Assumption 6.1 *The matrix B_u has the full row rank, i.e., $\text{rank}(B_u) = n < m$.*

Assumption 6.2 *The control input $u(t)$ lies in a compact set Ω_u described as:*

$$u(t) \in \Omega_u = \{u(t) \in \mathbb{R}^m | u_{\min} \leq u(t) \leq u_{\max}\} \quad (6-5)$$

where $u_{\min} = \{u_{1\min}, u_{2\min}, \dots, u_{m\min}\}$ and $u_{\max} = \{u_{1\max}, u_{2\max}, \dots, u_{m\max}\}$.

Assumption 6.1 implies a necessary condition for a system to be over-actuated. In this chapter, the number of redundant actuators is chosen to be four in order to accommodate actuator failures and also due to the special symmetrical configuration of the original quadrotor helicopter. In this case, the rank of the control effectiveness matrix B_u is four. The control input constraints described in Assumption 6.2 are the same for all the actuators in this chapter. For simplicity of the expression, the notation t is omitted in the following sections, e.g., $x(t)$ is expressed as x .

6.2.3 Formulation of the Transformed System

The actuators used in the octorotor helicopter can provide not only required torques but also forces to maintain the demanded attitude and height. Therefore, the attitude and height controllers are both directly related to the actuators. Then, the state vector is defined as follows:

$$\begin{aligned} x &= [z_e \ \dot{z}_e \ \phi \ \dot{\phi} \ \theta \ \dot{\theta} \ \psi \ \dot{\psi}]^T \\ &= [x_1 \ x_2 \ x_3 \ x_4 \ x_5 \ x_6 \ x_7 \ x_8]^T. \end{aligned} \quad (6-6)$$

With this state vector, the dynamic equations of the octorotor helicopter in (6–1) can be resolved into the following subsystems.

Height subsystem:

$$\begin{aligned}\dot{x}_1 &= x_2 \\ \dot{x}_2 &= f_1(x) + h_1\nu_1 + d_1\end{aligned}\tag{6–7}$$

where $f_1(x) = -g$, $h_1 = \cos \phi \cos \theta / m$, and $d_1 = -K_3 \dot{z}_e / m$.

Roll subsystem:

$$\begin{aligned}\dot{x}_3 &= x_4 \\ \dot{x}_4 &= f_2(x) + h_2\nu_2 + d_2\end{aligned}\tag{6–8}$$

where $f_2(x) = x_6 x_8 (I_{yy} - I_{zz}) / I_{xx}$, $h_2 = 1 / I_{xx}$, and $d_2 = -I_r \dot{\theta} \Omega / I_{xx} - K_4 L_d \dot{\phi} / I_{xx}$.

Pitch subsystem:

$$\begin{aligned}\dot{x}_5 &= x_6 \\ \dot{x}_6 &= f_3(x) + h_3\nu_3 + d_3\end{aligned}\tag{6–9}$$

where $f_3(x) = x_4 x_8 (I_{zz} - I_{xx}) / I_{yy}$, $h_3 = 1 / I_{yy}$, and $d_3 = I_r \dot{\phi} \Omega / I_{yy} - K_5 L_d \dot{\theta} / I_{yy}$.

Yaw subsystem:

$$\begin{aligned}\dot{x}_7 &= x_8 \\ \dot{x}_8 &= f_4(x) + h_4\nu_4 + d_4\end{aligned}\tag{6–10}$$

where $f_4(x) = x_4 x_6 (I_{xx} - I_{yy}) / I_{zz}$, $h_4 = 1 / I_{zz}$, and $d_4 = -K_6 \dot{\psi} / I_{zz}$.

Therefore, in this transformed system, there are four system outputs, four actuators and four redundant actuators. Then, each subsystem can be written as a single-input nonlinear system with the help of the virtual control input given by:

$$\begin{aligned}\dot{x}_{2i-1} &= x_{2i} \\ \dot{x}_{2i} &= f_i(x) + h_i\nu_i + d_i\end{aligned}\tag{6–11}$$

where $i = 1, 2, 3, 4$ represents each subsystem.

6.3 Adaptive Fault-Tolerant Control Allocation

In this section, an adaptive sliding mode control allocation (ASMCA) scheme is designed to accommodate actuator faults for the modified octorotor helicopter. The control allocation and re-allocation scheme itself could compensate actuator fault/failure without affecting the high-level control performance when only one of the actuators in the same group malfunctions. In the case of simultaneous actuator faults in the same group, not only the control re-allocation scheme needs to be triggered to redistribute more control signals to the less affected actuators, but also the synthesized adaptive scheme is employed to adjust the control gains for the high-level sliding mode controller to compensate the virtual control error. In such a way, the overall system performance can be maintained in both single and simultaneous actuator fault/failure conditions. The schematic of the proposed adaptive fault-tolerant control strategy is depicted in Fig. 6.2.

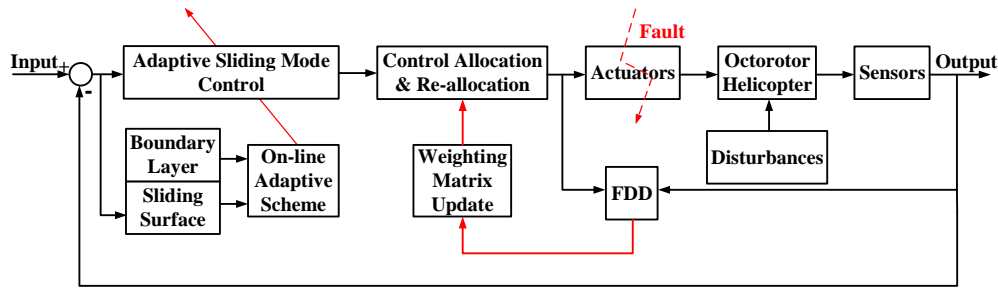


Figure 6.2: The schematic of the proposed adaptive fault-tolerant control strategy.

6.3.1 Fault-Tolerant Control Allocation

One way to achieve fault-tolerance for control allocation scheme is to solve a constrained optimization problem on-line at every sampling instant. The 2-norm (quadratic) formulation seems to be favorable over the 1-norm (linear) formulation since the solution tends to combine the use of all control surfaces rather than just a few [64].

Considering the implementation of the control scheme in real systems, the control re-allocation needs to be triggered instantly when actuator fault/failure occurs. Given the system in (6–3), the

control input u is computed employing quadratic optimization approach, such that conditions as shown in (6–4) and (6–5) can be satisfied.

Lemma 6.1 *The quadratic programming approach based on minimizing control input can be described as [38]:*

$$\begin{aligned} J &= \arg \min_u u^T W u \\ s.t. \quad \nu_i &= B_{ui} u, \end{aligned} \tag{6–12}$$

and it has an explicit solution as follows [38]:

$$u = W B_{ui}^T (B_{ui} W B_{ui}^T)^{-1} \nu_i \tag{6–13}$$

where $W = W^T = \text{diag}([w_1, w_2, \dots, w_m])$ is a symmetric positive definite weighting matrix, $B_{ui} \in \mathbb{R}^m$ is the control effectiveness matrix directly related to actuators, and ν_i is the virtual control signal from the high-level controller.

Since the considered system is over-actuated and in principle there exists a set of admissible control inputs u . When some of the actuators encounter faults/failures, the control allocation scheme should have the capability to redistribute the control efforts from the faulty actuators to the healthier ones. In order to achieve this goal, the commonly used approach is to change the weighting matrix W , which requires fault information from the FDD module. The larger of the corresponding gain in the weighting matrix, the less of the control input to the corresponding actuator.

In the case of single actuator fault/failure, the weighting matrix is updated according to the fault information from the FDD module without affecting the high-level controller, namely, $w_j = 1/l_{cj}$ ($j = 1, 2, \dots, m$). In this situation, more control efforts will be distributed to the healthier actuators. Specially, when the j th actuator experiences complete failure, the corresponding weighting parameter w_j will become infinity which means there will be no control effort distributed to this actuator.

In the case of simultaneous actuator faults, where control allocation and re-allocation scheme fails to maintain the closed-loop system stability, an adaptive scheme is synthesized to compensate this faulty condition. In this circumstance, the condition described in (6–4) cannot be satisfied due to the control input constraints described in (6–5), which will result in errors between the generated virtual control signals from the low-level control allocation module and the desired ones from the high-level virtual control module.

Let $\nu_i = \nu_{id} + \tilde{\nu}_i$, the following system dynamics can be obtained:

$$\dot{x}_{2i} = f_i(x) + h_i\nu_{id} + h_i\tilde{\nu}_i + d_i \quad (6-14)$$

where $\tilde{\nu}_i$ denotes the virtual control error.

In order to maintain the closed-loop system performance, the high-level sliding mode controller needs to be reconfigured. For this reason, an adaptive approach is employed.

6.3.2 Design of High-Level Sliding Mode Control

The design of a sliding mode controller is typically composed of two steps. The first step features the construction of a sliding surface, on which the system performance could be maintained as expected. The second step is concerned with the selection of the control law to force the sliding variable reach the sliding surface, and hereafter keep the sliding motion within the close neighborhood of the sliding surface. However, during the reaching phase, the insensitivity of the controller cannot be ensured. One way to solve this problem is to employ integral SMC scheme, such that the robustness of the system can be guaranteed throughout the entire response of the system starting from the initial time instant [161].

The integral sliding surface for the system is defined by the following set:

$$S_i = \{x \in \mathbb{R}^n : \sigma_i(x) = 0\}. \quad (6-15)$$

The switching function $\sigma_i(x)$ is defined as:

$$\sigma_i(x) = \sigma_{i0}(x) + z_i \quad (6-16)$$

$$\sigma_{i0}(x) = C_i^T x \quad (6-17)$$

where $C_i \in \mathbb{R}^n$, $\sigma_{i0}(x)$ is the linear combination of the states, which is similar to the conventional SMC design, and z_i includes the integral term.

The choice of z_i is determined by the following equations in order to guarantee that $\sigma_i(x, t_0) = 0$.

$$\dot{z}_i = -C_i^T(f_i^0(x^0) + h_i^0\nu_i^0) \quad (6-18)$$

$$z_i(0) = -C_i^T x(t_0) \quad (6-19)$$

i.e.,

$$z_i = -C_i^T[x(t_0) + \int_{t_0}^t (f_i^0(x^0(\tau)) + h_i^0\nu_i^0(\tau))d\tau]. \quad (6-20)$$

Due to this definition of z_i , $\sigma_i(x(t_0), t_0) = \sigma_{i0}(x(t_0), t_0) + z_i(0) = 0$ can be obtained and sliding motion occurs at the initial time instant t_0 . Hence, the system trajectory under integral SMC starts from the designed sliding surface and the reaching phase is eliminated accordingly in contrast with conventional SMC.

Then, after obtaining the sliding surface, the problem is to design an appropriate control law to make the sliding surface attractive. The control law is designed in the following form:

$$\nu_i = \nu_{i0} + \nu_{i1} \quad (6-21)$$

where ν_{i0} is the continuous nominal control part to stabilize the ideal system without actuator faults and disturbances and guide it to a given trajectory with satisfactory accuracy. ν_{i1} is the discontinuous control part for compensating the perturbations and disturbances in order to ensure the sliding motion.

For $\forall i = 1, 2, 3, 4$, denoting x_{2i-1}^d and x_{2i}^d as the desired trajectories, the tracking errors can be defined as $\tilde{x}_{i1} = x_{2i-1} - x_{2i-1}^d$ and $\tilde{x}_{i2} = x_{2i} - x_{2i}^d$. According to the definition of the integral sliding surface in (6–16)–(6–20), the switching function can be rewritten as:

$$\sigma_{i0} = c_i \tilde{x}_{i1} + \tilde{x}_{i2} \quad (6-22)$$

$$\begin{aligned} \dot{\tilde{x}}_i &= -c_i \tilde{x}_{i2} + k_{i2} \tilde{x}_{i2} + k_{i1} \tilde{x}_{i1} \\ z_i(0) &= -c_i \tilde{x}_{i1}(t_0) - \tilde{x}_{i2}(t_0). \end{aligned} \quad (6-23)$$

Such that,

$$\sigma_i = \tilde{x}_{i2} + k_{i2} \tilde{x}_{i1} + k_{i1} \int_{t_0}^t \tilde{x}_{i1}(\tau) d\tau - k_{i2} \tilde{x}_{i1}(t_0) - \tilde{x}_{i2}(t_0). \quad (6-24)$$

From the switching function defined in (6–24), it can be observed that regardless of the values of x_{2i-1}^d and x_{2i}^d at t_0 , the sliding variable is already on the sliding surface once the sliding motion begins. The positive constant c_i is used to define the switching function as shown in (6–22) and (6–23). However, c_i does not appear in (6–24), which means c_i is not necessary here to obtain the sliding surface. Therefore, no matter what the value of c_i is, the sliding motion will not be affected.

In order to analyze the sliding motion associated with the switching function as shown in (6–24), the time derivative of the switching function is computed as follows:

$$\dot{\sigma}_i = \dot{\tilde{x}}_{i2} + k_{i2} \tilde{x}_{i2} + k_{i1} \tilde{x}_{i1}. \quad (6-25)$$

The equivalent control ν_{i0} is designed by equalizing $\dot{\sigma}_i = 0$. In this case, the disturbance d_i is omitted, and the system is given as:

$$\dot{x}_{2i} = f_i(x) + h_i \nu_i. \quad (6-26)$$

Substituting (6–26) into (6–25) yields:

$$f_i(x) + h_i \nu_i - \dot{x}_{2i}^d + k_{i2} \tilde{x}_{i2} + k_{i1} \tilde{x}_{i1} = 0. \quad (6-27)$$

In the presence of disturbance d_i , substituting (6–27) into (6–11), the resultant error dynamics can be written as:

$$\dot{\tilde{x}}_{i2} + k_{i2}\tilde{x}_{i2} + k_{i1}\tilde{x}_{i1} = d_i. \quad (6-28)$$

One can easily tell from (6–28) that no matter what values of the constant parameters k_{i1} and k_{i2} are, the tracking error \tilde{x}_{i1} and its derivatives \tilde{x}_{i2} and $\dot{\tilde{x}}_{i2}$ will not tend to zero due to the presence of disturbance. To this end, a discontinuous control part is synthesized to reject the disturbance as shown below:

$$\nu_{i1} = -h_i^{-1}k_{ci}\text{sat}(\sigma_i/\Phi_i) \quad (6-29)$$

where k_{ci} is a positive high gain that rejects the disturbance and makes the sliding surface attractive, Φ_i is the boundary layer thickness with positive value, and the sat function is defined as:

$$\text{sat}(\sigma_i/\Phi_i) = \begin{cases} \text{sign}(\sigma_i) & \text{if } |\sigma_i| \geq \Phi_i \\ \sigma_i/\Phi_i & \text{if } |\sigma_i| < \Phi_i \end{cases}. \quad (6-30)$$

Therefore, the control law can be developed as:

$$\nu_i = h_i^{-1}(\dot{x}_{2i}^d - k_{i2}\tilde{x}_{i2} - k_{i1}\tilde{x}_{i1} - f_i(x)) - h_i^{-1}k_{ci}\text{sat}(\sigma_i/\Phi_i). \quad (6-31)$$

6.3.3 Adaptive Sliding Mode Control Allocation

By recalling (6–14), in order to maintain the tracking performance of the high-level sliding mode controller when there is an error between ν_i and ν_{id} , the parameter h_i needs to be adjusted accordingly to eliminate this error. In this case, the term $h_i\tilde{\nu}_i$ in (6–14) can be expressed as $\tilde{h}_i\nu_{id}$. Then, (6–14) can be rewritten as:

$$\begin{aligned} \dot{x}_{2i} &= f_i(x) + (h_i + \tilde{h}_i)\nu_{id} + d_i \\ &= f_i(x) + \hat{h}_i\nu_{id} + d_i. \end{aligned} \quad (6-32)$$

In this case, denoting $\hat{\Upsilon}_i = \hat{h}_i^{-1}$ and considering the sliding surface in (6–24), the high-level SMC law is redesigned by using the estimated $\hat{\Upsilon}_i$ as follows:

$$\nu_i = \hat{\Upsilon}_i(\dot{x}_{2i}^d - k_{i2}\tilde{x}_{i2} - k_{i1}\tilde{x}_{i1} - f_i(x)) - \hat{\Upsilon}_i k_{ci} \text{sat}(\sigma_i/\Phi_i). \quad (6-33)$$

In order to develop the adaptive scheme to update the estimated parameter $\hat{\Upsilon}_i$, a new variable is defined based on the switching function and boundary layer as follows:

$$\sigma_{\Delta i} = \sigma_i - \Phi_i \text{sat}(\sigma_i/\Phi_i) \quad (6-34)$$

where $\sigma_{\Delta i}$ is the measurement of the algebraic distance between the current state and the boundary layer. It features $\dot{\sigma}_{\Delta i} = \dot{\sigma}_i$ outside the boundary layer and $\sigma_{\Delta i} = 0$ inside the boundary layer.

Based on this newly-defined variable, the on-line adaptive scheme is formulated as:

$$\dot{\hat{\Upsilon}}_i = (-\dot{x}_{2i}^d + k_{i2}\tilde{x}_{i2} + k_{i1}\tilde{x}_{i1} + f_i(x) + k_{ci} \text{sat}(\sigma_i/\Phi_i))\sigma_{\Delta i}. \quad (6-35)$$

With the help of the adaptive scheme, as long as the sliding variable is out of the boundary layer where the control performance is unacceptable, the adaptation will be triggered to bring the sliding variable back inside the boundary layer to maintain system tracking performance.

Remark 6.1 *The variable $\sigma_{\Delta i}$ used to construct the adaptive scheme can cease the behavior of adaptation when the sliding variable reaches the boundary layer. Overestimation of the parameter is avoided in such a way compared to the adaptive approaches in the literature where the adaptation cannot stop due to the use of sliding variable for designing the adaptive scheme.*

Theorem 6.1 *Consider a nonlinear system with simultaneous actuator faults in the same group (both of the actuators cannot encounter complete failure together) and bounded disturbance in (6–11). Given the sliding surface in (6–24) and control input constraints in (6–5), by employing the feedback control laws in (6–13) and (6–33) and the on-line adaptive scheme in (6–35), the sliding motion will be achieved and maintained on the sliding surface to ensure the closed-loop system*

tracking performance with the discontinuous gain chosen as $k_{ci} \geq \eta_i + D_i$ regardless of the virtual control error, i.e., $\tilde{\nu}_i = \nu_i - \nu_{id} \neq 0$.

Proof 6.1 Consider the following Lyapunov candidate function:

$$\begin{aligned} V_7 &= \sum_{i=1}^4 V_{7i} \\ &= \sum_{i=1}^4 \frac{1}{2} \left[\sigma_{\Delta i}^2 + \Upsilon_i^{-1} (\hat{\Upsilon}_i - \Upsilon_i)^2 \right]. \end{aligned} \quad (6-36)$$

Then, the derivative of the selected Lyapunov candidate function would be:

$$\begin{aligned} \dot{V}_7 &= \sum_{i=1}^4 \left[\sigma_{\Delta i} \dot{\sigma}_{\Delta i} + \Upsilon_i^{-1} (\hat{\Upsilon}_i - \Upsilon_i) \dot{\hat{\Upsilon}}_i \right] \\ &= \sum_{i=1}^4 \left[\sigma_{\Delta i} (f_i(x) + \Upsilon_i^{-1} \hat{\Upsilon}_i (\dot{x}_{2i}^d - k_{i2} \tilde{x}_{i2} - k_{i1} \tilde{x}_{i1} - f_i(x) \right. \\ &\quad \left. - k_{ci} \text{sat}(\sigma_i/\Phi_i)) + d_i - \dot{x}_{2i}^d + k_{i2} \tilde{x}_{i2} + k_{i1} \tilde{x}_{i1}) + \Upsilon_i^{-1} (\hat{\Upsilon}_i - \Upsilon_i) \dot{\hat{\Upsilon}}_i \right] \\ &= \sum_{i=1}^4 \left[(\Upsilon_i^{-1} \hat{\Upsilon}_i - 1) (\dot{x}_{2i}^d - k_{i2} \tilde{x}_{i2} - k_{i1} \tilde{x}_{i1} - f_i(x)) \sigma_{\Delta i} \right. \\ &\quad \left. + (\Upsilon_i^{-1} \hat{\Upsilon}_i - 1) \dot{\hat{\Upsilon}}_i - \Upsilon_i^{-1} \hat{\Upsilon}_i k_{ci} \text{sat}(\sigma_i/\Phi_i) \sigma_{\Delta i} + d_i \sigma_{\Delta i} \right] \quad (6-37) \\ &= \sum_{i=1}^4 \left[(\Upsilon_i^{-1} \hat{\Upsilon}_i - 1) (\dot{x}_{2i}^d - k_{i2} \tilde{x}_{i2} - k_{i1} \tilde{x}_{i1} - f_i(x)) \sigma_{\Delta i} + (\Upsilon_i^{-1} \hat{\Upsilon}_i - 1) \dot{\hat{\Upsilon}}_i \right. \\ &\quad \left. - (\Upsilon_i^{-1} \hat{\Upsilon}_i - 1) k_{ci} \text{sat}(\sigma_i/\Phi_i) \sigma_{\Delta i} - k_{ci} \text{sat}(\sigma_i/\Phi_i) \sigma_{\Delta i} + d_i \sigma_{\Delta i} \right] \\ &= \sum_{i=1}^4 \left[(\Upsilon_i^{-1} \hat{\Upsilon}_i - 1) [\dot{\hat{\Upsilon}}_i + (\dot{x}_{2i}^d - k_{i2} \tilde{x}_{i2} - k_{i1} \tilde{x}_{i1} - f_i(x) \right. \\ &\quad \left. - k_{ci} \text{sat}(\sigma_i/\Phi_i)) \sigma_{\Delta i}] - k_{ci} \text{sat}(\sigma_i/\Phi_i) \sigma_{\Delta i} + d_i \sigma_{\Delta i} \right]. \end{aligned}$$

Substituting (6–35) into (6–37) leads to:

$$\begin{aligned}
\dot{V}_7 &= \sum_{i=1}^4 \left[-k_{ci} \text{sat}(\sigma_i/\Phi_i) \sigma_{\Delta i} + d_i \sigma_{\Delta i} \right] \\
&\leq \sum_{i=1}^4 \left[-(\eta_i + D_i) \text{sat}(\sigma_i/\Phi_i) \sigma_{\Delta i} + D_i \sigma_{\Delta i} \right] \\
&\leq \sum_{i=1}^4 \left[-\eta_i |\sigma_{\Delta i}| \right].
\end{aligned} \tag{6–38}$$

Therefore, with the proposed control scheme, the performance of the closed-loop system is maintained in the presence of simultaneous actuator faults.

Remark 6.2 It can be observed that although the simultaneous actuator faults is considered during the design of the controller, the value of the discontinuous gain is not increased with the help of the adaptive scheme. This feature will preserve the original tracking performance and prevent the chattering effect in the fault-free condition.

6.4 Simulation Results

In this section, in order to demonstrate the performance of the proposed ASMCA scheme, simulations based on the modified octorotor helicopter under different fault/failure scenarios are carried out. The initial attitude orientation of the octorotor helicopter is set to be $\phi(0) = \theta(0) = \psi(0) = 0 \text{ deg}$ and the initial altitude is $z_e(0) = 0 \text{ m}$. For a purpose of comparison, the linear quadratic regulator (LQR) and the normal SMC (NSMC) are also demonstrated as the high-level controller combined with control allocation in the following simulation scenarios.

Simulation scenarios: Firstly the octorotor helicopter is lifted up to 0.5 m, after that it is controlled to follow a set of pre-designed pitch command which is generated from the following pre-filter:

$$\ddot{\theta}_d + 3\dot{\theta}_d + 4\theta_d = 4\theta^* \tag{6–39}$$

where θ^* changes from 0 to 5 deg at 5 s, and goes back to 0 at 10 s, then changes to –5 deg at 15

s, and goes back to 0 at 20 s, after that, remains on 0 for 10 s.

- i) Case 1: Only one actuator encounters fault/failure at 14 s. The loss of control effectiveness of actuator #1 changes from 0 to 100%;
- ii) Case 2: Two actuators encounter simultaneous faults at 14 s. Actuator #1 encounters a complete failure, and actuator #5 experiences a 40% loss of control effectiveness fault.

6.4.1 Case 1: Single Actuator Fault/Failure

In this section, the fault is only considered occurring in actuator #1. For the proposed ASMCA scheme, the control parameters in (6–33) are chosen as $k_{11} = 25, k_{21} = 100, k_{31} = 100, k_{41} = 25, k_{12} = 10, k_{22} = 20, k_{32} = 20, k_{42} = 10, k_{c1} = 5, k_{c2} = 10, k_{c3} = 10, k_{c4} = 5$, and $\Phi = 0.1$. For comparison, the same control parameters are chosen for the normal sliding mode control allocation (NSMCA) scheme, and the control parameters for the compared linear quadratic regulator control allocation (LQRCA) scheme can refer to [21]. The loss of control effective fault is changed from 0 to 100% to demonstrate the effectiveness of the control allocation scheme. The tracking performances of height and pitch motion are shown in Figs. 6.3(a) and 6.3(b), respectively. All of the demonstrated three controllers show good tracking performances for both height and pitch motion in the presence of single actuator fault/failure. Regardless of the percentage of loss of control effectiveness, this kind of fault is handled within the control allocation scheme without affecting the tracking performance of the high-level controller. Since actuator #5 is underneath actuator #1, both of them have the same effect on the octorotor helicopter and can be treated as the grouped actuators. When actuator #1 experiences fault, the control input of actuator #5 will increase correspondingly to eliminate the impact of fault. Figure 6.4 shows the control inputs of actuators #1 and #5. With the increase of loss of control effectiveness in actuator #1, the control input of actuator #5 is increased correspondingly with the control re-allocation scheme to accommodate such a fault. Therefore, when an actuator fault occurs, the control re-allocation scheme delivers more control inputs to the healthy actuator to avoid using the faulty one. Figure 6.5 shows the sliding surfaces

and virtual control inputs of height and pitch motion. With only one actuator fault/failure, the generated virtual control signals can still meet the desired ones and the sliding surfaces are within the boundary layer. Therefore, there is no degradation of the tracking performances no matter what kind of high-level controller it is.

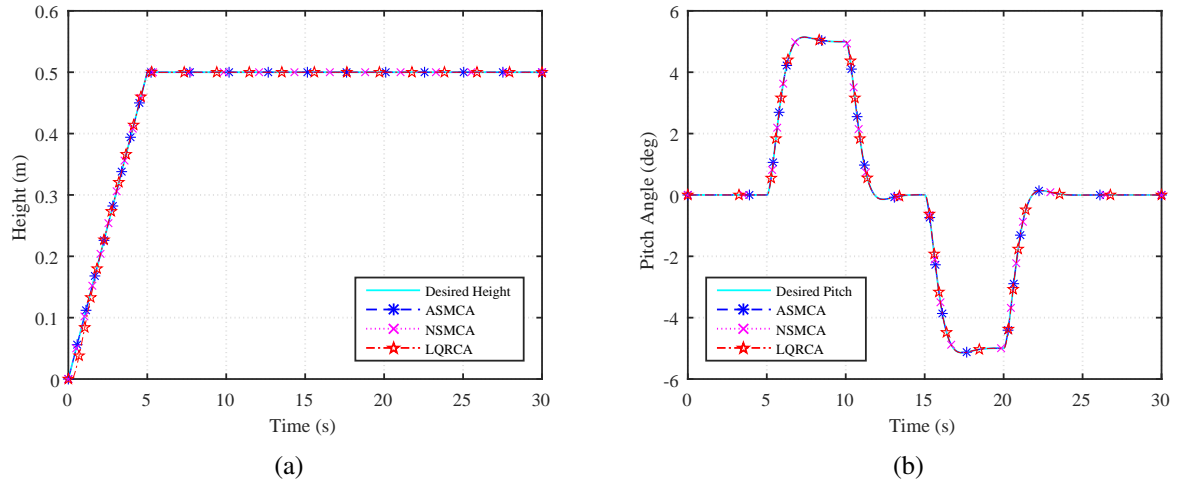


Figure 6.3: Tracking performances of height and pitch motion in the presence of single actuator fault/failure.

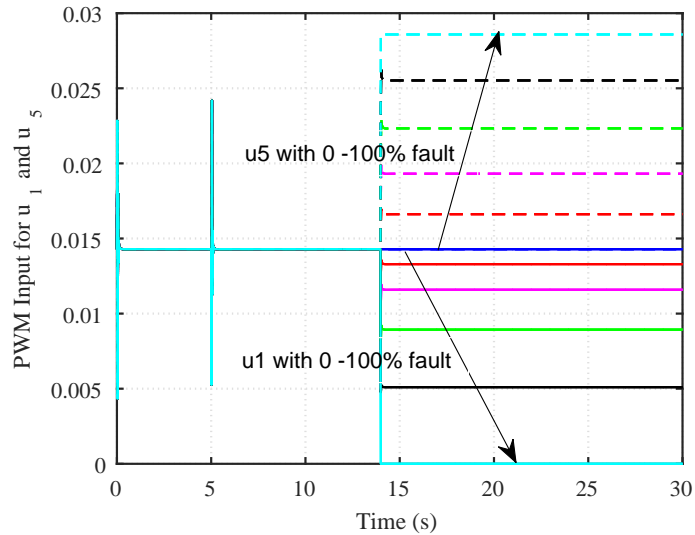


Figure 6.4: Control inputs for actuators #1 and #5.

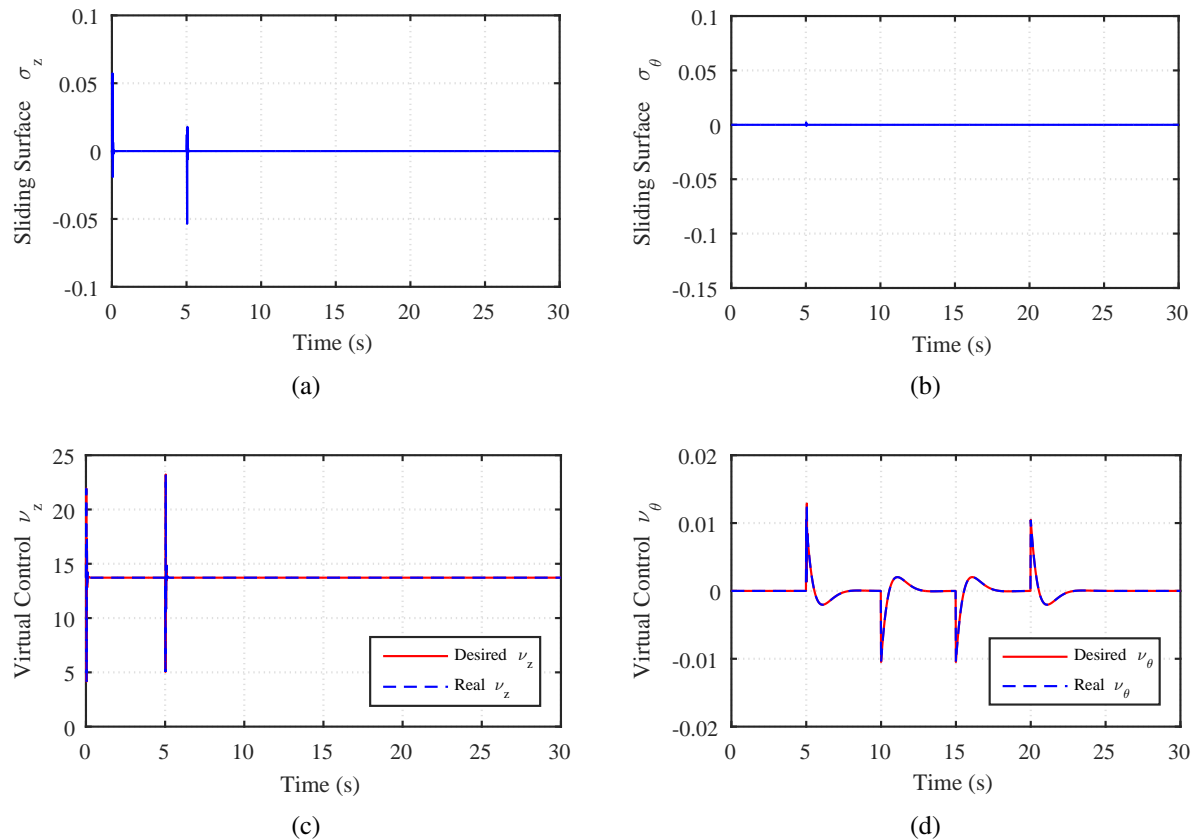


Figure 6.5: Sliding surfaces and virtual control inputs for height and pitch motion in the presence of single actuator fault/failure.

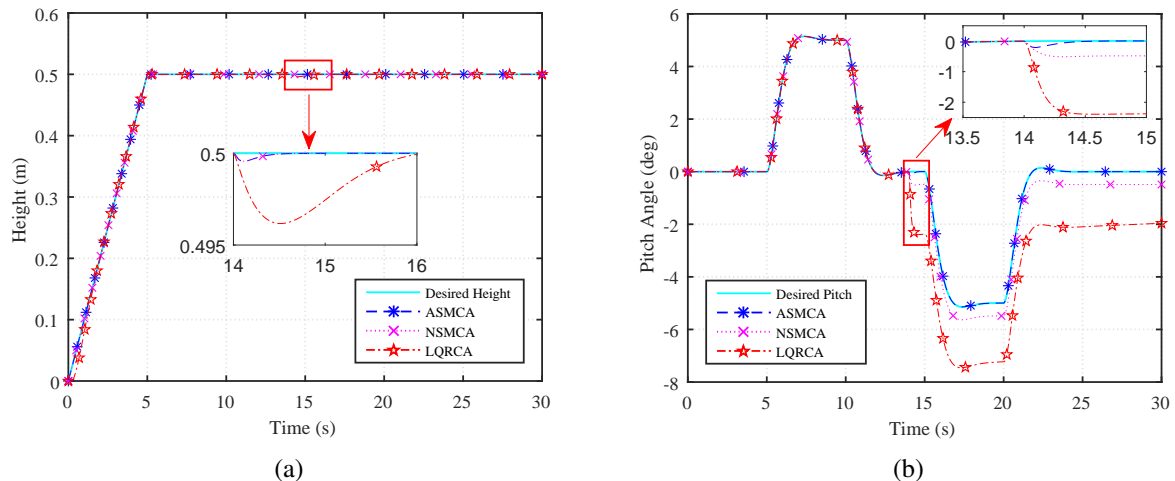


Figure 6.6: Tracking performances of height and pitch motion in the presence of simultaneous actuator faults.

6.4.2 Case 2: Simultaneous Actuator Faults

The case of simultaneous actuator faults is investigated in this section. Since actuators #1 and #5 are mounted on the same corner of the octorotor helicopter, if both of them encounter complete failures, it would be impossible for any controller to stabilize it. So the worst case considered here is a complete failure in actuator #1 and a 40% loss of control effectiveness fault in actuator #5. In order to make a comparison, control parameters for the demonstrated three controllers are chosen the same as case 1. As shown in Figs. 6.9(c) and 6.9(d), control allocation and re-allocation scheme cannot effectively maintain the closed-loop system performance in the presence of simultaneous actuator faults due to the existence of virtual control error. The tracking performances of height and pitch motion are shown in Figs. 6.6(a) and 6.6(b), respectively. It can be seen that the height is less affected than the pitch motion in this case, and the sliding surface for height controller is still within the boundary layer as shown in Fig. 6.9(a). This is because all of the eight actuators can contribute to compensate the loss of height. Therefore, with more available healthy actuators, the virtual control error of height control allocation scheme is less than that of pitch motion. For the pitch motion control, after faults occur, compared to the NSMCA and LQRCA, the proposed ASMCA can make a quicker compensation to maintain a better tracking performance and the sliding surface is brought within the boundary layer again as shown in Figs. 6.6(b) and 6.9(b) with the change of adaptive control parameter regardless of the virtual control error, which is shown in Fig. 6.8. On the contrary, due to the fact that the generated virtual control signal from the control allocation module cannot meet the desired one from the high-level virtual controller, the compared NSMCA and LQRCA cannot maintain the original tracking performance anymore. Figure 6.7 shows the control inputs of the actuators. Actuator #1 encounters a complete failure, therefore it has no control input. Since the consideration of fault in actuator #5 in this case, the control input of actuator #5 is larger than that in case 1 which can be observed from Figs. 6.4 and 6.7.

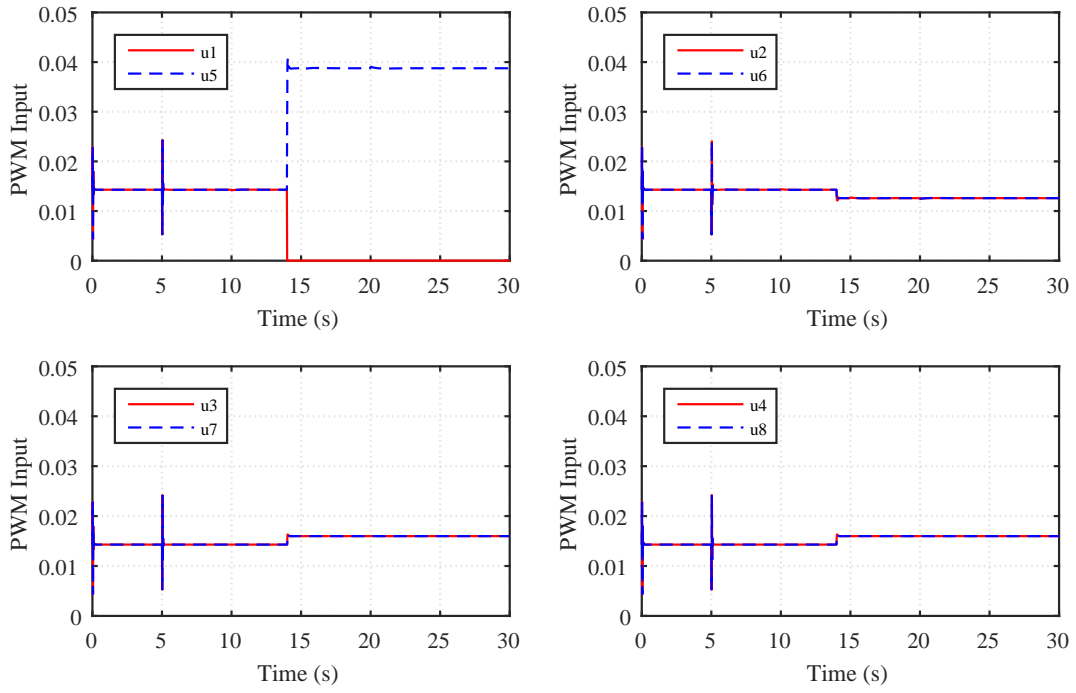


Figure 6.7: Control inputs of motors in the presence of simultaneous actuator faults.

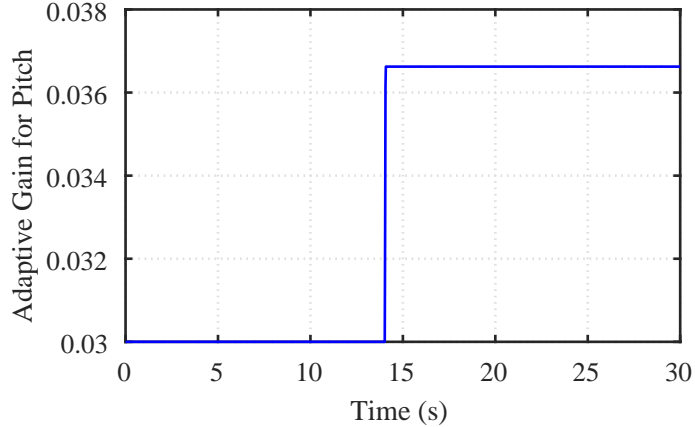


Figure 6.8: The change of adaptive parameter for pitch motion in the presence of simultaneous actuator faults.

6.5 Experimental Results

As demonstrated in the previous section, the proposed ASMCA shows a good tracking performance in the presence of both single and simultaneous actuator faults/failures. In order to validate the control effectiveness in real applications, some experiments are carried out in this section. The

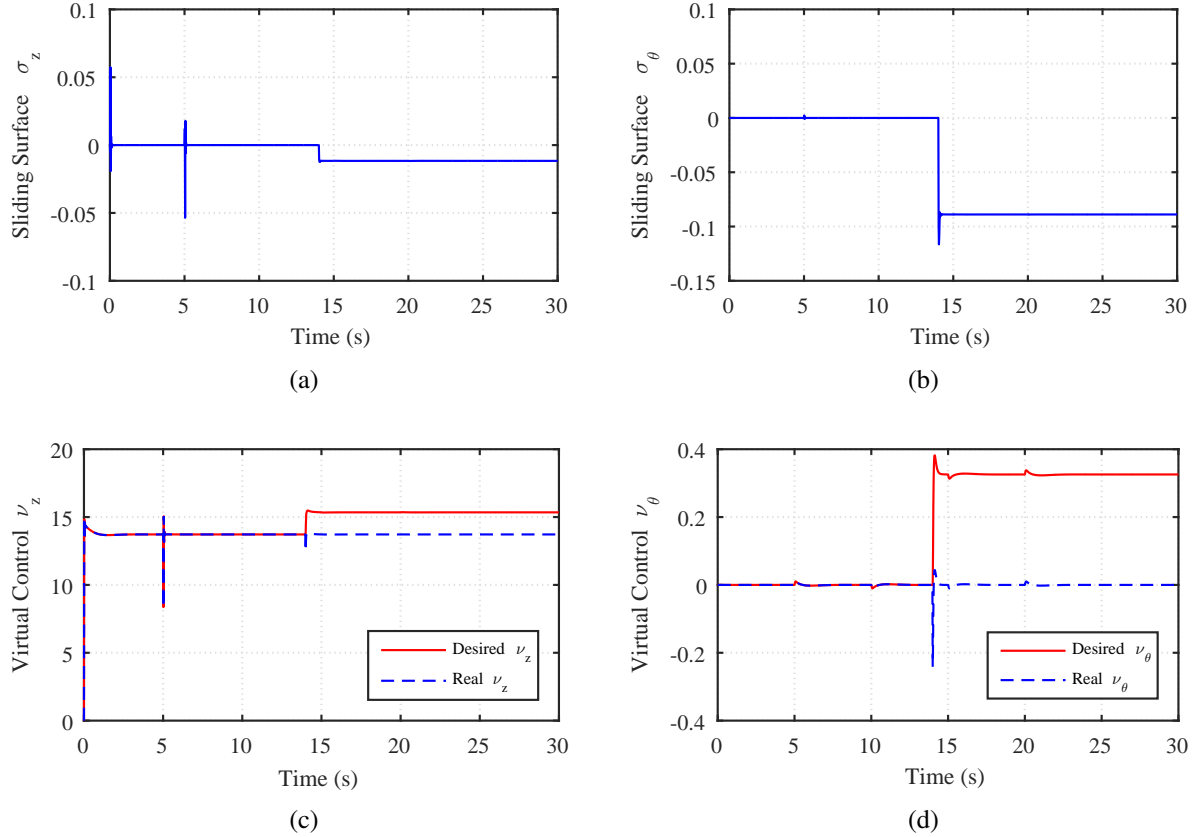


Figure 6.9: Sliding surfaces and virtual control inputs for height and pitch motion in the presence of simultaneous actuator faults.

performances of NSMCA and LQRCA are also demonstrated for comparison. The thickness of the boundary layer for both sliding mode controllers are chosen as $\Phi = 0.2$.

Experimental scenarios:

- i) Case 1: A 100% loss of control effectiveness fault is only introduced to actuator #1 at 20 s;
- ii) Case 2: Faults are injected into two actuators at 20 s. Actuator #1 encounters a complete failure, and actuator #5 experiences a 40% loss of control effectiveness fault.

Remark 6.3 Due to the reason that some controllers may have bad performance and lead to crash when simultaneous actuator faults is considered. In order to maintain the safety of the octorotor helicopter in real flight test when one actuator has already encountered a complete failure, only a 40% loss of control effectiveness fault is injected to another actuator.

6.5.1 Description of the Experiment Setup

The schematic of the experiment setup is demonstrated in Fig. 6.10. In the whole system, besides the octorotor helicopter itself, there is another subsystem called OptiTrack which includes twenty-four cameras as an indoor positioning system providing the position and attitude of the octorotor helicopter. For calculating the attitude of the octorotor helicopter, the on-board IMU can also be used which is called HiQ. The sampling rates for the on-board accelerometer, gyroscope, and magnetometer are set as 200Hz. The control algorithm is written with Simulink blocks which can be compiled to C-code with the help of a real-time control software, namely QuaRC. The compiled code runs on an embedded Linux-based system, Gumstix, that uses an ARM Cortex-M4 single-chip computer in real-time. Desired inputs are given from the host computer to the on-board processor of the octorotor helicopter through Wi-Fi wireless communication.

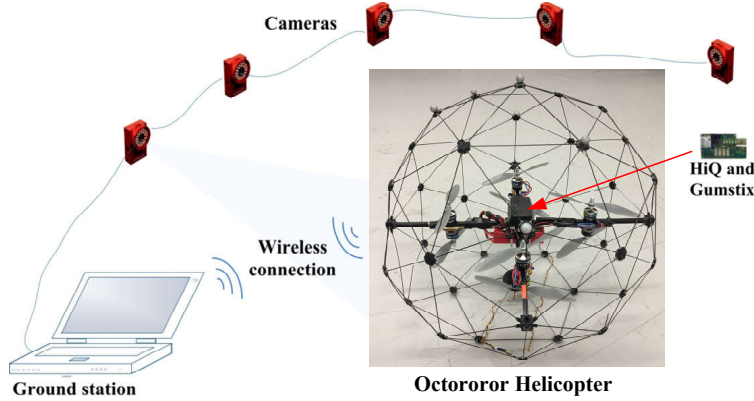


Figure 6.10: The schematic of the experiment setup.

6.5.2 Case 1: Single Actuator Complete Failure

Since the height is less affected than the pitch motion, only results related to pitch motion are shown in this section. The tracking performance of pitch motion in the presence of single actuator failure is shown in Fig. 6.11. Since the sliding surface does not exceed the defined boundary layer as shown in Fig. 6.12 in this faulty condition, only the performances of ASMCA and LQRCA are shown for comparison. It also implies that the control allocation and re-allocation scheme

is capable to handle such a fault without the help of the adaptive scheme. In theory, both of the controllers should have the same performance because only control re-allocation is triggered in this faulty condition. However, as shown in Fig. 6.11 the proposed ASMCA has a better performance than LQRCA at the very beginning of faulty stage although both of them can finally track the reference command. It is because the robustness of SMC to disturbances make it less affected during reconfiguring the control allocation scheme. The related actuator inputs for pitch motion are shown in Fig. 6.13.

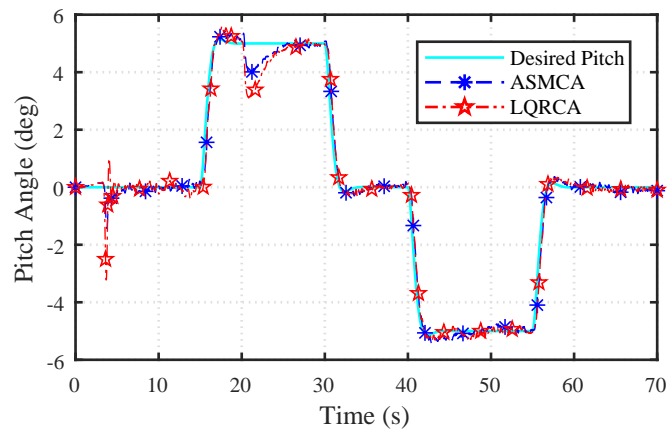


Figure 6.11: Tracking performance of pitch motion in the presence of single actuator failure in real flight test.

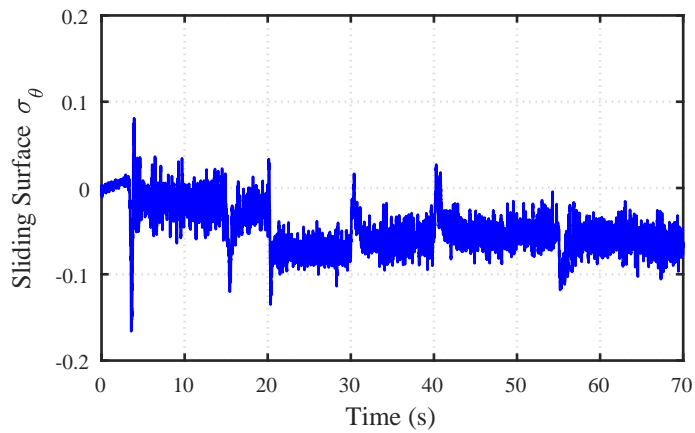


Figure 6.12: Sliding surface of ASMCA for pitch motion in the presence of single actuator failure in real flight test.

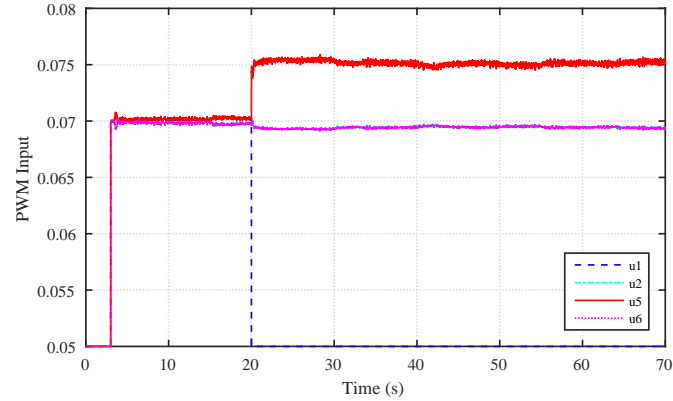


Figure 6.13: Control inputs of related actuators for pitch motion in the presence of single actuator failure in real flight test.

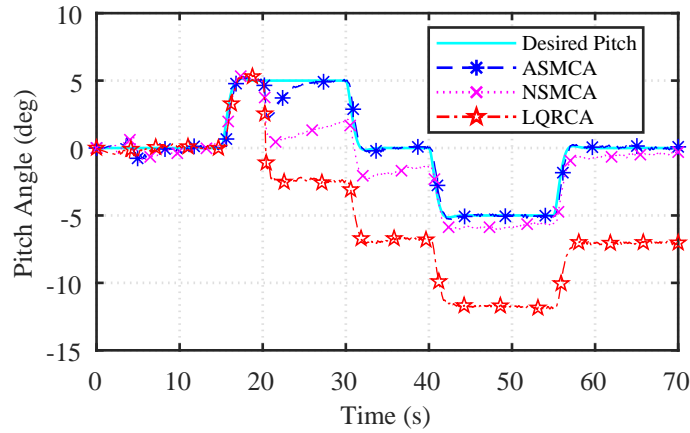


Figure 6.14: Tracking performance of pitch motion in the presence of simultaneous actuator faults in real flight test.

6.5.3 Case 2: Simultaneous Actuator Faults

In this case, simultaneous actuator faults is studied through real flight experiment. The tracking performance of pitch motion in the presence of simultaneous actuator faults is shown in Fig. 6.14. The LQRCA has the worst tracking performance after faults occur, whereas the NSMCA can gradually decrease the tracking error but still cannot achieve the original tracking performance. Compared to NSMCA and LQRCA, the proposed ASMCA can make a quicker compensation to maintain the original tracking performance with the help of the synthesized adaptive scheme. After faults occurrence, the control re-allocation scheme will be triggered firstly. Since actuator #1

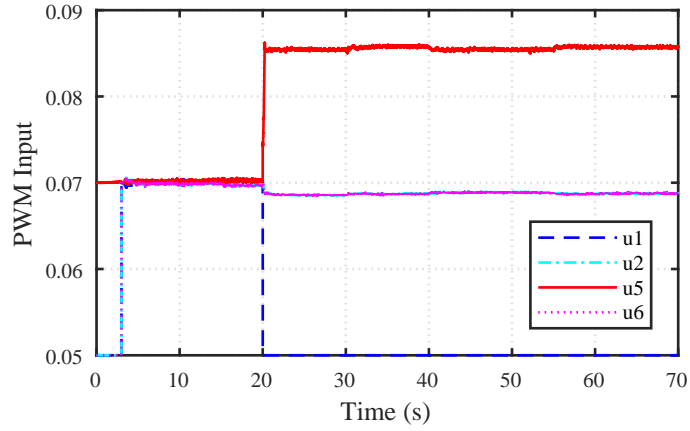


Figure 6.15: Control inputs of related actuators for pitch motion in the presence of simultaneous actuator faults in real flight test.

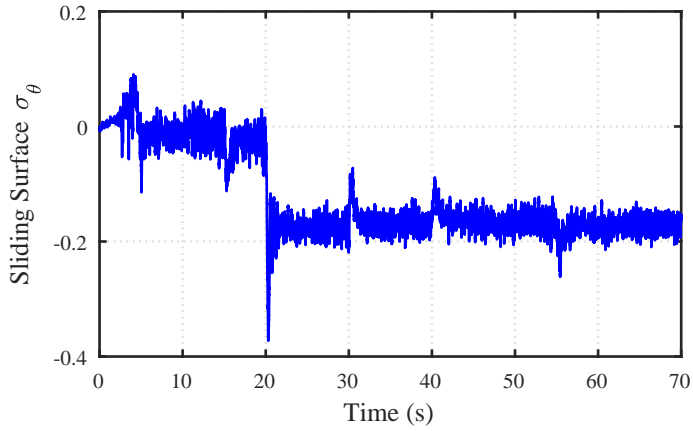


Figure 6.16: Sliding surface of ASMCA for pitch motion in the presence of simultaneous actuator faults in real flight test.

completely fails, no control effort will be distributed to it, and more control effort will be distributed to the less affected actuator #5, which can be observed from Fig. 6.15. Note that, the range of actuator input is [0.05 0.1]. Moreover, as can be observed from Fig. 6.16, after faults occurrence at 20 s, due to the virtual control error, which is shown in Fig. 6.17, caused by the simultaneous actuator faults and the corresponding inputs decrease in actuators #2 and #6 as shown in Fig. 6.15, there is a big deviation of the sliding surface which will trigger the high-level adaptive scheme to increase the corresponding adaptive gain as shown in Fig. 6.18. With the change of the control gain of the high-level sliding mode controller, the sliding surface is brought into the boundary

layer again to maintain the original tracking performance. Therefore, the proposed control scheme is a robust and reliable control strategy which represents the ability to deal with both single and simultaneous actuator faults.

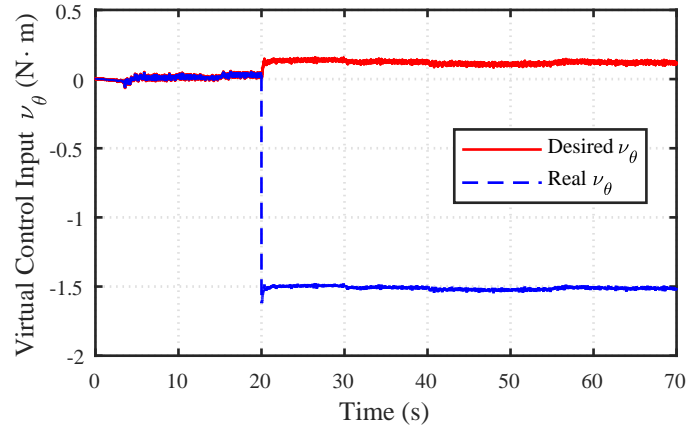


Figure 6.17: Virtual control input for pitch motion in the presence of simultaneous actuator faults in real flight test.

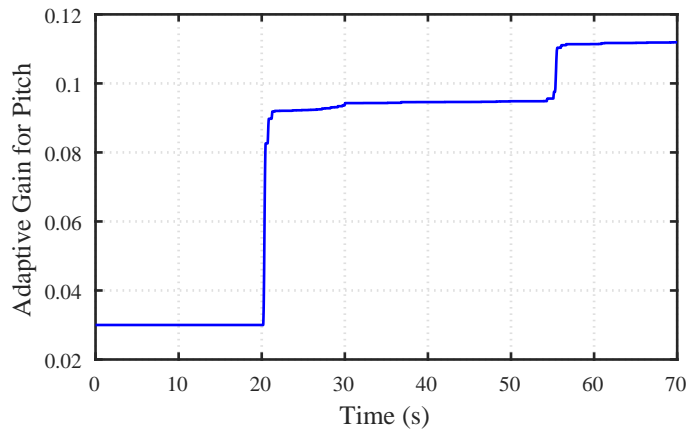


Figure 6.18: Adaptive parameter of ASMCA for pitch motion in the presence of simultaneous actuator faults in real flight test.

6.6 Conclusion

In this chapter, a novel adaptive sliding mode-based control allocation scheme is proposed for a modified octorotor helicopter to accommodate simultaneous actuator faults. The proposed control scheme includes two separate control modules: the low-level module and the high-level one. The low-level control allocation and re-allocation module is used to distribute the control signals among the required actuators, which can also reconfigure the distribution of the control signals in the presence of actuator faults. The high-level module is constructed by an adaptive sliding mode controller, which is employed to maintain the closed-loop system tracking performance. In the case of mild faulty conditions, the control allocation module can successfully deal with the fault independently. Whereas in the case of severe faulty conditions, the adaptive scheme will be triggered to compensate the virtual control error generated by the low-level control allocation module. With the help of the synthesized adaptive scheme, the high-level control gains can be changed adaptively to maintain the closed-loop system tracking performance. The demonstrated simulation and experimental results show the effectiveness and reliability of the proposed adaptive FTC strategy in the presence of both single and simultaneous actuator faults.

Chapter 7

Conclusions and Future Works

7.1 Conclusions

In this dissertation, several safety-critical issues on reliable control of UAVs are well studied, which include:

- 1) A comprehensive literature review on UAVs as well as their control approaches are provided.
- 2) An adaptive SMC method is proposed to control an unmanned quadrotor helicopter in the presence of actuator faults. After fault occurrence, the proposed adaptive SMC scheme is able to automatically provide robustness and maintain good tracking performance with even a large fault magnitude. Compared to the conventional SMC and existing adaptive SMC in the literature, the proposed control scheme can tolerate larger actuator fault in the system without stimulating control chattering. The proposed control scheme is validated under different faulty scenarios. The simulation results show that the proposed adaptive SMC achieves good tracking performance in both fault-free and faulty conditions.
- 3) An adaptive strategy based on an integral SMC, a fuzzy boundary layer, and a nonlinear disturbance observer is proposed to simultaneously accommodate parametric uncertainties, actuator faults, and external disturbances for a quadrotor helicopter. By virtue of using the

adaptive control parameters in both continuous and discontinuous control portions, the control discontinuity is significantly reduced in the presence of model uncertainties and actuator faults, which helps the system avoid control chattering. Furthermore, the fuzzy logic-based boundary layer and synthesized nonlinear disturbance observer can also help to maintain system stability and suppress control chattering. The simulation and experimental results of a quadrotor helicopter demonstrate the effectiveness and applicability of the proposed control strategy.

- 4) An active FTC strategy based on adaptive SMC and RNN is proposed to accommodate actuator faults and model uncertainties for a quadrotor helicopter. With the help of the developed online adaptive schemes, the proposed control strategy can adaptively generate appropriate control signals to compensate model uncertainties without the knowledge of uncertainty bounds to maintain tracking performance and stability of the quadrotor helicopter. Then, by designing a parallel bank of RNNs, the severity of the actuator faults can be precisely and reliably estimated, which is then synthesized with the proposed adaptive SMC to reconfigure the controller and accommodate actuator faults. Moreover, the actuator fault estimation error is explicitly considered, which can be compensated by the proposed adaptive control schemes. In this way, the robustness of the proposed active FTC strategy is improved. The simulation results show that the proposed scheme can effectively estimate the severity of various kinds of actuator faults in the closed-loop quadrotor helicopter system. Furthermore, the demonstrated experimental results confirm the effectiveness and superiority of the proposed active FTC strategy with comparison to a conventional SMC.
- 5) A reconfigurable control allocation scheme combined with adaptive SMC is proposed for a modified octocopter helicopter to accommodate both single and simultaneous actuator faults. In the case of mild faulty conditions, the control allocation/reallocation module can successfully deal with the fault independently. Whereas in the case of severe faulty conditions, the adaptive scheme will be triggered to compensate the virtual control error generated by the

low-level control allocation/reallocation module. With the help of the synthesized adaptive scheme, the high-level control gains can be changed adaptively to maintain the overall system tracking performance. The demonstrated simulation and experimental results show the effectiveness and reliability of the proposed adaptive FTC strategy in the presence of both single and simultaneous actuator faults.

7.2 Future Works

Following the current research in this dissertation, the following future directions are outlined:

- 1) The proposed control schemes in this dissertation are only validated on multirotor helicopters. In order to evaluate their practical usefulness, more tests need to be carried out on more different types of UAVs, such as fixed-wing UAVs.
- 2) The faults/failures considered in this dissertation only occur in actuators, while the sensor and communication faults/failures are not included, though they are of significance for safety-critical control system design as well. Therefore, the future work can be extended to the studies of more sorts of faults/failures in the sensors and communications.
- 3) Only loss of control effectiveness faults and complete failures are considered for controller design in this dissertation, more categories of faults need to be simultaneously considered in the future research to further increase the robustness and effectiveness of the proposed control schemes.
- 4) In the proposed reconfigurable control allocation scheme, the fault information is assumed to be known a prior. In the future research, an active fault diagnosis scheme can be incorporated with the designed control scheme to further validate its effectiveness. Moreover, the fault information error and delay should also be explicitly studied.
- 5) In the proposed control schemes, the design of the corresponding controllers are based on

state feedback. For some systems, the full states may not be available all the times. Therefore, the output feedback control for accommodating actuator faults, parametric uncertainties, and external disturbances needs to be further investigated.

- 6) More effective training algorithms for the proposed parallel bank of RNNs need to be further studied to improve the training accuracy and convergence rate.

Bibliography

- [1] H. Lee and H. J. Kim, “Estimation, control, and planning for autonomous aerial transportation,” *IEEE Transactions on Industrial Electronics*, vol. 64, no. 4, pp. 3369–3379, 2017.
- [2] N. Michael, J. Fink, and V. Kumar, “Cooperative manipulation and transportation with aerial robots,” *Autonomous Robots*, vol. 30, no. 1, pp. 73–86, 2011.
- [3] C. Yuan, Y. M. Zhang, and Z. X. Liu, “A survey on technologies for automatic forest fire monitoring, detection, and fighting using unmanned aerial vehicles and remote sensing techniques,” *Canadian Journal of Forest Research*, vol. 45, no. 7, pp. 783–792, 2015.
- [4] J. Capitán, L. Merino, and A. Ollero, “Cooperative decision-making under uncertainties for multi-target surveillance with multiples UAVs,” *Journal of Intelligent & Robotic Systems*, vol. 84, no. 1-4, pp. 371–386, 2016.
- [5] Z. Li, Y. Liu, R. Walker, R. Hayward, and J. Zhang, “Towards automatic power line detection for a UAV surveillance system using pulse coupled neural filter and an improved Hough transform,” *Machine Vision and Applications*, vol. 21, no. 5, pp. 677–686, 2010.
- [6] M. Dunbabin and L. Marques, “Robots for environmental monitoring: Significant advancements and applications,” *IEEE Robotics & Automation Magazine*, vol. 19, no. 1, pp. 24–39, 2012.

- [7] H. Xiang and L. Tian, “Development of a low-cost agricultural remote sensing system based on an autonomous unmanned aerial vehicle (UAV),” *Biosystems Engineering*, vol. 108, no. 2, pp. 174–190, 2011.
- [8] S. Siebert and J. Teizer, “Mobile 3D mapping for surveying earthwork projects using an Unmanned Aerial Vehicle (UAV) system,” *Automation in Construction*, vol. 41, pp. 1–14, 2014.
- [9] G. J. Ducard, *Fault-tolerant Flight Control and Guidance Systems: Practical Methods for Small Unmanned Aerial Vehicles*. Springer Science & Business Media, 2009.
- [10] K. P. Valavanis and G. J. Vachtsevanos, *Handbook of Unmanned Aerial Vehicles*. Springer Science & Business Media, 2015.
- [11] Y. M. Zhang and J. Jiang, “Bibliographical review on reconfigurable fault-tolerant control systems,” *Annual Reviews in Control*, vol. 32, no. 2, pp. 229–252, 2008.
- [12] X. Yu and J. Jiang, “A survey of fault-tolerant controllers based on safety-related issues,” *Annual Reviews in Control*, vol. 39, pp. 46–57, 2015.
- [13] S. Yin, B. Xiao, S. X. Ding, and D. Zhou, “A review on recent development of spacecraft attitude fault tolerant control system,” *IEEE Transactions on Industrial Electronics*, vol. 63, no. 5, pp. 3311–3320, 2016.
- [14] Y. M. Zhang, A. Chamseddine, C. Rabbath, B. Gordon, C.-Y. Su, S. Rakheja, C. Fulford, J. Apkarian, and P. Gosselin, “Development of advanced FDD and FTC techniques with application to an unmanned quadrotor helicopter testbed,” *Journal of the Franklin Institute*, vol. 350, no. 9, pp. 2396–2422, 2013.
- [15] B. Wang and Y. M. Zhang, “Adaptive sliding mode fault-tolerant control for an unmanned aerial vehicle,” *Unmanned Systems*, vol. 5, no. 04, pp. 209–221, 2017.

- [16] Q. Hu and B. Xiao, “Fault-tolerant sliding mode attitude control for flexible spacecraft under loss of actuator effectiveness,” *Nonlinear Dynamics*, vol. 64, no. 1-2, pp. 13–23, 2011.
- [17] B. Xiao, M. Huo, X. Yang, and Y. M. Zhang, “Fault-tolerant attitude stabilization for satellites without rate sensor,” *IEEE Transactions on Industrial Electronics*, vol. 62, no. 11, pp. 7191–7202, 2015.
- [18] H. Badihi, Y. M. Zhang, and H. Hong, “Wind turbine fault diagnosis and fault-tolerant torque load control against actuator faults,” *IEEE Transactions on Control Systems Technology*, vol. 23, no. 4, pp. 1351–1372, 2015.
- [19] B. Wang, L. X. Mu, and Y. M. Zhang, “Adaptive robust control of quadrotor helicopter towards payload transportation applications,” in *Proceedings of the 36th Chinese Control Conference (CCC)*, pp. 4774–4779, 2017.
- [20] J. Li and Y. Li, “Dynamic analysis and PID control for a quadrotor,” in *Proceedings of the IEEE International Conference on Mechatronics and Automation (ICMA)*, pp. 573–578, 2011.
- [21] B. Wang, K. A. Ghamry, and Y. M. Zhang, “Trajectory tracking and attitude control of an unmanned quadrotor helicopter considering actuator dynamics,” in *Proceedings of the 35th Chinese Control Conference (CCC)*, pp. 10795–10800, 2016.
- [22] B. Yu, Y. M. Zhang, I. Minchala, and Y. Qu, “Fault-tolerant control with linear quadratic and model predictive control techniques against actuator faults in a quadrotor UAV,” in *Proceedings of the Conference on Control and Fault-Tolerant Systems (SysTol)*, pp. 661–666, 2013.
- [23] T. Li, Y. M. Zhang, and B. W. Gordon, “Passive and active nonlinear fault-tolerant control of a quadrotor unmanned aerial vehicle based on the sliding mode control technique,” *Proceedings of the Institution of Mechanical Engineers, Part I: Journal of Systems and Control Engineering*, vol. 227, no. 1, pp. 12–23, 2013.

- [24] M. Mahmoud, J. Jiang, and Y. M. Zhang, *Active Fault Tolerant Control Systems: Stochastic Analysis and Synthesis*. Springer Science & Business Media, 2003.
- [25] J. Jiang and Q. Zhao, “Design of reliable control systems possessing actuator redundancies,” *Journal of Guidance, Control, and Dynamics*, vol. 23, no. 4, pp. 709–718, 2000.
- [26] F. Liao, J. L. Wang, and G.-H. Yang, “Reliable robust flight tracking control: an LMI approach,” *IEEE Transactions on Control Systems Technology*, vol. 10, no. 1, pp. 76–89, 2002.
- [27] Y. M. Zhang and J. Jiang, “Active fault-tolerant control system against partial actuator failures,” *IEE Proceedings-Control Theory and Applications*, vol. 149, no. 1, pp. 95–104, 2002.
- [28] H. Badihi, Y. M. Zhang, and H. Hong, “Fuzzy gain-scheduled active fault-tolerant control of a wind turbine,” *Journal of the Franklin Institute*, vol. 351, no. 7, pp. 3677–3706, 2014.
- [29] J. Jiang and X. Yu, “Fault-tolerant control systems: A comparative study between active and passive approaches,” *Annual Reviews in Control*, vol. 36, no. 1, pp. 60–72, 2012.
- [30] R. Isermann, *Fault-Diagnosis Applications: Model-based Condition Monitoring: Actuators, Drives, Machinery, Plants, Sensors, and Fault-Tolerant Systems*. Springer Science & Business Media, 2011.
- [31] C. Edwards, T. Lombaerts, and H. Smaili, *Fault Tolerant Flight Control: A Benchmark Challenge*. Springer Science & Business Media, 2010.
- [32] R. H. Chen and J. L. Speyer, “Sensor and actuator fault reconstruction,” *Journal of Guidance Control and Dynamics*, vol. 27, no. 2, pp. 186–196, 2004.
- [33] V. I. Utkin, “Variable structure systems with sliding modes,” *IEEE Transactions on Automatic Control*, vol. 22, no. 2, pp. 212–222, 1977.
- [34] V. I. Utkin, “Sliding mode control design principles and applications to electric drives,” *IEEE Transactions on Industrial Electronics*, vol. 40, no. 1, pp. 23–36, 1993.

- [35] V. Utkin, J. Guldner, and J. Shi, *Sliding Mode Control in Electro-Mechanical Systems*. CRC Press, 2009.
- [36] C. Edwards and S. Spurgeon, *Sliding Mode Control: Theory and Applications*. CRC Press, 1998.
- [37] L. Fridman, J. Moreno, and R. Iriarte, *Sliding Modes after the First Decade of the 21st Century*. Springer Science & Business Media, 2011.
- [38] H. Alwi and C. Edwards, “Fault detection and fault-tolerant control of a civil aircraft using a sliding-mode-based scheme,” *IEEE Transactions on Control Systems Technology*, vol. 16, no. 3, pp. 499–510, 2008.
- [39] T. Wang, W. Xie, and Y. M. Zhang, “Sliding mode fault tolerant control dealing with modeling uncertainties and actuator faults,” *ISA Transactions*, vol. 51, no. 3, pp. 386–392, 2012.
- [40] V. I. Utkin, *Sliding Modes in Control and Optimization*. Springer Science & Business Media, 2013.
- [41] Y. Shtessel, C. Edwards, L. Fridman, and A. Levant, *Sliding Mode Control and Observation*. Springer Science & Business Media, 2014.
- [42] J. Liu and X. Wang, *Advanced Sliding Mode Control for Mechanical Systems: Design, Analysis and MATLAB Simulation*. Tsinghua University Press, 2011.
- [43] F. Sharifi, M. Mirzaei, B. W. Gordon, and Y. M. Zhang, “Fault tolerant control of a quadrotor UAV using sliding mode control,” in *Proceedings of the Conference on Control and Fault-Tolerant Systems (SysTol)*, pp. 239–244, 2010.
- [44] Q. Shen, D. Wang, S. Zhu, and E. K. Poh, “Integral-type sliding mode fault-tolerant control for attitude stabilization of spacecraft,” *IEEE Transactions on Control Systems Technology*, vol. 23, no. 3, pp. 1131–1138, 2015.

- [45] M. T. Hamayun, C. Edwards, and H. Alwi, “Design and analysis of an integral sliding mode fault tolerant control scheme,” in *Fault Tolerant Control Schemes Using Integral Sliding Modes*, pp. 39–61, Springer Science & Business Media, 2016.
- [46] R. Hess and S. Wells, “Sliding mode control applied to reconfigurable flight control design,” *Journal of Guidance, Control, and Dynamics*, vol. 26, no. 3, pp. 452–462, 2003.
- [47] B. Xiao, Q. Hu, and Y. M. Zhang, “Adaptive sliding mode fault tolerant attitude tracking control for flexible spacecraft under actuator saturation,” *IEEE Transactions on Control Systems Technology*, vol. 20, no. 6, pp. 1605–1612, 2012.
- [48] Q. Hu and B. Xiao, “Adaptive fault tolerant control using integral sliding mode strategy with application to flexible spacecraft,” *International Journal of Systems Science*, vol. 44, no. 12, pp. 2273–2286, 2013.
- [49] D. Brière and P. Traverse, “AIRBUS A320/A330/A340 electrical flight controls—a family of fault-tolerant systems,” in *Digest of Papers FTCS-23 The Twenty-Third International Symposium on Fault-Tolerant Computing*, pp. 616–623, 1993.
- [50] L. Forssell and U. Nilsson, *ADMIRE The Aero-Data Model In a Research Environment Version 4.0, Model Description*. FOI-Totalförsvarets Forskningsinstitut, 2005.
- [51] Y. Ikeda and M. Hood, “An application of L1 optimization to control allocation,” in *Proceedings of the AIAA Guidance, Navigation and Control Conference and Exhibit*, 2000.
- [52] W. C. Durham, “Constrained control allocation,” *Journal of Guidance, Control, and Dynamics*, vol. 16, no. 4, pp. 717–725, 1993.
- [53] W. C. Durham, “Attainable moments for the constrained control allocation problem,” *Journal of Guidance, Control, and Dynamics*, vol. 17, no. 6, pp. 1371–1373, 1994.
- [54] W. C. Durham, “Efficient, near-optimal control allocation,” *Journal of Guidance, Control, and Dynamics*, vol. 22, no. 2, pp. 369–372, 1999.

- [55] J. D. Boskovic and R. K. Mehra, “Control allocation in overactuated aircraft under position and rate limiting,” in *Proceedings of the American Control Conference*, pp. 791–796, 2002.
- [56] O. Härkegård, “Dynamic control allocation using constrained quadratic programming,” *Journal of Guidance, Control, and Dynamics*, vol. 27, no. 6, pp. 1028–1034, 2004.
- [57] T. A. Johansen, T. P. Fuglseth, P. Tøndel, and T. I. Fossen, “Optimal constrained control allocation in marine surface vessels with rudders,” *Control Engineering Practice*, vol. 16, no. 4, pp. 457–464, 2008.
- [58] J. Virnig and D. Bodden, “Multivariable control allocation and control law conditioning when control effectors limit,” in *Proceedings of the AIAA Guidance, Navigation, and Control Conference*, p. 3609, 1994.
- [59] D. Enns, “Control allocation approaches,” in *Proceedings of the AIAA Guidance, Navigation, and Control Conference*, p. 4109, 1998.
- [60] W. C. Durham, “Constrained control allocation: Three-moment problem,” *Journal of Guidance, Control, and Dynamics*, vol. 17, no. 2, pp. 330–336, 1994.
- [61] T. A. Johansen, T. I. Fossen, and S. P. Berge, “Constrained nonlinear control allocation with singularity avoidance using sequential quadratic programming,” *IEEE Transactions on Control Systems Technology*, vol. 12, no. 1, pp. 211–216, 2004.
- [62] M. Bodson, “Evaluation of optimization methods for control allocation,” *Journal of Guidance, Control, and Dynamics*, vol. 25, no. 4, pp. 703–711, 2002.
- [63] R. L. Eberhardt and D. G. Ward, “Indirect adaptive flight control of a tailless fighter aircraft,” in *Proceedings of the AIAA Guidance, Navigation, and Control Conference and Exhibit*, pp. 466–476, 1999.

- [64] J. A. Petersen and M. Bodson, “Constrained quadratic programming techniques for control allocation,” *IEEE Transactions on Control Systems Technology*, vol. 14, no. 1, pp. 91–98, 2006.
- [65] J. J. Burken, P. Lu, Z. Wu, and C. Bahm, “Two reconfigurable flight-control design methods: Robust servomechanism and control allocation,” *Journal of Guidance, Control, and Dynamics*, vol. 24, no. 3, pp. 482–493, 2001.
- [66] Y. M. Zhang, V. S. Suresh, B. Jiang, and D. Theilliol, “Reconfigurable control allocation against aircraft control effector failures,” in *Proceedings of the IEEE International Conference on Control Applications*, pp. 1197–1202, 2007.
- [67] Y. M. Zhang, C. A. Rabbath, and C.-Y. Su, “Reconfigurable control allocation applied to an aircraft benchmark model,” in *Proceedings of the American Control Conference*, pp. 1052–1057, 2008.
- [68] M. T. Hamayun, C. Edwards, and H. Alwi, “A fault tolerant control allocation scheme with output integral sliding modes,” *Automatica*, vol. 49, no. 6, pp. 1830–1837, 2013.
- [69] Q. Hu, B. Li, and A. Zhang, “Robust finite-time control allocation in spacecraft attitude stabilization under actuator misalignment,” *Nonlinear Dynamics*, vol. 73, no. 1-2, pp. 53–71, 2013.
- [70] A. Cristofaro and T. A. Johansen, “Fault-tolerant control allocation: an unknown input observer based approach with constrained output fault directions,” in *Proceedings of the IEEE 52nd Annual Conference on Decision and Control (CDC)*, pp. 3818–3824, 2013.
- [71] A. Cristofaro, M. M. Polycarpou, and T. A. Johansen, “Fault diagnosis and fault-tolerant control allocation for a class of nonlinear systems with redundant inputs,” in *Proceedings of the IEEE 54th Annual Conference on Decision and Control (CDC)*, pp. 5117–5123, 2015.

- [72] Q. Shen, B. Jiang, and P. Shi, *Fault Diagnosis and Fault-Tolerant Control Based on Adaptive Control Approach*. Springer Science & Business Media, 2017.
- [73] A. Pouliezos and G. S. Stavrakakis, *Real Time Fault Monitoring of Industrial Processes*. Springer Science & Business Media, 2013.
- [74] R. Mohammadi, E. Naderi, K. Khorasani, and S. Hashtrudi-Zad, “Fault diagnosis of gas turbine engines by using dynamic neural networks,” in *Proceedings of the ASME Turbo Expo 2010: Power for Land, Sea, and Air*, pp. 365–376, 2010.
- [75] H. A. Talebi, K. Khorasani, and S. Tafazoli, “A recurrent neural-network-based sensor and actuator fault detection and isolation for nonlinear systems with application to the satellite’s attitude control subsystem,” *IEEE Transactions on Neural Networks*, vol. 20, no. 1, pp. 45–60, 2009.
- [76] M. R. Napolitano, C. Neppach, V. Casdorph, S. Naylor, M. Innocenti, and G. Silvestri, “Neural-network-based scheme for sensor failure detection, identification, and accommodation,” *Journal of Guidance, Control, and Dynamics*, vol. 18, no. 6, pp. 1280–1286, 1995.
- [77] S. Simani and C. Fantuzzi, “Fault diagnosis in power plant using neural networks,” *Information Sciences*, vol. 127, no. 3, pp. 125–136, 2000.
- [78] L. Yuan, Y. He, J. Huang, and Y. Sun, “A new neural-network-based fault diagnosis approach for analog circuits by using kurtosis and entropy as a preprocessor,” *IEEE Transactions on Instrumentation and Measurement*, vol. 59, no. 3, pp. 586–595, 2010.
- [79] S. S. Tayarani-Bathaie, Z. S. Vanini, and K. Khorasani, “Dynamic neural network-based fault diagnosis of gas turbine engines,” *Neurocomputing*, vol. 125, pp. 153–165, 2014.
- [80] T. De Bruin, K. Verbert, and R. Babuška, “Railway track circuit fault diagnosis using recurrent neural networks,” *IEEE Transactions on Neural Networks and Learning Systems*, vol. 28, no. 3, pp. 523–533, 2017.

- [81] M. H. Amoozgar, A. Chamseddine, and Y. M. Zhang, “Experimental test of a two-stage Kalman filter for actuator fault detection and diagnosis of an unmanned quadrotor helicopter,” *Journal of Intelligent & Robotic Systems*, vol. 70, no. 1-4, pp. 107–117, 2013.
- [82] Z. Cen, H. Noura, T. B. Susilo, and Y. A. Younes, “Robust fault diagnosis for quadrotor UAVs using adaptive Thau observer,” *Journal of Intelligent & Robotic Systems*, vol. 73, no. 1-4, pp. 573–588, 2014.
- [83] R. C. Avram, X. Zhang, and J. Muse, “Quadrotor actuator fault diagnosis and accommodation using nonlinear adaptive estimators,” *IEEE Transactions on Control Systems Technology*, vol. 25, no. 6, pp. 2219–2226, 2017.
- [84] Y. Park, “Robust and optimal attitude stabilization of spacecraft with external disturbances,” *Aerospace Science and Technology*, vol. 9, no. 3, pp. 253–259, 2005.
- [85] B. Wang, L. X. Mu, and Y. M. Zhang, “Adaptive robust tracking control of quadrotor helicopter with parametric uncertainty and external disturbance,” in *Proceedings of the International Conference on Unmanned Aircraft Systems (ICUAS)*, pp. 402–407, 2017.
- [86] S. Li, J. Yang, W.-H. Chen, and X. Chen, *Disturbance Observer-Based Control: Methods and Applications*. CRC Press, 2014.
- [87] J. Han, “From PID to active disturbance rejection control,” *IEEE Transactions on Industrial Electronics*, vol. 56, no. 3, pp. 900–906, 2009.
- [88] H. Xu, M. D. Mirmirani, and P. A. Ioannou, “Adaptive sliding mode control design for a hypersonic flight vehicle,” *Journal of Guidance, Control, and Dynamics*, vol. 27, no. 5, pp. 829–838, 2004.
- [89] L. Fiorentini, A. Serrani, M. A. Bolender, and D. B. Doman, “Nonlinear robust adaptive control of flexible air-breathing hypersonic vehicles,” *Journal of Guidance, Control, and Dynamics*, vol. 32, no. 2, pp. 401–416, 2009.

- [90] S. Ding and S. Li, “Stabilization of the attitude of a rigid spacecraft with external disturbances using finite-time control techniques,” *Aerospace Science and Technology*, vol. 13, no. 4, pp. 256–265, 2009.
- [91] Z. Chen and J. Huang, “Attitude tracking and disturbance rejection of rigid spacecraft by adaptive control,” *IEEE Transactions on Automatic Control*, vol. 54, no. 3, pp. 600–605, 2009.
- [92] C. Wen, J. Zhou, Z. Liu, and H. Su, “Robust adaptive control of uncertain nonlinear systems in the presence of input saturation and external disturbance,” *IEEE Transactions on Automatic Control*, vol. 56, no. 7, pp. 1672–1678, 2011.
- [93] X. Chen, J. Yang, S. Li, and Q. Li, “Disturbance observer based multi-variable control of ball mill grinding circuits,” *Journal of Process Control*, vol. 19, no. 7, pp. 1205–1213, 2009.
- [94] C. Johnson, “Accommodation of external disturbances in linear regulator and servomechanism problems,” *IEEE Transactions on Automatic Control*, vol. 16, no. 6, pp. 635–644, 1971.
- [95] S. Kwon and W. K. Chung, “A discrete-time design and analysis of perturbation observer for motion control applications,” *IEEE Transactions on Control Systems Technology*, vol. 11, no. 3, pp. 399–407, 2003.
- [96] J.-H. She, M. Fang, Y. Ohyama, H. Hashimoto, and M. Wu, “Improving disturbance-rejection performance based on an equivalent-input-disturbance approach,” *IEEE Transactions on Industrial Electronics*, vol. 55, no. 1, pp. 380–389, 2008.
- [97] Y. Xia, P. Shi, G. Liu, D. Rees, and J. Han, “Active disturbance rejection control for uncertain multivariable systems with time-delay,” *IET Control Theory & Applications*, vol. 1, no. 1, pp. 75–81, 2007.

- [98] T. Umeno, T. Kaneko, and Y. Hori, “Robust servosystem design with two degrees of freedom and its application to novel motion control of robot manipulators,” *IEEE Transactions on Industrial Electronics*, vol. 40, no. 5, pp. 473–485, 1993.
- [99] W.-H. Chen, D. J. Ballance, P. J. Gawthrop, and J. O’Reilly, “A nonlinear disturbance observer for robotic manipulators,” *IEEE Transactions on Industrial Electronics*, vol. 47, no. 4, pp. 932–938, 2000.
- [100] K. Ohishi, M. Nakao, K. Ohnishi, and K. Miyachi, “Microprocessor-controlled DC motor for load-insensitive position servo system,” *IEEE Transactions on Industrial Electronics*, vol. 34, no. 1, pp. 44–49, 1987.
- [101] W.-H. Chen, “Nonlinear disturbance observer-enhanced dynamic inversion control of missiles,” *Journal of Guidance, Control, and Dynamics*, vol. 26, no. 1, pp. 161–166, 2003.
- [102] W.-H. Chen, “Disturbance observer based control for nonlinear systems,” *IEEE/ASME Transactions on Mechatronics*, vol. 9, no. 4, pp. 706–710, 2004.
- [103] L. Besnard, Y. B. Shtessel, and B. Landrum, “Quadrotor vehicle control via sliding mode controller driven by sliding mode disturbance observer,” *Journal of the Franklin Institute*, vol. 349, no. 2, pp. 658–684, 2012.
- [104] J. Yang, S. Li, C. Sun, and L. Guo, “Nonlinear-disturbance-observer-based robust flight control for airbreathing hypersonic vehicles,” *IEEE Transactions on Aerospace and Electronic Systems*, vol. 49, no. 2, pp. 1263–1275, 2013.
- [105] W.-H. Chen, J. Yang, L. Guo, and S. Li, “Disturbance-observer-based control and related methods-An overview,” *IEEE Transactions on Industrial Electronics*, vol. 63, no. 2, pp. 1083–1095, 2016.

- [106] X. Wei and L. Guo, “Composite disturbance-observer-based control and H_∞ control for complex continuous models,” *International Journal of Robust and Nonlinear Control*, vol. 20, no. 1, pp. 106–118, 2010.
- [107] L. Guo and S. Cao, “Anti-disturbance control theory for systems with multiple disturbances: A survey,” *ISA Transactions*, vol. 53, no. 4, pp. 846–849, 2014.
- [108] B. Wang and Y. M. Zhang, “An adaptive fault-tolerant sliding mode control allocation scheme for multirotor helicopter subject to simultaneous actuator faults,” *IEEE Transactions on Industrial Electronics*, vol. 65, no. 5, pp. 4227–4236, 2018.
- [109] T. Bresciani, “Modelling, identification and control of a quadrotor helicopter,” Master’s thesis, Lund University, Sweden, 2008.
- [110] G. Pajares, “Overview and current status of remote sensing applications based on unmanned aerial vehicles (UAVs),” *Photogrammetric Engineering & Remote Sensing*, vol. 81, no. 4, pp. 281–329, 2015.
- [111] K. Nonami, “Prospect and recent research & development for civil use autonomous unmanned aircraft as UAV and MAV,” *Journal of System Design and Dynamics*, vol. 1, no. 2, pp. 120–128, 2007.
- [112] I. Sadeghzadeh, M. Abdolhosseini, and Y. M. Zhang, “Payload drop application using an unmanned quadrotor helicopter based on gain-scheduled PID and model predictive control,” *Unmanned Systems*, vol. 2, no. 1, pp. 39–52, 2014.
- [113] F. Sharifi, M. Mirzaei, Y. M. Zhang, and B. W. Gordon, “Cooperative multi-vehicle search and coverage problem in an uncertain environment,” *Unmanned Systems*, vol. 3, no. 1, pp. 35–47, 2015.

- [114] L. Merino, F. Caballero, J. R. Martínez-de Dios, I. Maza, and A. Ollero, “An unmanned aircraft system for automatic forest fire monitoring and measurement,” *Journal of Intelligent & Robotic Systems*, vol. 65, no. 1-4, pp. 533–548, 2012.
- [115] Z. Liu, C. Yuan, X. Yu, and Y. M. Zhang, “Fault-tolerant formation control of unmanned aerial vehicles in the presence of actuator faults and obstacles,” *Unmanned Systems*, vol. 4, no. 3, pp. 197–211, 2016.
- [116] A. Chamseddine, D. Theilliol, Y. M. Zhang, C. Join, and C.-A. Rabbath, “Active fault-tolerant control system design with trajectory re-planning against actuator faults and saturation: Application to a quadrotor unmanned aerial vehicle,” *International Journal of Adaptive Control and Signal Processing*, vol. 29, no. 1, pp. 1–23, 2015.
- [117] Z. Liu, C. Yuan, Y. M. Zhang, and J. Luo, “A learning-based fault tolerant tracking control of an unmanned quadrotor helicopter,” *Journal of Intelligent & Robotic Systems*, vol. 84, no. 1-4, pp. 145–162, 2016.
- [118] M. Chadli, S. Aouaouda, H.-R. Karimi, and P. Shi, “Robust fault tolerant tracking controller design for a VTOL aircraft,” *Journal of the Franklin Institute*, vol. 350, no. 9, pp. 2627–2645, 2013.
- [119] M. Steinberg, “Historical overview of research in reconfigurable flight control,” *Proceedings of the Institution of Mechanical Engineers, Part G: Journal of Aerospace Engineering*, vol. 219, no. 4, pp. 263–275, 2005.
- [120] B. Xiao and S. Yin, “Velocity-free fault-tolerant and uncertainty attenuation control for a class of nonlinear systems,” *IEEE Transactions on Industrial Electronics*, vol. 63, no. 7, pp. 4400–4411, 2016.
- [121] B. Mu, K. Zhang, and Y. Shi, “Integral sliding mode flight controller design for a quadrotor and the application in a heterogeneous multi-agent system,” *IEEE Transactions on Industrial Electronics*, vol. 64, no. 12, pp. 9389–9398, 2017.

- [122] M. Abdolhosseini, Y. M. Zhang, and C. A. Rabbath, “An efficient model predictive control scheme for an unmanned quadrotor helicopter,” *Journal of Intelligent & Robotic Systems*, vol. 70, no. 1-4, pp. 27–38, 2013.
- [123] H. Liu, D. Li, Z. Zuo, and Y. Zhong, “Robust three-loop trajectory tracking control for quadrotors with multiple uncertainties,” *IEEE Transactions on Industrial Electronics*, vol. 63, no. 4, pp. 2263–2274, 2016.
- [124] F. Chen, Q. Wu, B. Jiang, and G. Tao, “A reconfiguration scheme for quadrotor helicopter via simple adaptive control and quantum logic,” *IEEE Transactions on Industrial Electronics*, vol. 62, no. 7, pp. 4328–4335, 2015.
- [125] Q. Hu, Y. M. Zhang, X. Huo, and B. Xiao, “Adaptive integral-type sliding mode control for spacecraft attitude maneuvering under actuator stuck failures,” *Chinese Journal of Aeronautics*, vol. 24, no. 1, pp. 32–45, 2011.
- [126] X. Yu, P. Li, and Y. M. Zhang, “The design of fixed-time observer and finite-time fault-tolerant control for hypersonic gliding vehicles,” *IEEE Transactions on Industrial Electronics*, vol. 65, no. 5, pp. 4135–4144, 2018.
- [127] X. Yu, Y. Fu, and X. Peng, “Fuzzy logic aided fault-tolerant control applied to transport aircraft subject to actuator stuck failures,” *IEEE Transactions on Fuzzy Systems*, 2017. doi: 10.1109/TFUZZ.2017.2760860.
- [128] Q. Shen, B. Jiang, and V. Cocquempot, “Fault-tolerant control for T-S fuzzy systems with application to near-space hypersonic vehicle with actuator faults,” *IEEE Transactions on Fuzzy Systems*, vol. 20, no. 4, pp. 652–665, 2012.
- [129] Q. Shen, B. Jiang, and V. Cocquempot, “Fuzzy logic system-based adaptive fault-tolerant control for near-space vehicle attitude dynamics with actuator faults,” *IEEE Transactions on Fuzzy Systems*, vol. 21, no. 2, pp. 289–300, 2013.

- [130] Q. Shen, B. Jiang, P. Shi, and J. Zhao, “Cooperative adaptive fuzzy tracking control for networked unknown nonlinear multiagent systems with time-varying actuator faults,” *IEEE Transactions on Fuzzy Systems*, vol. 22, no. 3, pp. 494–504, 2014.
- [131] X. Yu, Y. Fu, P. Li, and Y. M. Zhang, “Fault-tolerant aircraft control based on self-constructing fuzzy neural networks and multivariable SMC under actuator faults,” *IEEE Transactions on Fuzzy Systems*, 2017. doi: 10.1109/TFUZZ.2017.2773422.
- [132] J.-J. Slotine and S. S. Sastry, “Tracking control of non-linear systems using sliding surfaces, with application to robot manipulators,” *International Journal of Control*, vol. 38, no. 2, pp. 465–492, 1983.
- [133] B. Wang and Y. M. Zhang, “Fuzzy adaptive fault-tolerant control for quadrotor helicopter,” in *Proceedings of the International Conference on Unmanned Aircraft Systems (ICUAS)*, pp. 945–950, 2017.
- [134] G. Heredia, A. Ollero, M. Bejar, and R. Mahtani, “Sensor and actuator fault detection in small autonomous helicopters,” *Mechatronics*, vol. 18, no. 2, pp. 90–99, 2008.
- [135] J. Seshadrinath, B. Singh, and B. K. Panigrahi, “Incipient interturn fault diagnosis in induction machines using an analytic wavelet-based optimized Bayesian inference,” *IEEE Transactions on Neural Networks and Learning Systems*, vol. 25, no. 5, pp. 990–1001, 2014.
- [136] S. C. Tan, J. Watada, Z. Ibrahim, and M. Khalid, “Evolutionary fuzzy ARTMAP neural networks for classification of semiconductor defects,” *IEEE Transactions on Neural Networks and Learning Systems*, vol. 26, no. 5, pp. 933–950, 2015.
- [137] B. Y. Vyas, B. Das, and R. P. Maheshwari, “Improved fault classification in series compensated transmission line: comparative evaluation of Chebyshev neural network training algorithms,” *IEEE Transactions on Neural Networks and Learning Systems*, vol. 27, no. 8, pp. 1631–1642, 2016.

- [138] F. Chen, R. Jiang, K. Zhang, B. Jiang, and G. Tao, “Robust backstepping sliding-mode control and observer-based fault estimation for a quadrotor UAV,” *IEEE Transactions on Industrial Electronics*, vol. 63, no. 8, pp. 5044–5056, 2016.
- [139] Z. X. Liu, C. Yuan, X. Yu, and Y. M. Zhang, “Retrofit fault-tolerant tracking control design of an unmanned quadrotor helicopter considering actuator dynamics,” *International Journal of Robust and Nonlinear Control*, 2017. doi: 10.1002/rnc.3889.
- [140] A.-R. Merheb, H. Noura, and F. Bateman, “Active fault tolerant control of quadrotor UAV using sliding mode control,” in *Proceedings of the International Conference on Unmanned Aircraft Systems (ICUAS)*, pp. 156–166, 2014.
- [141] X. Yu, P. Li, and Y. M. Zhang, “The design of fixed-time observer and finite-time fault-tolerant control for hypersonic gliding vehicles,” *IEEE Transactions on Industrial Electronics*, vol. 65, no. 5, pp. 4135–4144, 2018.
- [142] J. M. Andrade-Da Silva, C. Edwards, and S. K. Spurgeon, “Sliding-mode output-feedback control based on LMIs for plants with mismatched uncertainties,” *IEEE Transactions on Industrial Electronics*, vol. 56, no. 9, pp. 3675–3683, 2009.
- [143] K. Patan, *Artificial Neural Networks for the Modelling and Fault Diagnosis of Technical Processes*. Springer Science & Business Media, 2008.
- [144] R. J. Williams and D. Zipser, “A learning algorithm for continually running fully recurrent neural networks,” *Neural Computation*, vol. 1, no. 2, pp. 270–280, 1989.
- [145] J. L. Elman, “Finding structure in time,” *Cognitive Science*, vol. 14, no. 2, pp. 179–211, 1990.
- [146] M. I. Jordan, “Supervised learning and systems with excess degrees of freedom,” tech. rep., Amherst, MA, USA, 1988.

- [147] S. Haykin, *Neural Networks and Learning Machines*. Pearson Upper Saddle River, NJ, USA, 2009.
- [148] Y. M. Zhang and X. R. Li, “A fast UD factorization-based learning algorithm with applications to nonlinear system modeling and identification,” *IEEE Transactions on Neural Networks*, vol. 10, no. 4, pp. 930–938, 1999.
- [149] X. Zhang, M. M. Polycarpou, and T. Parisini, “A robust detection and isolation scheme for abrupt and incipient faults in nonlinear systems,” *IEEE Transactions on Automatic Control*, vol. 47, no. 4, pp. 576–593, 2002.
- [150] A. Abbaspour, P. Aboutalebi, K. K. Yen, and A. Sargolzaei, “Neural adaptive observer-based sensor and actuator fault detection in nonlinear systems: Application in UAV,” *ISA Transactions*, vol. 67, pp. 317–329, 2016.
- [151] M. W. Mueller and R. D’Andrea, “Stability and control of a quadrocopter despite the complete loss of one, two, or three propellers,” in *Proceedings of the IEEE International Conference on Robotics and Automation (ICRA)*, pp. 45–52, 2014.
- [152] A. Lanzon, A. Freddi, and S. Longhi, “Flight control of a quadrotor vehicle subsequent to a rotor failure,” *Journal of Guidance, Control, and Dynamics*, vol. 37, no. 2, pp. 580–591, 2014.
- [153] P. Lu and E.-J. Van Kampen, “Active fault-tolerant control for quadrotors subjected to a complete rotor failure,” in *Proceedings of the IEEE/RSJ International Conference on Intelligent Robots and Systems (IROS)*, pp. 4698–4703, 2015.
- [154] S. Osder, “Practical view of redundancy management application and theory,” *Journal of Guidance, Control, and Dynamics*, vol. 22, no. 1, pp. 12–21, 1999.

- [155] A. Chamseddine, D. Theilliol, I. Sadeghzadeh, Y. M. Zhang, and P. Weber, “Optimal reliability design for over-actuated systems based on the MIT rule: Application to an octocopter helicopter testbed,” *Reliability Engineering & System Safety*, vol. 132, pp. 196–206, 2014.
- [156] G.-X. Du, Q. Quan, and K.-Y. Cai, “Controllability analysis and degraded control for a class of hexacopters subject to rotor failures,” *Journal of Intelligent & Robotic Systems*, vol. 78, no. 1, pp. 143–157, 2015.
- [157] V. G. Adîr and A. M. Stoica, “Integral LQR control of a star-shaped octorotor,” *Incas Bulletin*, vol. 4, no. 2, pp. 1–16, 2012.
- [158] B. Arain and F. Kendoul, “Real-time wind speed estimation and compensation for improved flight,” *IEEE Transactions on Aerospace and Electronic Systems*, vol. 50, no. 2, pp. 1599–1606, 2014.
- [159] J. P. V. Cunha, R. R. Costa, L. Hsu, and T. R. Oliveira, “Output-feedback sliding-mode control for systems subjected to actuator and internal dynamics failures,” *IET Control Theory & Applications*, vol. 9, no. 4, pp. 637–647, 2015.
- [160] M. Wang, J. Yang, G. Qin, and Y. Yan, “Adaptive fault-tolerant control with control allocation for flight systems with severe actuator failures and input saturation,” in *Proceedings of the American Control Conference (ACC)*, pp. 5134–5139, 2013.
- [161] V. Utkin and J. Shi, “Integral sliding mode in systems operating under uncertainty conditions,” in *Proceedings of the 35th IEEE Conference on Decision and Control (CDC)*, pp. 4591–4596, 1996.

List of Publications

Journal Papers

- (1) Ban Wang, and Youmin Zhang (2017), “Adaptive sliding mode fault-tolerant control for an unmanned aerial vehicle,” *Unmanned Systems*, 5(4), pp. 209–221.
- (2) Ban Wang, and Youmin Zhang (2018), “An adaptive fault-tolerant sliding mode control allocation scheme for multirotor helicopter subject to simultaneous actuator faults,” *IEEE Transactions on Industrial Electronics*, 65(5), pp. 4227–4236.
- (3) Ban Wang, Xiang Yu, Lingxia Mu, and Youmin Zhang (2018), “An adaptive fault-tolerant control for a quadrotor helicopter against actuator faults and model uncertainties,” *IEEE Transactions on Industrial Informatics* (Under review).
- (4) Ban Wang, Yanyan Shen, and Youmin Zhang (2018), “Active fault-tolerant control for a quadrotor helicopter against faults and uncertainties,” *IEEE Transactions on Industrial Electronics* (Under revision).
- (5) Ban Wang, Xiang Yu, Lingxia Mu, and Youmin Zhang (2018), “Disturbance observer-based adaptive fault-tolerant control for a quadrotor helicopter subject to parametric uncertainties and external disturbances,” *Mechanical Systems and Signal Processing* (Under review).

Conference Papers

- (1) Ban Wang, and Youmin Zhang (2018), “Fault-tolerant control for a quadrotor helicopter with parametric uncertainty,” in *Proceedings of the International Conference on Sensing,*

Diagnostics, and Control (SDPC 2018), August 15-17, 2018, Xi'an, China.

- (2) Ban Wang, Lingxia Mu, and Youmin Zhang (2017), “Adaptive robust control of quadrotor helicopter towards payload transportation applications,” in *Proceedings of the 36th Chinese Control Conference (CCC 2017)*, pp. 4774–4779, July 26-28, 2017, Dalian, China.
- (3) Ban Wang, Youmin Zhang, Jean-Christophe Ponsart, and Didier Theilliol (2017), “Fault-tolerant adaptive control allocation for unmanned multirotor helicopter,” in *Proceedings of the 20th World Congress of the International Federation of Automatic Control*, 50(1), pp. 5269–5274, July 9-14, 2017, Toulouse, France.
- (4) Ban Wang, and Youmin Zhang (2017), “Fuzzy adaptive fault-tolerant control for quadrotor helicopter,” in *Proceedings of the International Conference on Unmanned Aircraft Systems (ICUAS 2017)*, pp. 945–950, June 13-16, 2017, Miami, FL, USA.
- (5) Ban Wang, Lingxia Mu, and Youmin Zhang (2017), “Adaptive robust tracking control of quadrotor helicopter with parametric uncertainty and external disturbance,” in *Proceedings of the International Conference on Unmanned Aircraft Systems (ICUAS 2017)*, pp. 402–407, June 13-16, 2017, Miami, FL, USA.
- (6) Ban Wang, and Youmin Zhang (2017), “Fault-tolerant control for quadrotor helicopter with parametric uncertainty based on integral sliding mode control,” in *Proceedings of the 26th Canadian Congress of Applied Mechanics*, pp. 1–6, May 29-June 1, 2017, Victoria, BC, Canada.
- (7) Ban Wang, Khaled A. Ghamry, and Youmin Zhang (2016), “Trajectory tracking and attitude control of an unmanned quadrotor helicopter considering actuator dynamics,” in *Proceedings of the 35th Chinese Control Conference (CCC 2016)*, pp. 10795–10800, July 27-29, 2016, Chengdu, China.
- (8) Ban Wang, and Youmin Zhang (2016), “Adaptive sliding mode fault-tolerant control for an

unmanned quadrotor helicopter,” in *Proceedings of the Canadian Society for Mechanical Engineering International Congress*, pp. 1–6, June 26-29, 2016, Kelowna, BC, Canada.

- (9) Lingxia Mu, Xiang Yu, Ban Wang, Youmin Zhang, Xinmin Wang, and Ping Li (2018), “Second-order sliding mode guidance for 3D gliding motion,” in *Proceedings of the 33rd Youth Academic Annual Conference of Chinese Association of Automation (YAC 2018)*, May 18-20, 2018, Nanjing, China.
- (10) Lingxia Mu, Xiang Yu, Ban Wang, Youmin Zhang, Xinmin Wang, and Ping Li (2018), “Sliding mode guidance for 3D gliding motions with bank limitations,” in *Proceedings of the IEEE/CSAA Guidance, Navigation and Control Conference*, August 10-12, 2018, Xiamen, China.